PRELIMINARY STUDY OF BYPASS FLOW IN PRISMATIC CORE OF VERY HIGH TEMPERATURE REACTOR USING SMALL-SCALE MODEL

A Dissertation

by

WORASIT KANJANAKIJKASEM

Submitted to the Office of Graduate Studies of
Texas A&M University
in partial fulfillment of the requirements for the degree of

DOCTOR OF PHILOSOPHY

Approved by:

Chair of Committee,	Yassin A. Hassan
Committee Members,	Sai Lau
	Kalyan Annamalai
	William H. Marlow
Head of Department,	Jerald Caton

December 2012

Major Subject: Mechanical Engineering

ABSTRACT

Very high temperature reactor (VHTR) is one of the candidates for Generation IV reactor. It can be continuously operated with average core outlet temperature between 900°C and 950°C, so the core temperature is one of the key features in the design of VHTR. Bypass flow in the prismatic core of VHTR is not a designed feature but it is inevitable due to the combination of several causes and considerably affects the core temperature. Although bypass flow has been studied extensively, the current status of research on thermal/hydraulic core flow of VHTR is far from completion. Present study is the starting of bypass flow characteristic investigation using small-scale model that will fulfill understandings of bypass flow in the prismatic core of VHTR.

Bypass flow experiments are conducted by using three small-scale models of prismatic blocks. They are stacked in a test section to form bypass gaps of single-layer blocks as exist in prismatic core of VHTR. Three bypass gap widths set in air and water flow experiments are 6.1, 4.4 and 2.7 mm. Experimental data shows that bypass flow fraction depends on bypass gap width and downstream condition of prismatic blocks, while pressure drop of flow through bypass gaps depends on bypass gap width only.

Bypass flow simulations are performed by using STAR-CCM+ software after meshing parameters were determined from simulation exercises and grid independent study. Three turbulence models are employed in all bypass flow simulations which are stopped at physical time of 100 seconds marching by implicit unsteady scheme. Bypass flow fraction, coolant channel Reynolds number and bypass gap Reynolds number from

air flow and water flow simulations with 6.1-mm bypass gap width are very close to experimental data. This is because bypass flow fractions from experiments at this bypass gap width are matched in construction of the simulation models. Discrepancies between results from simulations and experiments for remaining gaps increase when bypass gap width becomes smaller. Finally, guidelines for bypass flow experiments and simulations are drawn from the data in present study to improve bypass flow study in the future.

DEDICATION

To my parents

ACKNOWLEDGEMENTS

I would like to thank my committee chair, Dr. Yassin A. Hassan, and my committee members, Dr. Sai Lau, Dr. Kalyan Annamalai, and Dr. William H. Marlow, for their guidance and support during the course of this research.

Special thanks also go to my colleagues, Elvis Dominguez-Onteveros and Huhu Wang, for their collaboration on working for bypass flow experiments. The Texas A&M University Supercomputing center and their support on bypass flow simulations is indispensable and appreciated. I am thankful for the help and support from all of my friends in Thai Student Association and my research group that makes my time at Texas A&M University a good memory in my life.

Finally, I want to express my highest gratitude to my parents for their support and encouragement when I have difficult times during my doctoral study.

TABLE OF CONTENTS

Page

LIST OF FIGURES

LIST OF TABLES

1. INTRODUCTION

This section is intended to provide important basics for present study. It starts with introduction to Generation IV Reactor and all of its candidates. Very high-temperature gas-cooled reactor, one of the candidates for Generation IV Reactor, is focused in more details. Concepts about core flow distribution and core temperature are briefly introduced and followed by related literatures. Finally, objectives of present study are drawn as closure of the section.

1.1 Generation IV Reactor

The Generation IV Forum (GIF) was initiated in 2000 [1] and formally chartered in July 2001 with nine members which are Argentina, Brazil, Canada, France, Japan, the Republic of Korea, the Republic of South Africa, the United Kingdom, and the United States [2]. Subsequently, it was signed by Switzerland in 2002, the European Atomic Energy Community (EURATOM) in 2003, and the People's Republic of China and the Russian Federation, both in 2006 [2].

Late in 2002, GIF announced the selection of six reactor technologies which were believed to represent the future shape of nuclear energy are: gas-cooled fast reactor (GFR); lead-cooled fast reactor (LFR); molten salt reactor (MSR); sodium-cooled fast reactor (SFR); supercritical water-cooled reactor (SCWR); and very high-temperature gas-cooled reactor (VHTR) [3]. These reactor types were selected on the basis of being clean, safe, cost-effective, resistant to diversion of materials for weapons proliferation, and secure from terrorist attacks [1]. The Generation IV systems are expected to become

available for commercial introduction in the period between 2015 and 2030 or beyond. Evolution of all generations of nuclear systems is shown in Figure 1 [2].

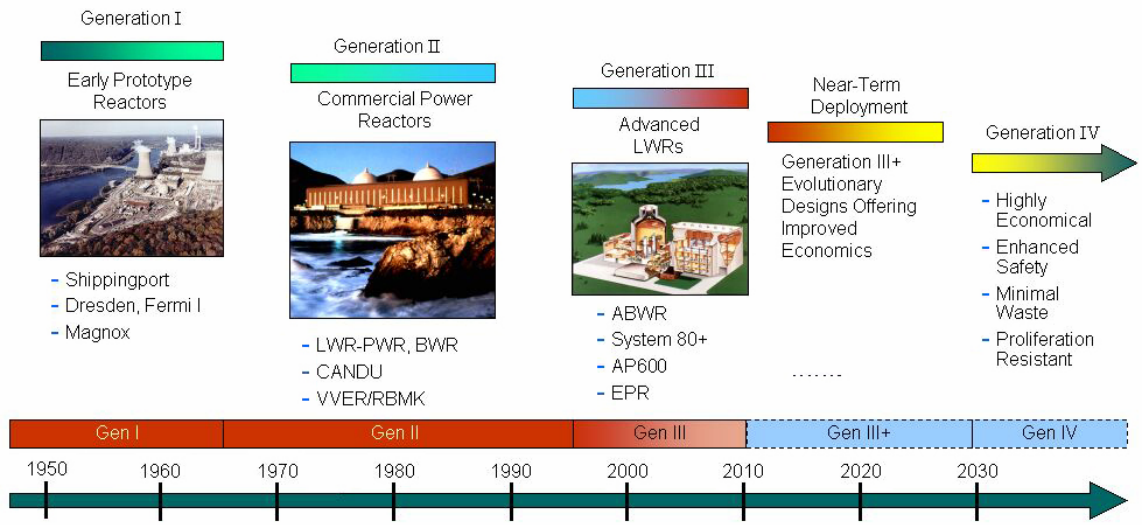

Figure 1. Evolution of nuclear systems

1.2 Very High-Temperature Gas-Cooled Reactor

Very high-temperature gas-cooled reactor (VHTR) is a graphite-moderated, helium-cooled, thermal neutron spectrum reactor with a once-through uranium fuel cycle [4]. The reactor core can be either a *prismatic block* or a *pebble-bed* core. The VHTR system is designed to be a high-efficiency system that can supply process heat to a broad spectrum of high-temperature and energy-intensive, non-electric processes [5] and can be continuously operated with average core outlet temperature between 900°C and 950°C [6]. Schematic concept of the VHTR is shown in Figure 2 [7].

The overall good safety characteristics of this reactor are due to: a) high heat capacity of the graphite core; b) high temperature capability of core components; c) chemical stability and inertness of fuel, coolant, and moderator; d) high retention of

fission products by fuel coatings; e) single phase characteristics of helium coolant; and f) inherent negative temperature coefficient of core reactivity [8].

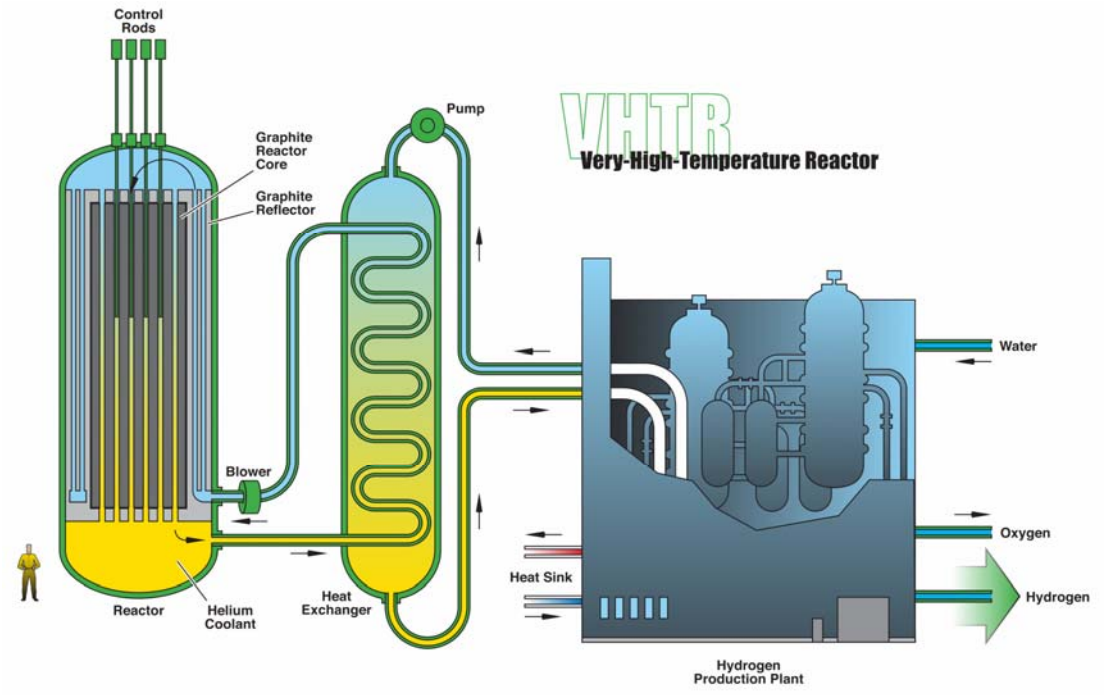

Figure 2. Schematic concept of the VHTR

The earlier version of the VHTR is known as high-temperature gas-cooled reactor (HTR). The HTR design was first proposed by the Staff of the Power Pile Division of the Clinton Laboratories (Oak Ridge National Laboratory) in 1947 [9]. Experimental HTRs with prismatic block core were developed in United Kingdom (Dragon reactor, 20 MW thermal) and in the United States (Peach Bottom, 40 MW electrical, operated from 1967 to 1974) [10]. They were followed by Fort St. Vrain Generating Station (330 MW electrical) operated from 1979 to 1989 [10].

Germany built a pebble bed reactor, Arbeitsgemeinschaft Versuchsreaktor (AVR, 15 MW electrical, operated from 1966 to 1987), at the research center of Julich.

Following the experience from AVR, the Thorium High Temperature Reactor (THTR-300, 300 MW electrical) was built and operated as prototype of power reactor. It was suffered from a number of technical difficulties and finally closed. There was no further development until late of 1990s when the interest in HTRs was revived by the needs of low carbon high temperature supply for various industrial processes [10].

Nowadays, there are several projects of VHTR prototypes planned for the period of 2015 to 2025 [10] which are the High Temperature Test Reactor (HTTR, using prismatic fuel with capacity of 30 MW thermal) in parallel with Gas Turbine High Temperature Reactor (GTHTR300C, based on HTTR derivative technology) in Japan, HTR-10 (a 10 MW thermal pebble bed high temperature reactor prototype) and two pebble-bed HTRs (scaled up from HTR-10, each with 250 MW thermal) which are under construction with the date of completion around 2013 [11] in China, Pebble Bed Modular Reactor (PBMR, 165 MW electrical) in the Republic of South Africa, Next Generation Nuclear Project (NGNP) in the United States, and Nuclear Hydrogen Development and Demonstration (NHDD) in Korea.

1.2.1 Modular Helium Reactor

In the 1980s, evaluation of the reasons for the dearth of new nuclear plants orders in the United States led to the conclusion that smaller, simpler nuclear power plants with inherent safety characteristics were needed for public acceptance. The modular high temperature gas reactor (MHTGR) was conceived to meet these needs [12].

Because helium is inert and single phase, modular helium reactor (MHR) can operate at higher temperature and results in higher efficiency of the plant. Therefore, the

gas turbine modular helium reactor (GT-MHR) was developed as a new turbine generating system because it is a cleaner, more economical and safer way to generate electricity [13]. Because GT-MHR is referred as reference reactor in several researches, GT-MHR system and its cross sectional view are shown in Figure 3 [14] and Figure 4 for better understanding about the prismatic block core nuclear reactor.

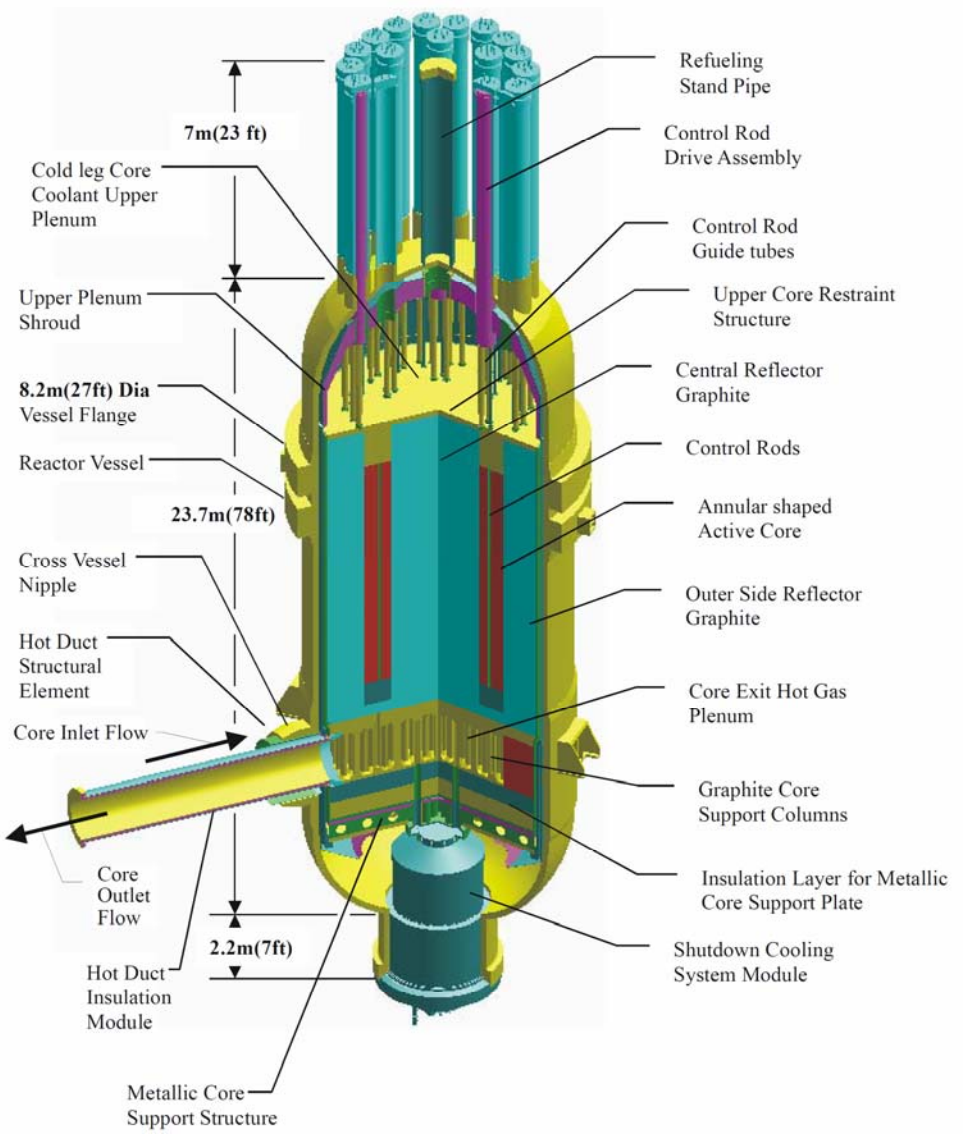

Figure 3. GT-MHR system

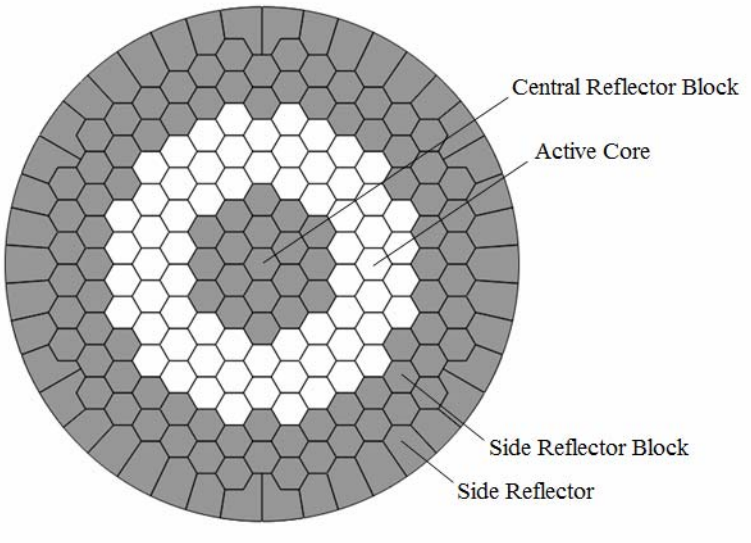

Figure 4. Cross sectional view of the prismatic block core

1.3 High Temperature Reactor Core Flow

Helium coolant is delivered from the circulators to the large plenum above the core. The helium coolant flows downward in various paths through the core from the upper plenum. Flow distribution control in the core of HTR is used because the helium coolant temperature rise in HTR core is large under normal operating conditions and the graded fuel cycle management results in relatively large differences in radial power generation in the core. Flow distribution through the core is controlled by remotely operable flow control valves [15].

Most of the helium coolant entering the upper core plenum passes through the coolant channels within the fuel elements of the core, and a small fraction of the helium coolant bypasses these coolant channels and passes through alternate flow paths to provide cooling to fuel elements and other components within the reactor core cavity. Each of the flow passage in HTR core cavity are defined below [15]:-

Coolant Channel Flow

Almost all of the coolant entering refueling region through variable flow control valves flows through the coolant channels within top reflector, active core, and bottom reflector which are hexagonal graphite blocks. The coolant from each coolant channel is collected into a single plenum within the bottom reflector element just above the core support block.

Bypass Flow

The coolant flow that does not pass through the fuel element coolant channels is called bypass flow. Bypass flow varies with fuel age and with axial position in the core. Bypass flow increases as spaces between elements increase due to fast neutron-induced fuel element shrinkage. Also, bypass flow provides cooling to components of reactor core, i.e. control rod channel, gaps between fuel columns and crossflow gaps, and side reflector and reflector gaps.

1.3.1 Terminology of Flows That Bypass Coolant Channels

Because only the flow through vertical gaps between the walls of fuel elements are focused in present study, a terminology of all the flows contribute to bypass flow is needed to clarify them and used throughout this dissertation. All of them are named based on flow passages shown in Figure 5 which is the prismatic block model used in present study. It can be seen that there are three major flows contribute to the flow that bypasses coolant channels: 1) *bypass flow* which is the flow through vertical gaps formed by the walls of two adjacent fuel columns; 2) *side gap flow* which is the flow through vertical gaps formed by the walls of fuel column and side reflector; and 3)

crossflow which is the flow through horizontal gap formed by two fuel layers stacked in the same column. It should be noted that the new definition of bypass flow is difference from the original definition and it will be referred to throughout this dissertation.

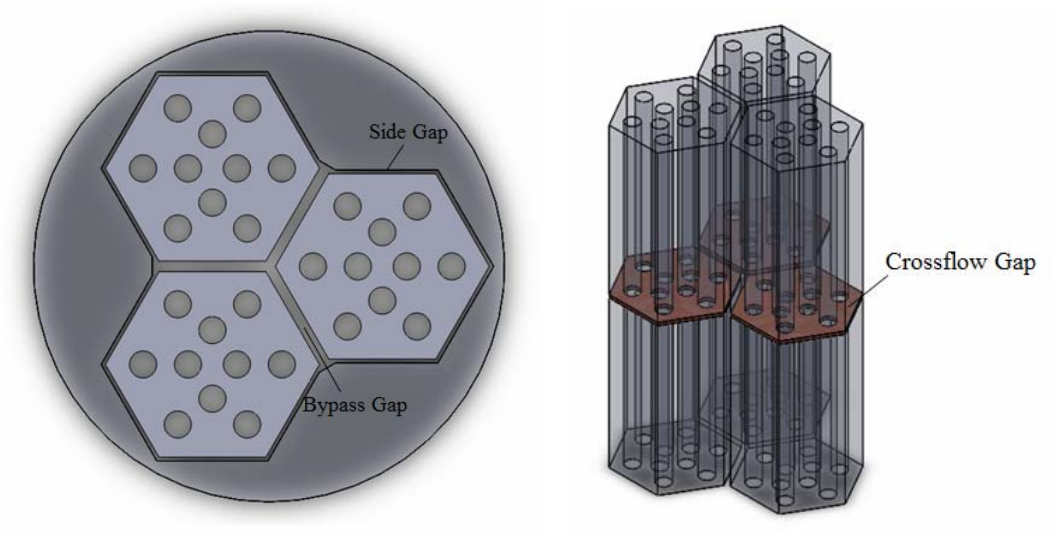

(a) bypass gap and side gap (b) crossflow gap

Figure 5. Bypass passages in core flow

1.4 High Temperature Reactor Core Temperature

Temperature in the core have to be kept below values that begin to cause damage to fission product barriers, produce structural material weakness, and lead to excessive chemical reaction rates. The temperature limitations are defined quantitatively based on four categories of plant conditions: 1) normal operating transients; 2) upset transients; 3) emergency transients; and 4) faulted transients [15].

In addition to the limitations mentioned above, the temperature distribution must not produce thermal stresses from fast neutron-induced dimensional changes that prevent core components from performing their function [15].

1.4.1 Unit Cell Models of Heat Flow in Fuel Elements

It can be noticed that the regular area in the interior of fuel element of large HTR is made up from triangular-shaped unit cells as shown in Figure 6. It is assumed that the unit cell is a symmetry section such that only heat generated in fuel and reflector in this triangular region is removed by coolant flowing in coolant hole within it. This means that heat conduction radially across fuel element is ignored. Even though the model is not accurate in every part of the core, various correction factors have been devised to account for other effects and it is possible to determine the temperatures of coolant, graphite, and fuel throughout the core by using the unit cell model [15].

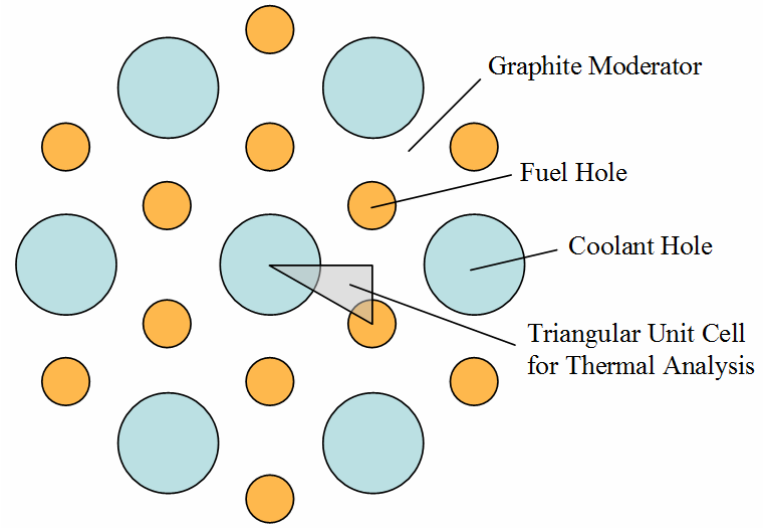

Figure 6. Coolant hole pattern and triangular unit cell

1.4.2 Core Power Distribution

It is obvious that the unit cell model cannot accurately predict temperature distribution in HTR core because heat production in the core is not uniform which causes radial heat conduction in the core fuel element. Therefore, the distribution of heat

production in the core of HTR must be included when more sophisticated approach is employed in core thermal analysis. In describing the distribution of heat production in HTR core, the power peaking factor at each point, $P(l,z)$, is calculated from the product of radial power peaking factor, $P(r)$, local radial intraregion tilt factor, $\alpha(l,r)$, and relative axial power factor, $A(l,z)$, where l is combination radial/azimuth coordinate, r is radial coordinate, and z is axial coordinate [15].

Power Peaking Factor: $$P(l,z) = P(r) \cdot \alpha(l,r) \cdot A(l,z) \tag{1.1}$$

1.4.3 Hot Spot Factors

Hot spot factors used in reactor core thermal-hydraulic analyses are analogous to safety factors in the design of structures and used to account for various uncertainties to assure that a specified maximum temperature in the reactor core is not exceeded at any time and at any location for normal power operation. Two methods can be used for determining hot spot factors: 1) totally deterministic method which all uncertainties are assumed to occur at their worst values all time and everywhere in the core and 2) semi-statistical method which each uncertainty is examined for its nature of occurrence. To combine the deterministic and statistical subfactors, the Monte Carlo method and the worst-value method have been developed [15].

The maximum fuel temperature can be evaluated by the following equation with nominal values from fuel temperature analysis (modified from [16]):

Maximum Fuel Temperature: $$Tf_{\max} = Tg_{in} + \sum_{i=1}^{n} F_i \times \Delta T_i \tag{1.2}$$

Tg_{in} is gas coolant inlet temperature to the core, ΔT_i is ith component of nominal temperature rise, F_i is ith component overall hot spot factor which is calculated from product of total systematic subfactor, Fs_i, and total random (statistical) subfactor, Fr_i.

Overall Hot Spot Factor: $$F_i = Fs_i \times Fr_i \quad (1.3)$$

1.5 Literature Review Related to Bypass Flow in HTR Core

The starting point when bypass flow in nuclear reactor core was firstly interested can be traced back until late of 1970s. In the operation of Fort St. Vrain plant, periodic changes in bypass flow and crossflow of primary coolant helium was mentioned as one cause of core outlet temperature fluctuations [17] occurred during the plant was risen to power above 50% in late 1977 [15]. 84 region constraint devices were installed on the top of the core in October 1979 [17] and they were shown in the following year to prevent temperature fluctuations [15].

In the early of 1980s, studies on prismatic block core flow in HTR which are the foundations of VHTR development have been started. The effects of crossflow on flow distribution through coolant channels were investigated by Groehn [18]. Experiments were carried out by introducing crossflow through a wedge-shaped gap located between two succeeding full-scale blocks model. From the measured results, it could be stated that the influence of crossflow was limited to the upstream block only, whereas the downstream block was not affected. The basic for estimation of the influence of crossflow on main coolant flow was established by finding the most affected coolant channel and then representing the decrease of velocity in that channel as function of the

ratio of crossflow to main flow. The predicted velocity diminutions as function of driving pressure of crossflow were presented. The plots were supposed to be valid when Reynolds number is greater than 60000 under the assumption that flow characteristics do not change and the resistance coefficient follows the derived correlations for greater Reynolds numbers. Groehn [19] continued his study about the effects crossflow on flow distribution through coolant channels by modifying the arrangement of blocking pieces around the circumference of crossflow gap to change flow area geometry of crossflow.

Since the beginning state of studying of flow in VHTR, the projects of VHTR prototypes were committed and now are under developing and operating in many countries. Therefore, it is convenient to categorize all literatures about thermal/hydraulic aspects of VHTR core by existing projects as follows.

1.5.1 Literatures Related to High Temperature Test Reactor

Japan Atomic Energy Research Institute (JAERI) has carried out research and development on HTR since late of 1960s [20]. The construction of the high temperature test reactor (HTTR) was decided in 1987 and started in 1991. From the starting point of HTTR project until it attained the first criticality in 1998, several research works related to prismatic core flow have been published and they are briefly review in the following paragraphs.

Two basic experiments using small-scale graphite blocks with nitrogen gas and experiment using full-scale fuel elements on crossflow with air as working fluid were conducted by Kaburaki and Takizuka [21]. In the basic experiments, crossflow rate through the gaps between contacting cylindrical graphite blocks was measured to predict

the interface equivalent crossflow gap width and the permeability of graphite material was determined by using cylindrical hollow graphite blocks. Experimental data of full-scale fuel elements was well predicted by using the data from the basic experiments.

Kaburaki and Takizuka [22] analyzed coolant flow distribution in the core by using a one-dimensional flow network model based on experiments. Air flow tests in a full-scale core column with one crossflow gap were carried out with a parallel gap and a simulated wedge-shaped gap with 1 mm width which consists of three cases: 1) parallel crossflow gap without orifice installation; 2) parallel crossflow gap with orifice installation; and 3) simulated wedge-shaped gap with orifice installation. After pressure distributions in the gaps between columns obtained from flow network models showed good agreements with experimental data, effects of the variation of crossflow and bypass gap width on flow distribution were studied by flow network model. It was concluded that static pressure distribution in the gaps between columns is very sensitive to the variation of bypass gap width especially for the column with orifice.

Pressure drop characteristics were determined experimentally and estimated numerically using finite element model based on one-sixth sector for parallel gaps and whole block interface for wedge-shaped gaps by Kaburaki and Takizuka [23]. The relation between mass flow rate and pressure difference was obtained experimentally through non-dimensional pressure loss coefficient and two distinct types of flow region were found. Crossflow loss coefficient factor was defined such that the cross-sectional area of the gap was included because the cross-sectional area of the crossflow path is complex and cannot easily be specified. Both parallel and wedge-shaped gap cases have

same tendency with higher crossflow loss coefficient factor for wedge-shaped gap. Finally, empirical crossflow equations were proposed based on the results obtained from the developed numerical code after the relation between crossflow loss coefficient factor and Reynolds number obtained from numerical results showed good agreements with experimental results.

Flat-shaped seal mechanism was devised and the characteristics of bypass flow under this developed seal mechanism were studied by Kaburaki and Takizuka [24]. It could be concluded that the flat-shaped seal mechanism is vulnerable to wedge-shaped block configurations. Then, a seal mechanism consists of graphite seal element with triangular cross section and V-shaped seal seat that gives stable and higher pressure loss coefficient factor under various conditions of seal and block configurations has been proposed by Kaburaki and Takizuka [25].

The helium engineering demonstration loop (HENDEL) was constructed for a large-scale component test of the VHTR under simulated reactor operating conditions. Thermal and hydraulic tests have been conducted using single-channel rig of the fuel stack test section [26]. Also, experimental and analytical investigations on thermal and hydraulic performance of fuel stack of VHTR were performed with multi-channel test rig of the fuel stack test section [27].

Hot spot factors selected in thermal and hydraulic design and their estimated values, and evaluation results of thermal and hydraulic characteristics of the HTTR were reported by Maruyama et al [16]. They were used in the core thermal and hydraulic design procedure of the HTTR which employed pin-in-block type fuel described by

Maruyama et al [28] where coolant flow rate and temperature distributions in a steady state were evaluated by the flow network analysis code FLOWNET (consists of one-dimensional flow branches and pressure nodes, which are junctions or terminals of the branches) and fuel temperatures were calculated by the fuel temperature analysis code TEMDIM (uses a cylindrical model, based on power distribution including local power peaking and coolant flow distribution including redistribution in fuel column and hot spot factors).

The maximum fuel temperature from the former design was revised by using of the operational data of the HTTR and reported by Takada et al [29]. The re-evaluation of the maximum fuel temperature was performed with the same method as in the thermal-hydraulic design and the revised hot spot factors from measurement data through rise-to-power test and gamma ray measurement of fuel block. It was concluded that the flow distribution in the HTTR core calculated by FLOWNET code was reliable.

Preliminary study of prism-type VHTR was carried out by Nakano et al [30]. Three-dimensional analysis of core internal and bypass flow was conducted by ANSYS v.10 code. It was found that the core internals that enable the coolant outlet temperature of 950°C required approximately 90% fuel flow fraction and could be achieved with the installation of seals in bottom blocks, coolant tubes in permanent side reflector (PSR), and core restraint devices; while the temperature distribution along fuel block height was comparable with the case when coolant outlet temperature was 850°C.

1.5.2 Literatures Related to Gas Turbine Modular Helium Reactor

Gas Turbine Modular Helium Reactor (GT-MHR) which is the gas turbine cycle developed to be coupled to Modular Helium Reactor (MHR) to form a new generating system. Therefore, the MHR was selected as the reference reactor for CFD analyses for reactor design. Tak et al [31] carried out a three-dimensional computational fluid dynamics analysis by using a commercial code CFX 11 to investigate the detailed temperature behaviors within the fuel assembly of a prismatic VHTR. A one-twelfth part of the fuel assembly and bypass gap were modeled in their simulations. The bypass gap width was kept at 1 mm and a uniform axial power profile was assumed in reference calculation. The standard k-ε turbulence model with scalable wall function was applied to main coolant flow, and bypass flow through the gaps was assumed to be laminar in the case of reference gap size.

A nominal flow rate which produces an average coolant outlet temperature of 950°C obtained from one-dimensional calculations by assuming the same pressure drop across entire height of the reactor core including top and bottom reflector blocks was set in reference simulation. The exit temperature of bypass flow was comparable to the average coolant exit temperature meant that bypass flow contributed effectively to the cooling of heat generated in fuel compacts. Larger gap sizes, expected to be increased during the life time of fuel blocks, resulted in higher maximum fuel temperature and lower bypass flow exit temperature. Finally, the variations of radial power profile which cannot be analyzed by the unit cell model were considered.

Sato et al [32] and Johnson and Sato [33] conducted three-dimensional CFD calculations of a typical prismatic VHTR to better understand bypass flow and establish an evaluation method for the reactor core using the commercial CFD code FLUENT. Same as previous work by Tak et al, the MHR was selected as the reference reactor for calculations. The effects of several factors; which include inter-column gap-width, turbulence model, axial heat generation profile and geometry change from irradiation-induced shrinkage in graphite block region; in a one-twelfth sector of a fuel column were considered. Simulations showed that bypass flow provided a significant cooling effect on the prismatic block. The maximum fuel temperature and coolant outlet temperature increased with an increase in bypass gap width. Also, the presence of bypass flow caused a large lateral temperature gradient in the block and dramatically increased the variation in coolant outlet temperatures. Tung et al [34] continued the work on bypass flow in the VHTR by including effects of graphite surface roughness using STAR-CCM+ software. Their results indicated that the maximum fuel and helium temperatures increased with increasing of graphite surface roughness.

1.5.3 Literatures Related to Nuclear Hydrogen Development and Demonstration

In Korea, the facility for measuring bypass flow fraction in prismatic core model was designed and setup by Yoon et al [35]. Air flow experiment and CFD analysis using CFX 10 code were carried out employing unit cell concept with various gap sizes and combinations of blocks. It was found that bypass flow fraction increased with increasing of bypass gap width and with decreasing of the number of fuel block in the unit cell arranged in experiments, and is independent of inlet mass flow rate if flow regime in

coolant channels and bypass gaps were turbulent. Yoon et al [36], [37] continued their preceding experiment by including multi-block effects and crossflow phenomena. CFX 12 code was validated by a comparison with experimental result and its reliability was confirmed.

Kim and Lim [38] investigated the influence of gap distributions on bypass flow and hot spot in a prismatic VHTR core. Gap distributions were calculated based on neutron fluence and temperature distribution obtained from one-sixth core model analysis. Their study showed that core restraint mechanisms preventing outward movement of graphite blocks reduced bypass gap size which resulted in decreasing of maximum fuel temperature higher than 100°C compared to the case without them.

1.5.4 Summary of Literature Review

To review research works related to bypass flow in VHTR core in short, all literatures in the preceding section are categorized by their related VHTR projects, features, and chronological orders; and are summarized in Table 1.

Table 1 Summary of literature review

Researchers	Year	Feature	Description	Approach
Literatures at the Beginning Period				
H. G. Olson et al [17]	1982	Crossflow & Bypass Flow	Temperature fluctuation troubleshooting	Practical Operation
H. G. Groehn [18]	1980	Crossflow	Effects of crossflow on coolant channel flows	Experiment
H. G. Groehn [19]	1982			
Literatures Related to HTTR				
H. Kaburaki & T. Takizuka [21]	1985	Crossflow & Permeation	Devise flow model from experimental data	Experiment & Mathematical Model
H. Kaburaki & T. Takizuka [22]	1987	Crossflow	Flow network model based on experiment	Experiment & Mathematical Model
H. Kaburaki & T. Takizuka [23]	1990	Crossflow	Empirical equations based on experimental and numerical results	Experiment & Mathematical Model
H. Kaburaki & T. Takizuka [24]	1987	Seal Mechanism	Pressure loss coefficient factor evaluation for plate seal mechanism	Experiment
H. Kaburaki & T. Takizuka [25]	1988	Seal Mechanism	Pressure loss coefficient factor evaluation for v-shaped seal mechanism	Experiment
S. Maruyama et al [26]	1987	Thermal/Hydraulic Characteristics	Single-channel thermal/hydraulic tests	Experiment & Mathematical Model
S. Maruyama et al [27]	1987	Thermal/Hydraulic Characteristics	Multi-channel thermal/hydraulic tests	Experiment & Mathematical Model
S. Maruyama et al [16]	1993	Thermal/Hydraulic Characteristics	Evaluate hot spot factors for thermal/hydraulic design	Numerical Calculation (FLOWNET, TEMDIM)
S. Maruyama et al [28]	1994	Thermal/Hydraulic Characteristics	Describe thermal/hydraulic core design	Numerical Calculation (FLOWNET, TEMDIM)

Table 1 continued

Researchers	Year	Feature	Description	Approach
E. Takada et al [29]	2004	Thermal/Hydraulic Characteristics	Re-evaluate of thermal/hydraulic design conditions	Numerical Calculation (FLOWNET, TEMDIM) & Operational Data
M. Nakano et al [30]	2008	Thermal/Hydraulic Characteristics	Enable 950°C of coolant outlet temperature	Numerical Simulation (ANSYS 10)
Literatures Related to GT-MHR				
N.-I. Tak et al [31]	2008	Thermal/Hydraulic Characteristics & Bypass	CFD analysis with the conditions that unit cell model cannot be used	Numerical Simulation (CFX 11)
H. Sato et al [32] R. W. Johnson & H. Sato [33]	2010 2012	Thermal/Hydraulic Characteristics & Bypass	CFD analysis with effects of several factors	Numerical Simulation (FLUENT 6.3.26)
Y. H. Tung et al [34]	2011	Thermal/Hydraulic Characteristics & Bypass	Surface roughness effects on thermal/hydraulic of bypass flow	Numerical Simulation (STAR-CCM+ 5.02.009)
Literatures Related to NHDD				
S. J. Yoon et al [35]	2007	Bypass Flow	Investigation of bypass flow fraction in prismatic core model	Experiment & Numerical Simulation (CFX 10)
S. J. Yoon et al [36] S. J. Yoon et al [37]	2011 2012	Crossflow & Bypass Flow	Including multi-block effects and crossflow to prismatic core model	Experiment & Numerical Simulation (CFX 12)
M.-H. Kim & H.-S. Lim	2011	Thermal/Hydraulic Characteristics & Bypass	Evaluation of influence of gap distributions on bypass flow and hot spot in VHTR core	Numerical Calculation (GAMMA+)

1.6 Objectives of Present Study

Bypass flow in the prismatic block core of VHTR is not a designed feature. It can be occurred from the combination of several causes such as tolerance in manufacturing process of fuel element blocks, inexactness of fuel element block installations, and change of graphite block geometry over the lifetime of reactor. Bypass flow can affect the occurrence of hot spots in the core and induce larger temperature variation of coolant jets exiting the core into lower plenum (hot streaking). Also, it can cause strong temperature variation in graphite block which affects structural integrity and fuel neutronics. Therefore, bypass flow is a very important issue to be studied extensively before the emerging of commercial construction of the Generation IV reactor.

It can be seen from the preceding section that the current status of research on thermal and hydraulic core flow of VHTR is very far from completion because many topics related to bypass flow still are not investigated. Because of the important of bypass flow mentioned in a large number of publications, present study will be the starting of bypass flow characteristic investigation using small-scale model that will fulfill understandings of bypass flow with the following features:-

(1) Flows through bypass gaps formed by three hexagonal prismatic blocks which is a part of multi-hole type core model (Figure 7) are studied experimentally using air and water as working fluids.

(2) Flow fraction in each flow passage, pressure drop, Reynolds number and velocity field obtained from three-dimensional CFD simulations performed by STAR-CCM+ are compared with those obtained from experiments to validate the code.

(3) Bypass flow simulations using p-cymene as working fluid are performed to provide the results to be compared with those obtained from bypass flow experiments including flow fields that will be obtained from Particle Image Velocimetry (PIV) technique.

(4) The data reduction procedures of flows through bypass gap for the existing small-scale model are demonstrated.

(5) All experiences from present study are summarized as guidelines for the design of new facility for bypass flow experiments and performing of bypass flow simulations in the future.

Figure 7. Prismatic block models

2. BYPASS FLOW EXPERIMENTS

An open loop for air flow experiments is built and two air flow experiments are conducted with bypass gap width of 6.1, 4.4, and 2.7 mm. In the first experiment, method of flow measurement and calculation are examined by balancing volume flow rate of all flow passages. It is found that all procedures are reliable but the result shows very high bypass flow fractions which are much higher than actual situation. Another air flow experiment is conducted after removing all flow meters connected from prismatic blocks and it yields lower bypass flow fractions as expected.

To attain higher Reynolds number of flow through coolant channels and bypass gaps, liquid loop is constructed for water flow experiments. All components of the loop are selected such that they can be run with p-cymene when Particle Image Velocimetry (PIV) is employed. Bypass gap widths in air flow and water flow experiments are same but only bypass gap width of 4.0 mm can be prepared for p-cymene flow experiments because method of varying bypass gap width in air flow and water flow experiments cannot be applied due to material integrity problem with p-cymene.

Bypass flow fractions from water flow experiments lie between bypass flow fractions from two air flow experiments, i.e. larger than air flow experiments without flow meter but smaller than air flow experiments with flow meters. Reynolds numbers of flow through coolant channels and bypass gaps in all experiments are much higher than their values in actual operation but they can be improved by adjusting flow resistance in each flow passage incorporated with changing porosity of the blocks.

2.1 Construction of the Loops

Two working fluids are used in present study to obtain experimental results for data reduction. Air and water are common and their experiments are not hard to be conducted. P-cymene which is chosen to be matched with refractive index of acrylic of prismatic block models is skipped but the liquid loop is prepared for it. Details of the loops for air and water flow experiments are explained in the following sub-sections.

2.1.1 Open Loop for Air Flow Experiments

Schematic diagram of open loop for air flow experiments is shown in Figure 8. Air is supplied through 8-inch-diameter pipe passes the location where inlet air velocity is measured and the location of upstream pressure tap. Air reaches flow straighteners installed just before the test section where three prismatic block models are stacked within it to form bypass gaps.

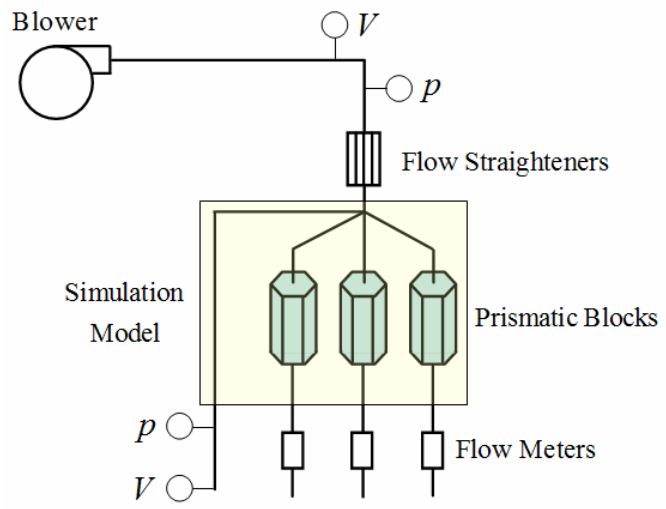

Figure 8. Schematic diagram of open loop for air flow experiments

Flow rate from each prismatic block is measured by 4000-Series flow meters in the first set of air flow experiments. All flow meters are removed for another set of air flow experiments. For the latter case, flow rate in each block can be found from one-third of difference between total flow rate and flow rate through bypass gaps under the assumption that air flows through each block equally.

Dash lines in Figure 8 indicate flow passages connected from bypass gaps to avoid confusions that all flow passages are intersected. Downstream pressure tap is located just after the test section. Outlet air velocity from bypass gap is measured by VelociCalc air velocity meter as for inlet air velocity at exit of 3-inch-diameter pipe connected from the end of the test section.

2.1.2 Liquid Loop for Water Flow Experiments

Schematic diagram of liquid loop for water flow experiments is shown in Figure 9. Water stored in an open container is supplied into the loop constructed from 3-inch-diameter pipes. Total flow rate is measured by turbine flow meter placed at location before water reaches flow straighteners and the test section. Flow rate from each block is measured by three identical flow meters. Bypass flow rate is calculated from difference between total flow rate and sum of flow rates from all blocks.

Two valves are installed to switch the operation to be cleaning working fluid if necessary. Drainage valve and ventilate valve (not shown in Figure 9) are attached just before and after the test section of the loop to help in draining process of water from the loop. A pressure gage is attached to the loop to roughly recheck pressure drop read from pressure transducers located just before and after the test section.

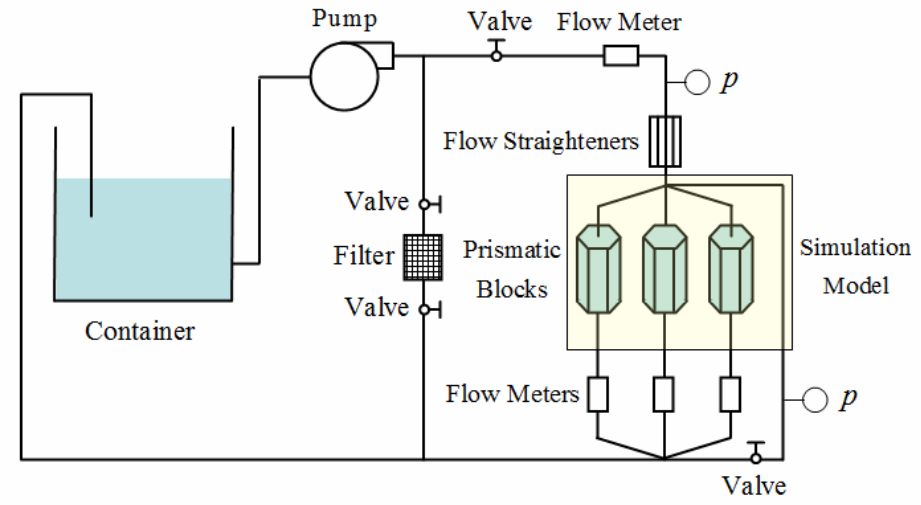

Figure 9. Schematic diagram of liquid loop for water flow experiments

2.2 Geometry of Prismatic Block and Bypass Gap

Geometry of prismatic block used in all experiments with important parameters, i.e., block height (h), block side length (l), and coolant channel diameter (d), is shown in Figure 10. The values of these parameters are h = 152 mm, l = 50 mm, and d = 12.7 mm. Because the number of coolant channels (n) and their locations are less important, they can be different from the prototype of VHTR core while block porosity (defined later) still be the same because of difficulties arisen in model fabricating process.

When a number of prismatic blocks are arranged to form a part of single-layer blocks in reactor core, additional parameters to be considered are number of columns stacked in test section (N_C), seal mechanism and its configuration, bypass gap width (b) and its configuration, and side gap width (s). If more than one block layers are under consideration, crossflow gap width (c) and its configuration and number of block layers (N_L) should be included. Because present study has only three prismatic blocks stacked

in the test section as single-layer blocks and has no seal mechanism, only bypass gap width (*b*) and side gap width (*s*) are parameters to be considered under the condition that they have rectangular shape and exactly lie in vertical planes. The top view of block combination is shown in Figure 11.

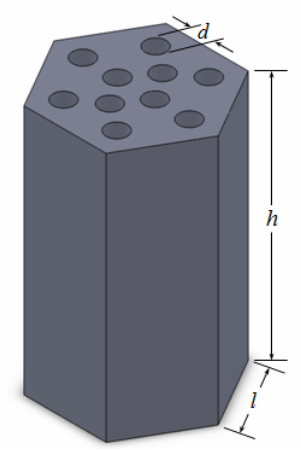

Figure 10. Geometry of prismatic block

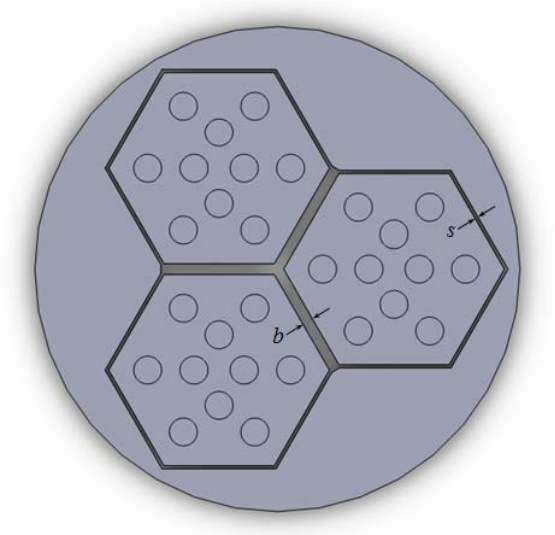

Figure 11. Top view of block combination

All side gaps are sealed by inserting plastic plates to fill them and then sealing the top of side gaps with silicone. Therefore, only bypass gap width (*b*) is varied to three values as shown in Figure 12 in air flow and water flow experiments. Only one bypass gap width shown in Figure 13 is prepared for p-cymene flow experiments because the method of side gap sealing is changed and the method of bypass gap varying cannot be applied due to material integrity problem between plastic plates and p-cymene.

Bypass gap widths mentioned above are taken from the top of the blocks where they are prevented from tilting by three obstructions shown in Figure 14. However, the blocks can be slightly tilted at the bottom of the blocks because the obstructions cannot be inserted due to the existence of collector results in narrower bypass gap width there.

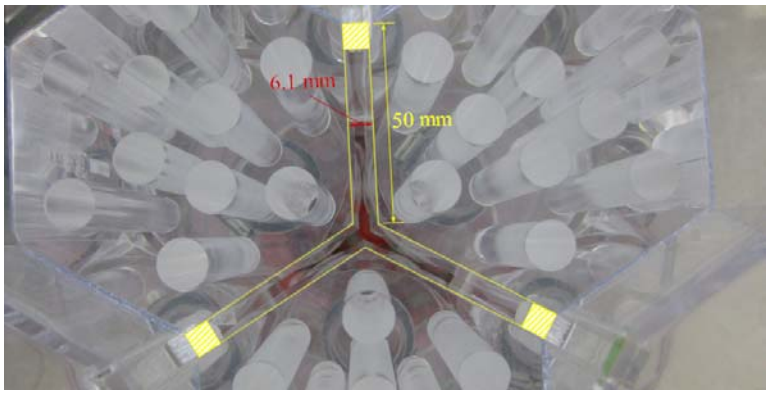

(a) 6.1 mm

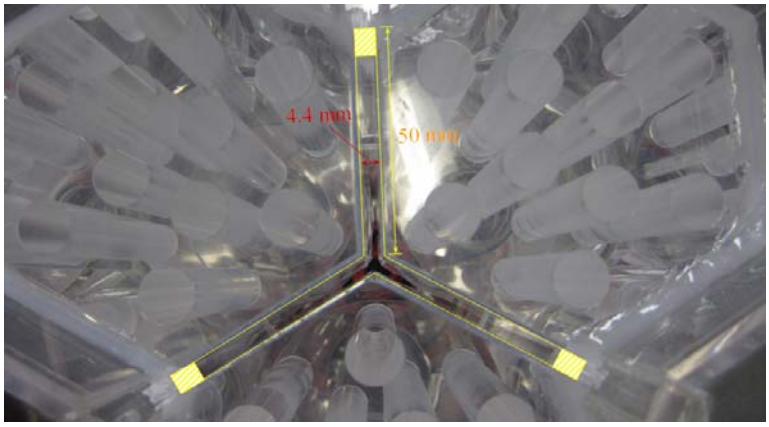

(b) 4.4 mm

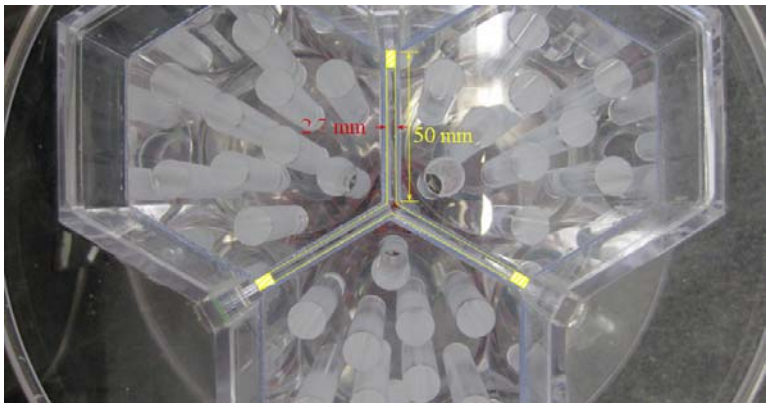

(c) 2.7 mm

Figure 12. Bypass gap widths in air and water flow experiments

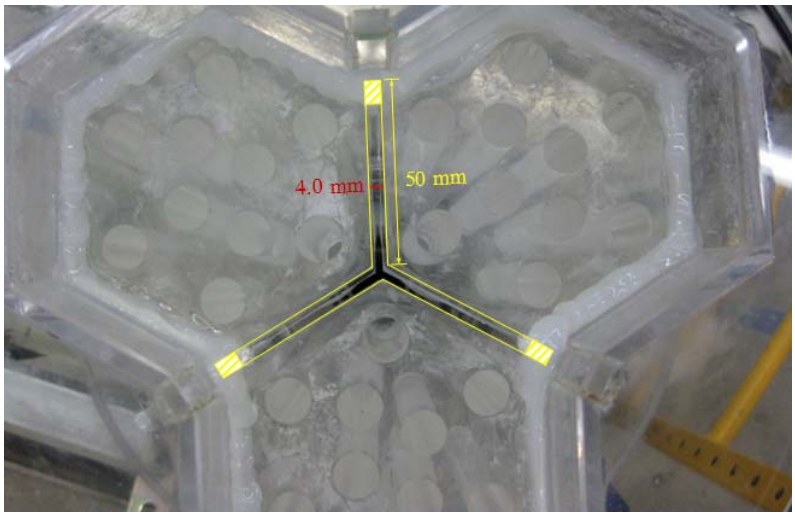

Figure 13. Bypass gap width of 4.0 mm prepared for p-cymene flow experiments

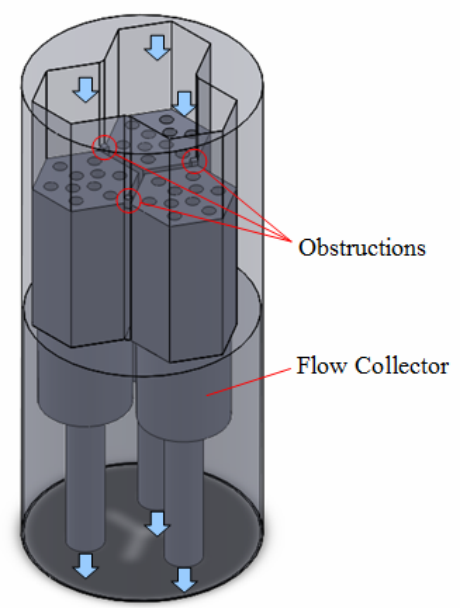

Figure 14. Test section for bypass flow experiments

2.3 Air Flow Experiments

An air flow experiment is conducted for bypass gap width of 6.1, 4.4, and 2.7 mm to examine method of flow measurement and calculation by taking (1) volume flow

rate, temperature, and pressure of air flow through each block, (2) pressure drop between locations before flow straighteners and after the exit of bypass gap, Δp, (3) maximum speed of air flow in *8-inch-diameter pipe* before flow straighteners, V_{Inlet}, and (4) maximum speed of air flow at the exit of *3-inch-diameter pipe* connected from bypass flow passage, V_{Bypass}.

Air flow rate through each prismatic block can be calculated from equation (2.1) by employing the data in part (1). Although volume flow rates taken in part (1) have unit of l/min, they can be converted into m^3/s or cfm and used in any plot.

Air Flow Rate from 4000 Series Flow Meter [39]:

$$Volumetric\ Flow = Std\ Flow\left[\frac{273.15+T_m}{273.15+21.11}\right]\left(\frac{101.3}{p_m}\right) \tag{2.1}$$

where *Std Flow* is standard flow rated read from the 4000 Series flow meter,

T_m is air temperature measured in unit of degree Celsius,

p_m is absolute pressure measured in unit of kPa.

Pressure drop in part (2) is measured in mm-H_2O and converted into kPa for plotting with bypass gap Reynolds number. The maximum flow speeds in part (3) and (4) are taken at the centerline of the pipes and used in flow rate estimations for inlet flow and bypass flow. Reynolds numbers (*Re*) in part (3) and (4) are calculated from average velocity (V) and hydraulic diameter (d_h) of each flow passage with air density (ρ) and dynamic viscosity (μ) of 1.18415 kg/m^3 and 1.85508×10^{-5} Pa·s, respectively.

Reynolds Number: $$Re = \frac{\rho V d_h}{\mu} \tag{2.2}$$

Firstly, turbulent flow regime is assumed with an initial guess of index of power law (n) for velocity profile of fully-developed turbulent flow in pipe. Then, Reynolds number is calculated from average velocity (V) in equation (2.4). Under the assumption of smooth pipe (roughness, e, equals to 0), the index of power law is found iteratively from the relation proposed by Nunner in equation (2.5) with the aid of Darcy friction factor (f) from Colebrook equation.

After the iteration is ended, average velocity of flow in each pipe is known and air flow rate can be estimated. If Reynolds number obtained from previous assumption is lower than 2300, laminar velocity profile should be assumed. Because low speed air flow can be treated as incompressible flow, conservation of mass can be examined by comparing inlet air flow rate from part (3) with sum of air flow rates from part (1) and (4) which is considered as exit flow. Air flow rates from this experiment are summarized in Table 2 to Table 4. Experimental data and details of calculations are in Appendix A.

Laminar Flow in Pipe: $$\frac{u}{u_{\max}} = 1 - \left(\frac{r}{R}\right)^2, \frac{V}{u_{\max}} = \frac{1}{2} \tag{2.3}$$

Turbulent Flow in Pipe: $$\frac{u}{u_{\max}} = \left(1 - \frac{r}{R}\right)^{1/n}, \frac{V}{u_{\max}} = \frac{2n^2}{(n+1)(2n+1)} \tag{2.4}$$

Relation Proposed by Nunner [40]: $$\frac{1}{n} = \sqrt{f} \tag{2.5}$$

Colebrook Equation [41]: $$\frac{1}{\sqrt{f}} = -2\log_{10}\left(\frac{e/d_h}{3.7} + \frac{2.51}{Re\sqrt{f}}\right) \tag{2.6}$$

Table 2 Flow rates in air flow experiments with flow meters with 6.1-mm bypass gap

No.	Block 1 (cfm)	Block 2 (cfm)	Block 3 (cfm)	Bypass (cfm)	Exit Flow (cfm)	Inlet Flow (cfm)	Difference (%)
1	1.122	1.147	1.087	12.476	15.832	17.922	13.20
	7.09%	*7.24%*	*6.87%*	*78.81%*	*100%*	-	-
2	2.528	2.588	2.412	27.112	34.640	36.293	4.77
	7.30%	*7.47%*	*6.96%*	*78.27%*	*100%*	-	-
3	4.049	4.107	3.809	41.774	53.738	54.917	2.19
	7.54%	*7.64%*	*7.09%*	*77.73%*	*100%*	-	-
4	5.707	5.703	5.236	56.219	72.866	73.006	0.19
	7.83%	*7.83%*	*7.19%*	*77.15%*	*100%*	-	-
5	7.377	7.390	6.666	71.713	93.146	91.654	-1.60
	7.92%	*7.93%*	*7.16%*	*76.99%*	*100%*	-	-
6	9.181	9.219	8.237	86.942	113.579	112.096	-1.31
	8.08%	*8.12%*	*7.25%*	*76.55%*	*100%*	-	-

Table 3 Flow rates in air flow experiments with flow meters with 4.4-mm bypass gap

No.	Block 1 (cfm)	Block 2 (cfm)	Block 3 (cfm)	Bypass (cfm)	Exit Flow (cfm)	Inlet Flow (cfm)	Difference (%)
1	1.137	1.159	1.104	8.480	11.879	13.185	10.99
	9.57%	*9.75%*	*9.29%*	*71.39%*	*100%*	-	-
2	2.561	2.607	2.455	17.667	25.291	27.011	6.80
	10.13%	*10.31%*	*9.71%*	*69.85%*	*100%*	-	-
3	4.107	4.132	3.868	27.750	39.857	39.922	0.16
	10.30%	*10.37%*	*9.71%*	*69.62%*	*100%*	-	-
4	5.784	5.735	5.325	37.475	54.319	53.733	-1.08
	10.65%	*10.56%*	*9.80%*	*68.99%*	*100%*	-	-
5	7.449	7.413	6.788	46.123	67.773	67.625	-0.22
	10.99%	*10.94%*	*10.02%*	*68.05%*	*100%*	-	-
6	9.263	9.235	8.394	53.550	80.442	80.729	0.36
	11.52%	*11.48%*	*10.43%*	*66.57%*	*100%*	-	-

Table 4 Flow rates in air flow experiments with flow meters with 2.7-mm bypass gap

No.	Block 1 (cfm)	Block 2 (cfm)	Block 3 (cfm)	Bypass (cfm)	Exit Flow (cfm)	Inlet Flow (cfm)	Difference (%)
1	1.162	1.184	1.125	1.870	5.341	4.189	-21.57
	21.75%	*22.17%*	*21.06%*	*35.02%*	*100%*	-	-
2	2.597	2.661	2.498	6.318	14.074	14.160	0.61
	18.45%	*18.90%*	*17.75%*	*44.89%*	*100%*	-	-
3	4.145	4.195	3.918	10.119	22.378	21.379	-4.46
	18.52%	*18.75%*	*17.51%*	*45.22%*	*100%*	-	-
4	5.824	5.831	5.365	14.272	31.291	28.117	-10.14
	18.61%	*18.63%*	*17.14%*	*45.61%*	*100%*	-	-
5	7.491	7.482	6.821	18.955	40.749	35.903	-11.89
	18.38%	*18.36%*	*16.74%*	*46.52%*	*100%*	-	-
6	9.279	9.279	8.413	23.490	50.461	42.833	-15.12
	18.39%	*18.39%*	*16.67%*	*46.55%*	*100%*	-	-

In above tables, negative difference in flow rate indicates that inlet flow rate is less than sum of outlet flow rates. At the minimum flow rate of experiments with bypass gap of 6.1 and 4.4 mm, differences in inlet and exit flow rate are larger than 10% because Reynolds numbers of flows in 8-inch diameter inlet pipe are in the transition regime and velocity profile cannot be accurately represented by the power law. For all remaining data of these two cases, balancing of inlet and exit air flow rate is excellent with differences less than 5%. This indicates that flow rate measurement and calculation methods are reliable for these two gap widths.

For air flow experiments with bypass gap of 2.7 mm, almost all of flow rate differences are negative with magnitude greater than 10%. It can be seen in Appendix A that all Reynolds numbers of air flow in 8-inch diameter inlet pipe are less than 10000 (but still higher than 2300 except for the minimum flow rate). Flow rate calculations in

this range of Reynolds number yield flow rates lower than the values as they should be. Therefore, this flow rate calculation method can be applied efficiently when Reynolds number is more than 10000, i.e., air flow rates in 8-inch and 3-inch diameter pipe are greater than 50 cfm and 20 cfm, respectively. Furthermore, actual bypass flow fractions should be higher than those presented for bypass gap of 2.7 mm.

Because bypass flow fractions from all gap widths are higher than a range from 10% to 25% mentioned in INEEL/EXT-05-02581 report [42], air flow experiment is modified by removing all flow meters connected from prismatic blocks and bypass flow fraction is expected to be decreased because pressure losses of flow through prismatic blocks is reduced. Air flow rates from new experiments summarized in Table 5 to Table 7 are kept in the same format as in previous set of air flow experiments for comparison. Experimental data and details of calculations are in Appendix A.

Table 5 Flow rates in air flow experiments without flow meter with 6.1-mm bypass gap

No.	Block 1 (cfm)	Block 2 (cfm)	Block 3 (cfm)	Bypass (cfm)	Exit Flow (cfm)	Inlet Flow (cfm)	Difference (%)
1	7.679	7.679	7.679	11.139	-	34.175	-
	22.47%	*22.47%*	*22.47%*	*32.59%*	-	*100%*	-
2	14.539	14.539	14.539	24.404	-	68.022	-
	21.37%	*21.37%*	*21.37%*	*35.88%*	-	*100%*	-
3	20.873	20.873	20.873	38.277	-	100.895	-
	20.69%	*20.69%*	*20.69%*	*37.94%*	-	*100%*	-
4	29.208	29.208	29.208	51.771	-	139.396	-
	20.95%	*20.95%*	*20.95%*	*37.14%*	-	*100%*	-
5	38.014	38.014	38.014	66.433	-	180.473	-
	21.06%	*21.06%*	*21.06%*	*36.81%*	-	*100%*	-
6	46.699	46.699	46.699	80.583	-	220.681	-
	21.16%	*21.16%*	*21.16%*	*36.52%*	-	*100%*	-

Table 6 Flow rates in air flow experiments without flow meter with 4.4-mm bypass gap

No.	Block 1 (cfm)	Block 2 (cfm)	Block 3 (cfm)	Bypass (cfm)	Exit Flow (cfm)	Inlet Flow (cfm)	Difference (%)
1	7.691	7.691	7.691	7.706	-	30.780	-
	24.99%	*24.99%*	*24.99%*	*25.03%*	-	*100%*	-
2	15.606	15.606	15.606	16.279	-	63.097	-
	24.73%	*24.73%*	*24.73%*	*25.80%*	-	*100%*	-
3	22.654	22.654	22.654	25.917	-	93.877	-
	24.13%	*24.13%*	*24.13%*	*27.61%*	-	*100%*	-
4	30.319	30.319	30.319	35.348	-	126.306	-
	24.00%	*24.00%*	*24.00%*	*27.99%*	-	*100%*	-
5	38.763	38.763	38.763	43.705	-	159.995	-
	24.23%	*24.23%*	*24.23%*	*27.32%*	-	*100%*	-
6	47.380	47.380	47.380	51.045	-	193.185	-
	24.53%	*24.53%*	*24.53%*	*26.42%*	-	*100%*	-

Table 7 Flow rates in air flow experiments without flow meter with 2.7-mm bypass gap

No.	Block 1 (cfm)	Block 2 (cfm)	Block 3 (cfm)	Bypass (cfm)	Exit Flow (cfm)	Inlet Flow (cfm)	Difference (%)
1	8.043	8.043	8.043	1.497	-	25.625	-
	31.39%	*31.39%*	*31.39%*	*5.84%*	-	*100%*	-
2	15.758	15.758	15.758	5.613	-	52.886	-
	29.80%	*29.80%*	*29.80%*	*10.61%*	-	*100%*	-
3	23.071	23.071	23.071	9.240	-	78.453	-
	29.41%	*29.41%*	*29.41%*	*11.78%*	-	*100%*	-
4	30.190	30.190	30.190	13.064	-	103.634	-
	29.13%	*29.13%*	*29.13%*	*12.61%*	-	*100%*	-
5	38.271	38.271	38.271	17.462	-	132.273	-
	28.93%	*28.93%*	*28.93%*	*13.20%*	-	*100%*	-
6	46.399	46.399	46.399	21.663	-	160.861	-
	28.84%	*28.84%*	*28.84%*	*13.47%*	-	*100%*	-

In air flow experiments without flow meter with bypass gap of 6.1 and 4.4 mm, experimental data at the minimum flow rate should be omitted based on the conclusion drawn in previous experiments because air flow rate in 8-inch diameter inlet pipe is less than 50 cfm and air flow rate in 3-inch diameter pipe connected from bypass flow passage is less than 20 cfm simultaneously. For all remaining data of these two gap widths, Reynolds numbers of flows in these two pipes are in the range that air flow rates can be estimated accurately.

In air flow experiments without flow meter with bypass gap of 2.7 mm, almost all of bypass flow rates calculated from flow in 3-inch diameter pipe are lower than 20 cfm. Based on the inlet flow rates in previous experiments with the same bypass gap width which are over 10% smaller than the actual values as they should be, actual bypass flow rates can be (at least) 10% higher than the values shown in Table 7 in the same range of Reynolds number. Or in other words, actual bypass flow fractions for No.3 to No.6 in this case may be up to 15% of total flow rate.

To distinguish the difference between two sets of air flow experiments, physical quantities measured in air flow experiments are summarized in Table 8.

Table 8 Physical quantities measured in air flow experiments

Flow Passage	Air Flow Experiments with Flow Meters	Air Flow Experiments without Flow Meter
Block 1	Flow Rate	-
Block 2	Flow Rate	-
Block 3	Flow Rate	-
Bypass	Velocity	Velocity
Total Flow (Inlet)	Velocity	Velocity

Bypass flow fractions from both air flow experiments are plotted versus total flow rate in Figure 15. It can be concluded that bypass flow fractions are almost constant and are not depended on total flow rate except for the data at the minimum flow rate in the cases with 2.7-mm bypass gap. This is because air flows through bypass gap in these cases are in laminar flow regime as seen from two lowest points in Figure 17.

Average velocity of flow through coolant channels and bypass gaps can be found by dividing flow rate through each flow passage with corresponding flow area. Then, Reynolds numbers based on hydraulic diameter (d_h) of flow through coolant channels (Re_C) and bypass gaps (Re_B, approximated by flow between two parallel plates) can be calculated and plotted in Figure 16 and Figure 17. It is obvious in Figure 17 that Re_B at the minimum flow rate of both air flow experiments are lower than 1400 which is critical Reynolds number of flow between two parallel plates.

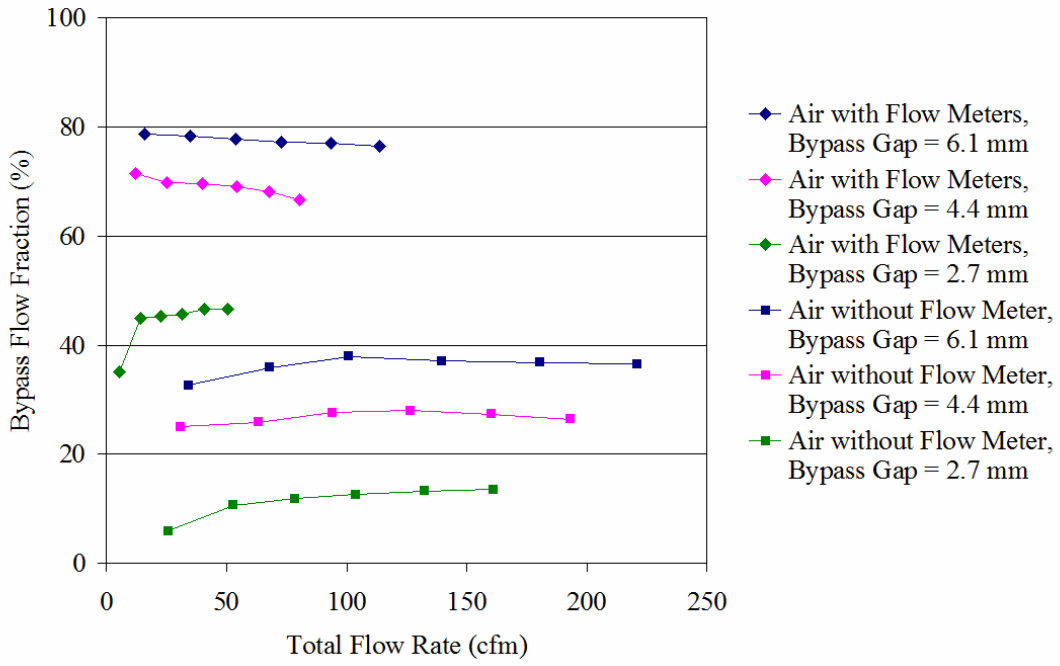

Figure 15. Bypass flow fractions from air flow experiments

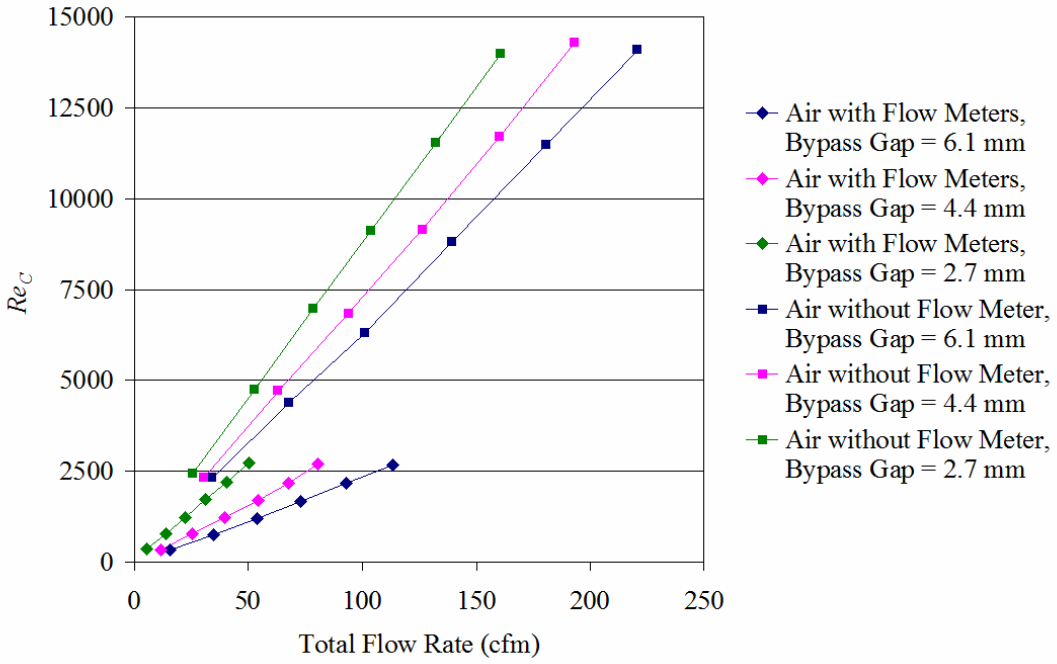

Figure 16. Coolant channel Reynolds numbers from air flow experiments

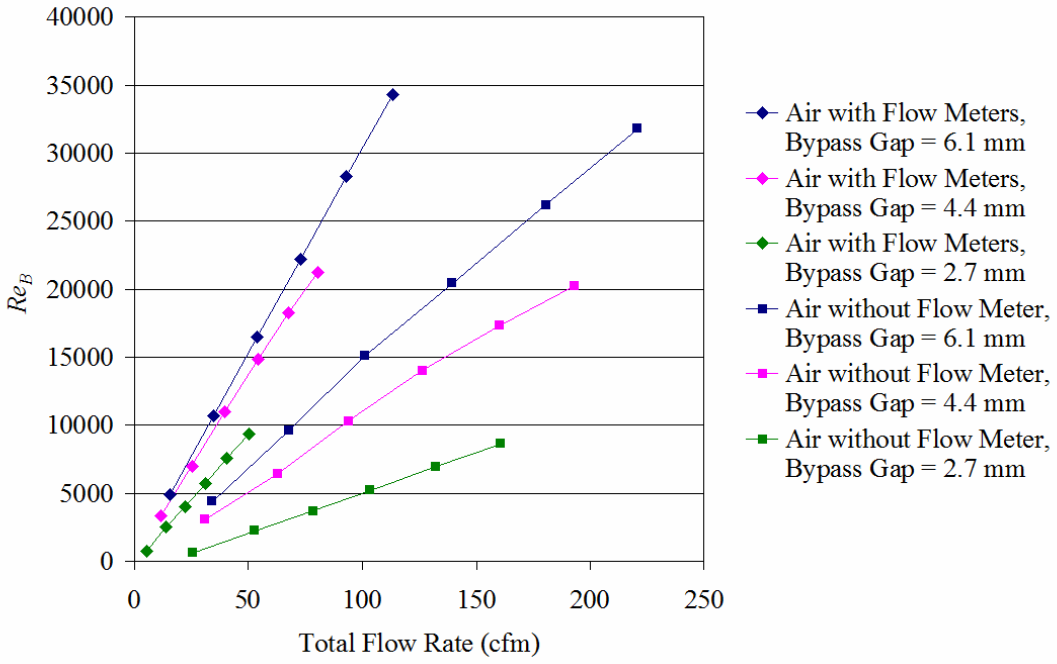

Figure 17. Bypass gap Reynolds numbers from air flow experiments

From Figure 16, the maximum Reynolds number of air flow through coolant channels (Re_C) that can be attained in both air flow experiments (about 2700 and 14000 for experiments with and without flow meter, respectively) is not depended on bypass gap width. It should be depended on block porosity (area ratio of coolant channel and cross section of the block) but this cannot be confirmed in present study because block porosity must be kept at the same value of fuel elements used in nuclear reactors. This means that air flow rates through prismatic block are not affected by bypass gap width and total flow rate increases when bypass gap becomes wider. Because bypass flow fraction in air flow experiments without flow meter decreases as expected, flow rate through each prismatic block increases and results in higher Reynolds number of flow through coolant channel (Re_C).

From Figure 17, the maximum Reynolds number of air flow through bypass gaps (Re_B) is strongly depended on bypass gap width. Their values for bypass gap of 6.1, 4.4 and 2.7 mm are about 34000, 21000 and 9000; respectively.

Although Re_C and Re_B in both air flow experiments still are very far from the desired values at 35000 and 2500, it can be suggested for bypass flow study in the future that flow fraction can be controlled by adjusting flow resistance in each flow passage. As seen from the experimental results, removing of flow meter reduces flow resistance of flow passage connected from each prismatic block results in higher flow rate through coolant channels and lower bypass flow fraction. However the desired values of Re_C and Re_B may not only be attained simultaneously by adjusting flow resistance in each flow passage, but also incorporated with changing of block porosity.

As closure of air flow experiments, pressure drops of flow through bypass gaps (i.e. pressure drop taken from the experiment subtracted by pressure drop due to flow straighteners estimated from data in Appendix B) are plotted versus Reynolds numbers of flow through bypass gaps (Re_B) in Figure 18. The plot shows that pressure drop at the same value of Re_B increases with decreasing of bypass gap width in both experiments and it does not depend on downstream condition of the blocks that is the existence of flow meters in present study. Therefore, Re_B can be used in data reduction representation but the relationship between pressure loss coefficient and Re_B will be plotted later.

It should be noted that no error bar appears in all plots in this dissertation because sample standard deviations of physical quantities in all data sets are only few percents and they are not clearly observable if they are included in the plots.

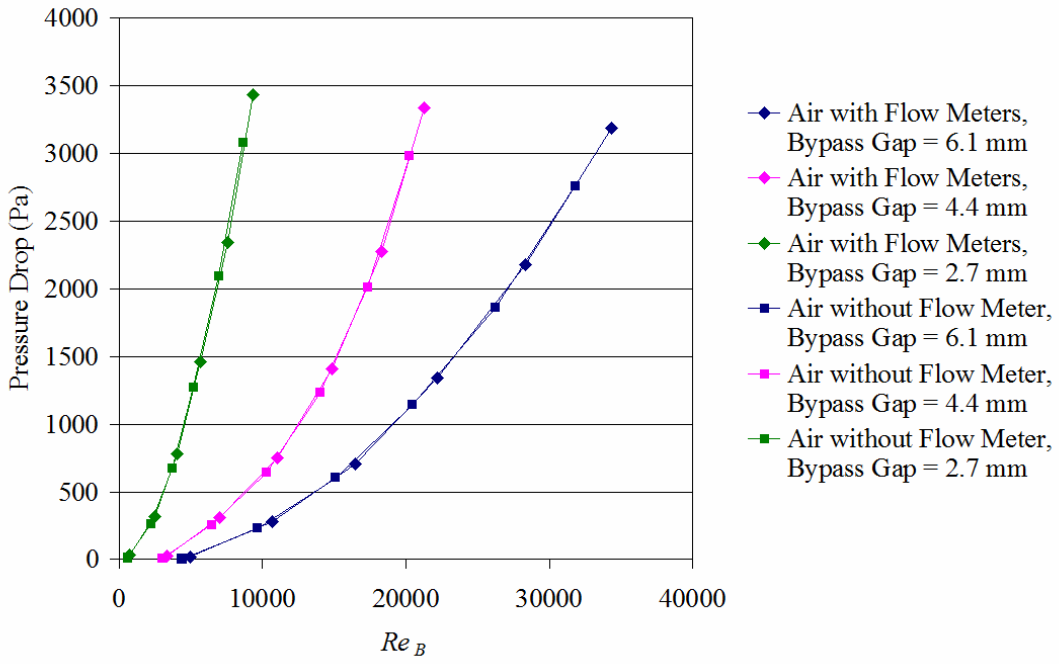

Figure 18. Pressure drops of flow through bypass gaps from air flow experiments

2.4 Water Flow Experiments

To attain higher Reynolds numbers of flow through coolant channels and bypass gaps, water flow experiments are conducted. All bypass gap widths are same as in air flow experiments because all obstructions used in preventing tilting of prismatic blocks in air flow experiments are placed in test section again. The difference in measurement method between water flow and air flow experiments is that there are flow meters for each block and total flow only. Therefore, bypass flow rate can be calculated from difference between total flow rate and sum of flow rates through all blocks. Quantities measured in each flow passage in water flow experiments are compared with those in air flow experiments in Table 9. Flow rates from water flow experiments are summarized in Table 10 to Table 12 and experimental data are in Appendix A.

Table 9 Physical quantities measured in air and water flow experiments

Flow Passage	Air Flow Experiments with Flow Meters	Air Flow Experiments without Flow Meter	Water Flow Experiments
Block 1	Flow Rate	-	Flow Rate
Block 2	Flow Rate	-	Flow Rate
Block 3	Flow Rate	-	Flow Rate
Bypass	Velocity	Velocity	-
Total Flow (Inlet)	Velocity	Velocity	Flow Rate

In Figure 19, bypass flow fractions for the case with 6.1-mm bypass gap are almost constant because all blocks are pushed into contact with the walls of test section chamber easily when water flow through bypass gaps even at low flow rate. But bypass flow fractions for the cases with bypass gap width of 4.4 and 2.7 mm increase with the increasing of total flow rates because larger pressure force applies on the walls of the

blocks that form bypass gaps pushes the blocks from slightly tilted positions to more favorable positions in vertical planes which results in higher bypass flow fractions.

Table 10 Flow rates in water flow experiments with 6.1-mm bypass gap

No.	Total Flow (gpm)	Block 1 (gpm)	Block 2 (gpm)	Block 3 (gpm)	Bypass (gpm)
1	92.0	12.00	13.20	13.30	53.50
	100%	*13.04%*	*14.35%*	*14.46%*	*58.79%*
2	117.0	15.50	16.64	16.94	67.92
	100%	*13.25%*	*14.22%*	*14.48%*	*58.05%*
3	141.6	18.90	20.10	20.60	82.00
	100%	*13.35%*	*14.19%*	*14.55%*	*57.91%*
4	165.8	22.20	23.42	24.20	95.98
	100%	*13.39%*	*14.13%*	*14.63%*	*57.89%*
5	189.4	25.52	26.76	27.70	109.42
	100%	*13.47%*	*14.13%*	*14.63%*	*57.77%*
6	215.0	28.68	30.02	31.14	125.16
	100%	*13.34%*	*13.96%*	*14.48%*	*58.21%*

Table 11 Flow rates in water flow experiments with 4.4-mm bypass gap

No.	Total Flow (gpm)	Block 1 (gpm)	Block 2 (gpm)	Block 3 (gpm)	Bypass (gpm)
1	55.6	11.48	11.60	11.94	20.58
	100%	*20.65%*	*20.86%*	*21.47%*	*37.01%*
2	76.2	15.40	15.50	15.90	29.40
	100%	*20.21%*	*20.34%*	*20.87%*	*38.58%*
3	98.6	19.20	19.38	19.90	40.12
	100%	*19.47%*	*19.66%*	*20.18%*	*40.69%*
4	122.6	22.98	23.20	23.90	52.52
	100%	*18.74%*	*18.92%*	*19.49%*	*42.84%*
5	146.4	26.58	26.84	27.76	65.22
	100%	*18.16*	*18.33%*	*18.96%*	*44.55%*

Table 12 Flow rates in water flow experiments with 2.7-mm bypass gap

No.	Total Flow (gpm)	Block 1 (gpm)	Block 2 (gpm)	Block 3 (gpm)	Bypass (gpm)
1	50.6	12.24	12.36	12.76	13.24
	100%	*24.19%*	*24.43%*	*25.22%*	*26.17%*
2	69.6	16.40	16.58	17.10	19.52
	100%	*23.56%*	*23.82%*	*24.57%*	*28.05%*
3	91.6	20.58	20.78	21.58	28.66
	100%	*22.47%*	*22.69%*	*23.56%*	*31.29%*
4	114.4	24.66	24.80	25.86	39.08
	100%	*21.56%*	*21.68%*	*22.60%*	*34.16%*

In Figure 20 and Figure 21, Reynolds numbers of flow through coolant channels (Re_C) and bypass gaps (Re_B) for 6.1-mm bypass gap form straight lines that pass through the origin. Bypass flow fractions for two remaining gap widths deviated from their ideal (constant) values at low flow rate as seen in Figure 19 causes the plots of Re_C and Re_B deviate slightly up and down from straight lines that pass through the origin. Water density and viscosity used in computations are 997.561 kg/m^3 and 8.8871×10^{-4} Pa$\cdot$s.

Although the maximum Re_C about 20000 for all bypass gap widths and the maximum Re_B up to 120000 depends on bypass gap width are very far from the desired values as in air flow experiments, it is confirmed that higher Reynolds number can be attained with the use of liquid as working fluid.

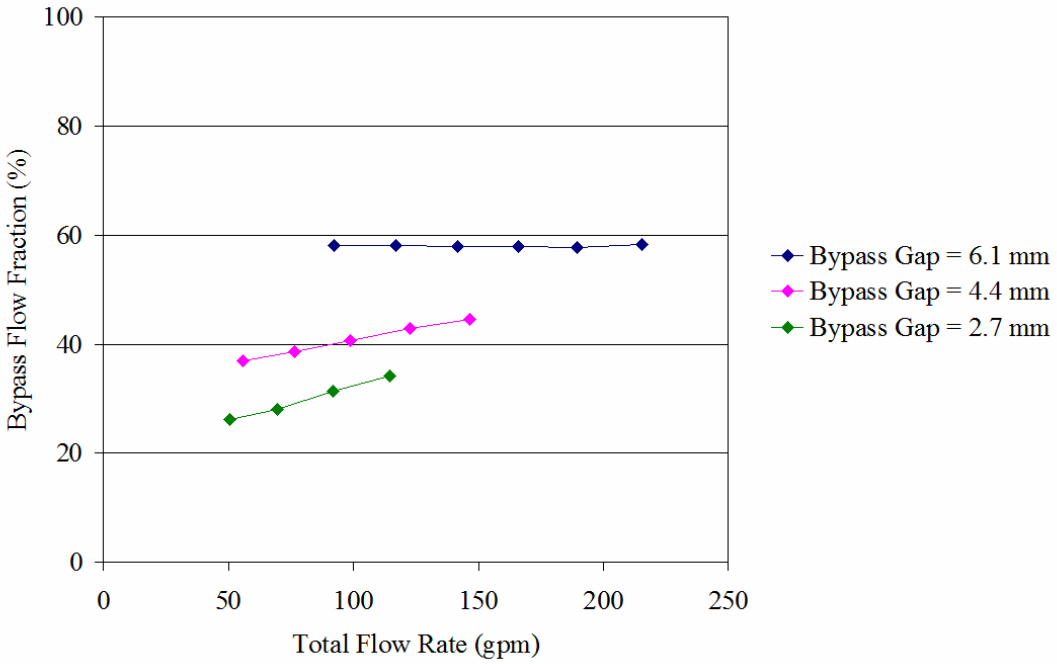

Figure 19. Bypass flow fractions from water flow experiments

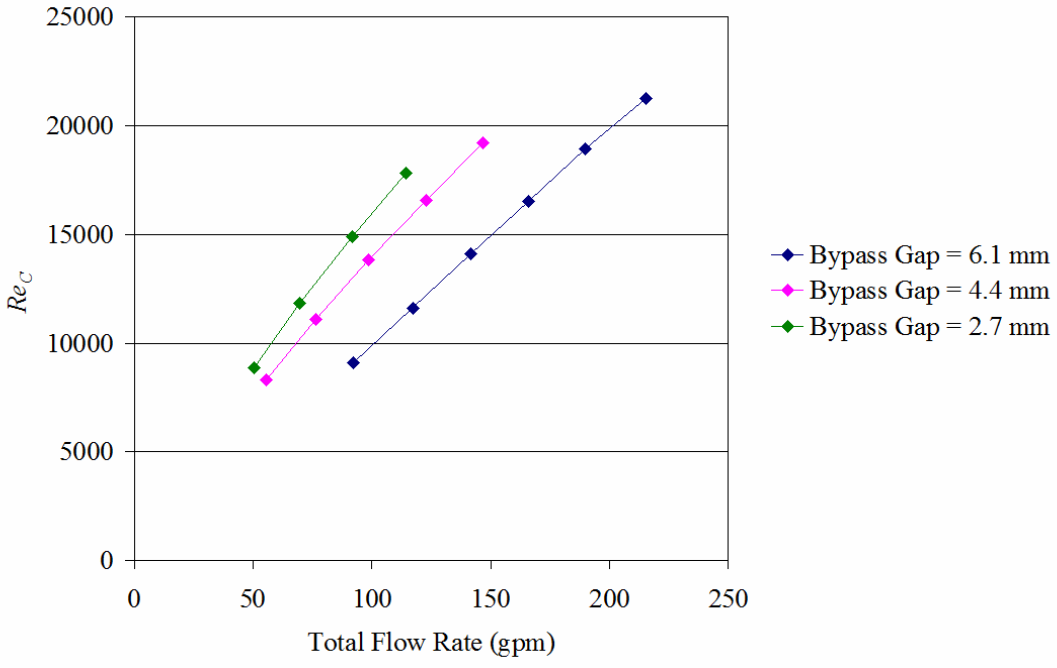

Figure 20. Coolant channel Reynolds numbers from water flow experiments

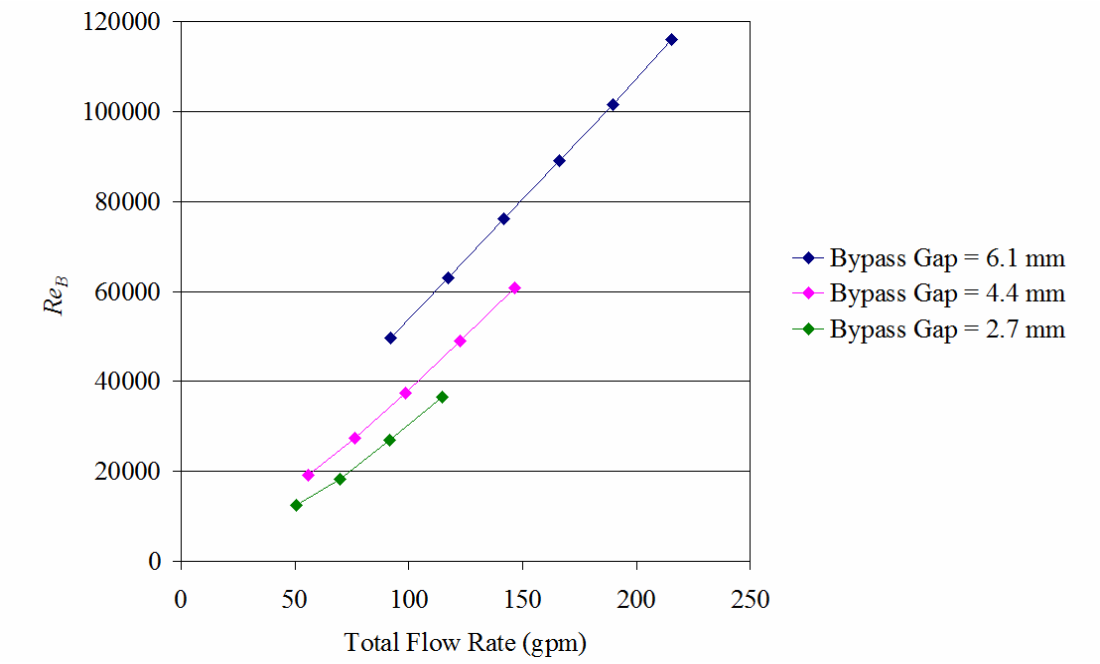

Figure 21. Bypass gap Reynolds numbers from water flow experiments

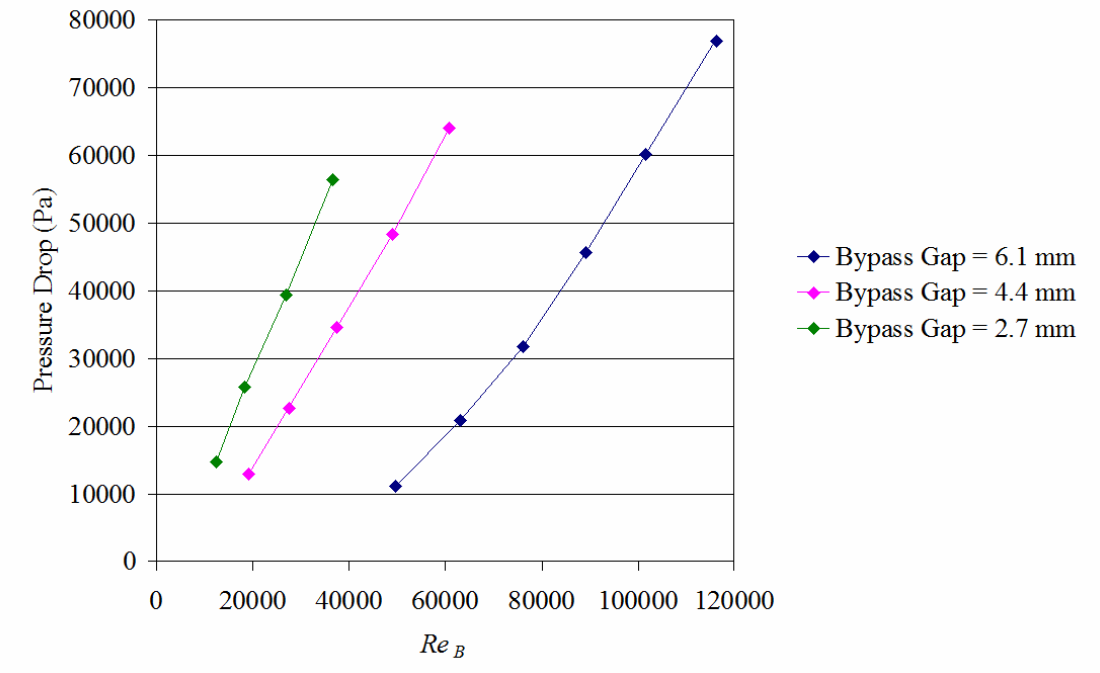

Figure 22. Pressure drops of flow through bypass gaps from water flow experiments

Pressure drops of flow through bypass gaps are plotted versus Reynolds number of flow through bypass gaps (Re_B) in Figure 22. It should be noted that the values of pressure drop in Figure 22 are subtracted by estimated pressure drop of flow through flow straighteners (Appendix B) and added by hydrostatic pressure of 42.5-inch of water which is difference in height of two locations where pressure transducers are placed to remove hydrostatic effects from measured pressure drops. There is no need to add hydrostatic pressure for pressure drop obtained from air flow experiments because air density is very small and 42.5-inch of air contributes about 10 Pa in error.

Actually, all curves of pressure drop in Figure 22 should be convex like those in Figure 18 but pressure drops for 4.4-mm and 2.7-mm bypass gap width are higher than the values as they should be at low Re_B (low flow rate). Therefore, their curves tend to be straight lines. This is because the method of bypass gap width varying makes all blocks tilt slightly closer to others at bottom portion which causes higher pressure drop especially at lower flow rate. Higher pressure force that pushes all blocks to favorable positions at higher flow rate results in higher bypass flow fraction. Although present study has some imperfections in experimental setup, it can be expected that bypass flow fraction for these two bypass gap widths will converge to constant values after block arrangement method is improved.

2.5 Conclusion

Bypass flow fraction depends on bypass gap width in all experiments. In air flow experiments, effects of changing of downstream condition of the blocks on bypass flow fraction are examined by attaching and removing flow meters. At the lowest flow rate in air flow experiments with 2.7-mm bypass gap, bypass flow fraction drops significantly from others because flow through bypass gaps is laminar. Also, flow in pipe connected from bypass gaps where the maximum speeds were taken is laminar which lead to inaccurate flow rate estimation. Therefore, if possible, measuring flow rate directly should be employed instead of estimating flow rate from maximum speeds which is accurate when Reynolds number of flow in that pipe is greater than 10000.

Bypass flow fractions in water flow experiments with 4.4- and 2.7-mm bypass gap increase with flow rate because the method of varying bypass gap width make the blocks slightly tilted and higher flow rate causes high pressure force that pushes the blocks to more favorable positions which result in higher bypass flow fractions.

Coolant channel Reynolds number (Re_C) and bypass gap Reynolds number (Re_B) vary with bypass flow fraction. Re_C increases and Re_B decreases when bypass flow fraction decreases with bypass gap width or vice versa. Pressure drop of flow through bypass gaps seem to be depended on both bypass gap width and downstream condition of the blocks when it is plotted with total flow rate. But its plot with Re_B from air flow experiments indicates that there is no effect from downstream condition of the blocks. Because other upstream and downstream conditions of flow passages are not changed, this conclusion is limited for downstream condition of the blocks only.

Bypass flow fractions from all bypass flow experiments are plotted together in Figure 23. The most representative curve is from air flow experiments with flow meters. It can be expected that bypass flow fraction should nonlinearly decrease with bypass gap width when it is large enough to let turbulent flow regime exists within bypass gaps and linearly decrease bypass gap width when flow regime in bypass gaps is laminar. For air flow experiments without flow meter, the trend of bypass flow fraction seems to follow the expectation but it is not obvious on this plotting scale. Unexpected trend of bypass flow fraction in water flow experiments indicates the problem in block arrangement and gap varying method which should be improved in the future.

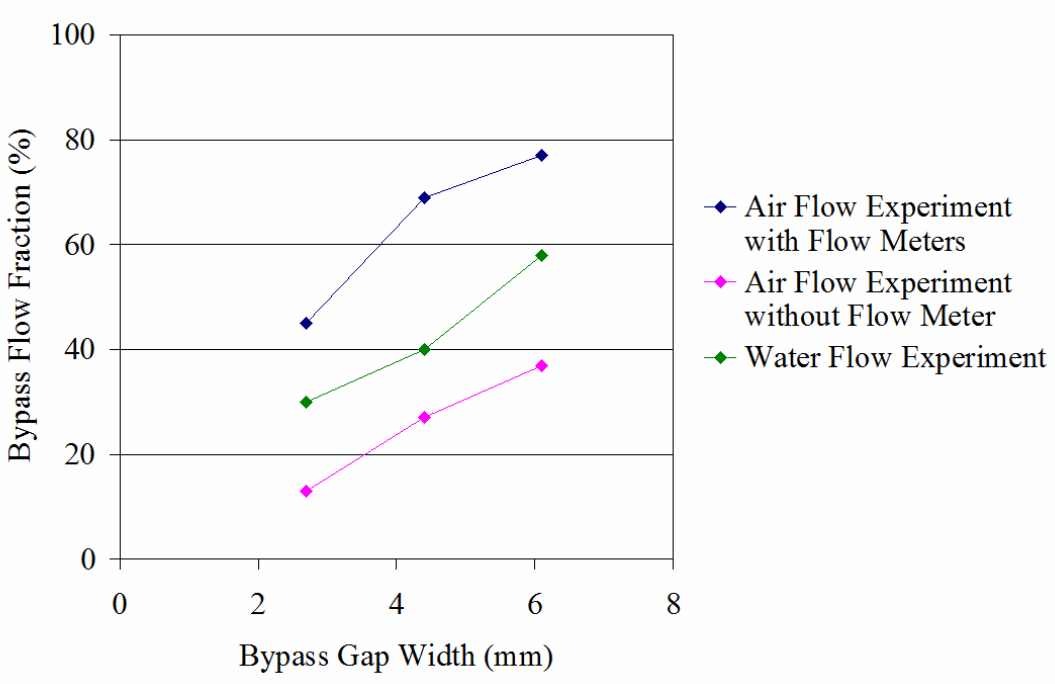

Figure 23. Bypass flow fraction as function of bypass gap width

3. BYPASS FLOW SIMULATIONS

Bypass flow simulations for bypass gap width of 6.1, 4.4 and 2.7 mm with air and water, and 4.0 mm with p-cymene as working fluid are performed by using STAR-CCM+ software. Total flow rates set in air flow simulations are from 33 to 133 cfm and 50 to 200 cfm to enable the comparison with air flow experiments with and without flow meter, respectively. For water and p-cymene, total flow rates set in bypass flow simulations are from 50 to 200 gpm.

Firstly, validation exercises are used in finding appropriate parameters for bypass flow simulations (Appendix C). Then, three models are constructed with bypass gap width of 6.1 mm and are analyzed based on 1.0-mm base size at 100 cfm for air and 100 gpm for water using realizable k-epsilon model with two-layer all *y*+ wall treatment. The models are adjusted at the exit of flow passage connected from prismatic blocks until they yield same bypass flow fractions as obtained from two sets of air flow experiments and one set of water flow experiments. Other six models are constructed for bypass gap width of 4.4 and 2.7 mm, three models for each bypass gap width, for air and water flow simulations. Grid independence of these models is examined using the same turbulence model to suggest appropriate cell base size set in bypass flow simulations.

Nine models are employed in bypass flow simulations by using realizable k-epsilon model with two-layer all *y*+ wall treatment, SST (Menter) k-omega model with all *y*+ wall treatment and Reynolds stress model with linear pressure strain and high *y*+ wall treatment. The model used in p-cymene flow simulations is the same model as used

in water flow simulations but bypass gap width is changed to be 4.0 mm because only this gap can be prepared in p-cymene flow experiments. Implicit unsteady scheme is employed with timestep of 1.0 second for all bypass flow simulations and is stopped at physical time of 100 seconds. Simulations with 1.0-mm cell base size constructed from trimmer meshes are compared with experimental data in Section 2 for all cases.

3.1 Computational Models for Bypass Flow Simulations

Models for bypass flow simulation are constructed in SolidWorks software (Figure 24) and then imported to STAR-CCM+ software to construct simulation meshes. Two features in the models that should be mentioned are:-

(1) Three obstructions used in preventing tilting of the blocks in all experiments are included in the models.

(2) At the exit of flow passage connected from each block (1.215-inch diameter), the model is modified to be sudden contraction and its inner diameter is adjusted until bypass flow fraction from simulation is matched with bypass flow fraction from each experiment. Changing of pressure specified at the exit of flow passage connected from each block (without making sudden contraction) is another approach for matching bypass flow fractions from simulations and experiments. But pressure drops are very sensitive both in bypass flow experiments and simulations. This means that if two pressures specified at the exit of this flow passage in two simulations are few percents different, they may yield very close bypass flow fractions and cause uncertainty in pressure drop comparison. Therefore, it should be preferred to change flow passage geometry instead of changing exit pressure in matching bypass flow fraction.

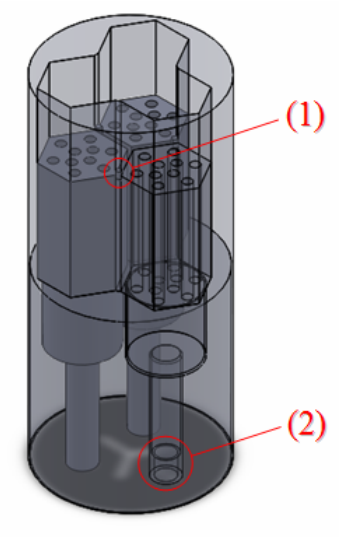

Figure 24. Model for constructing meshes used in bypass flow simulations

Based on the models with two features mentioned above, the models meshed with base size of 1.0 mm for 6.1-mm bypass gap width are analyzed by using STAR-CCM+ software. Implicit unsteady scheme is employed with timestep of 1.0 second and the simulations are stopped at physical time of 100 seconds. Inner diameters of sudden contraction that can match bypass flow fractions from simulations and experiments are summarized in Table 13. Numbers of cells constructed based on other 4 base sizes are summarized in the same table. These models are prepared for grid independence study which is conducted at *100 cfm* for air flow simulations and *100 gpm* for water flow simulations. Seven layers of prism-layered cell with stretching ratio of 1.35 are employed with constant absolute thickness of 0.4 mm (see Appendix C). This makes the number of total cells of the models with base size of 2.0 mm and 1.5 mm (Table 13) are comparable because the number of cells in prism layers of these models is a large portion compared with the number of total cells in the models.

Table 13 Number of cells in bypass flow simulations with 6.1-mm bypass gap

Sudden Contraction Inner Diameter (in.)	Bypass Flow Experiment	Number of Cells in the Model				
		Base Size 2.0 mm	Base Size 1.5 mm	Base Size 1.0 mm	Base Size 0.8 mm	Base Size 0.6 mm
0.416	Air flow with flow meters	3148913	3528872	8242374	13309746	25313224
0.994	Air flow without flow meter	3143118	3507328	8279213	13361739	25415772
0.646	Water flow	3131320	3497691	8258042	13328416	25351035

After using experimental data from the cases with 6.1-mm bypass gap width for calibrating model geometry, bypass gap width of the models is changed to 4.4 and 2.7 mm for air and water simulations. Additionally, bypass gap width of the model used in water flow simulations is changed to 4.0 mm for p-cymene simulations. Numbers of cells constructed based on 1.0-mm base size for all cases are summarized in Table 14. Boundary conditions and example of meshes on five plane sections of the computational models are shown in Figure 25 and Figure 26, respectively.

Table 14 Number of cells in bypass flow simulations with base size of 1.0 mm

Sudden Contraction Inner Diameter (in.)	Bypass Flow Experiment	Number of Cells in the Model			
		Bypass 6.1 mm	Bypass 4.4 mm	Bypass 2.7 mm	Bypass 4.0 mm
0.416	Air flow with flow meters	8242374	8223638	8166896	-
0.994	Air flow without flow meter	8279213	8254962	8200343	-
0.646	Water flow	8258042	8236520	8182639	-
0.646	P-cymene flow	-	-	-	8236635

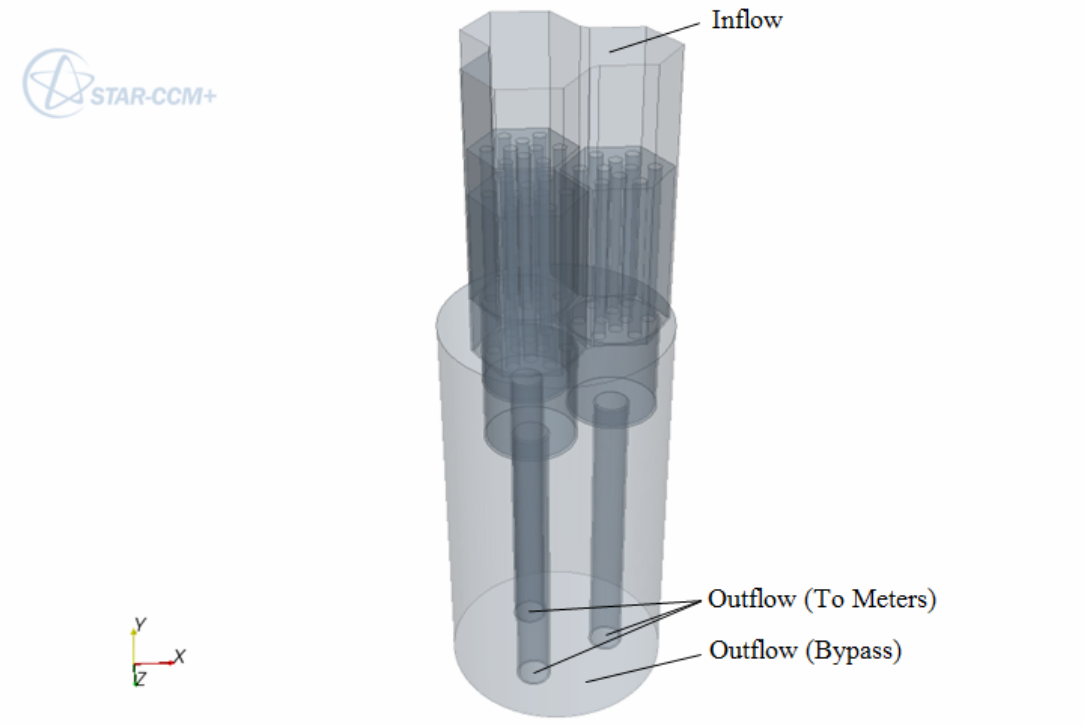

Figure 25. Boundary conditions of computational models

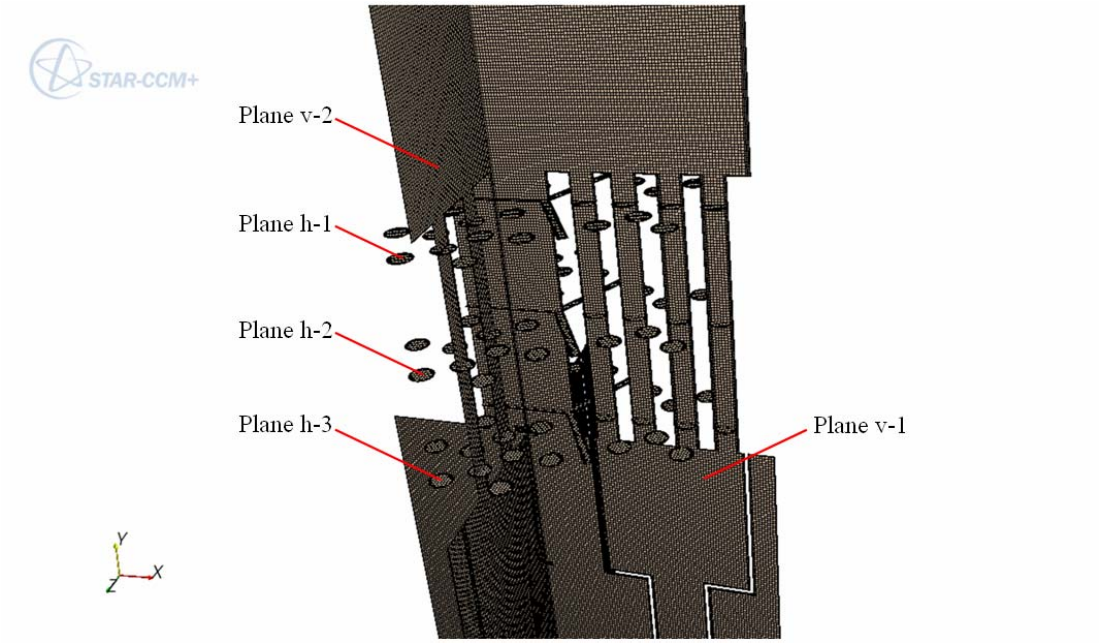

Figure 26. Example of mesh on five plane sections

3.2 Grid Independence Study

All bypass flow models, except the model for p-cymene simulations, are used in grid independence study. The selected flow rates are *100 cfm* for air flow simulations (0.416- and 0.994-in. sudden contraction inner diameter) and *100 gpm* for water flow simulations (0.664-in. sudden contraction inner diameter) and the turbulence model employed is realizable k-epsilon model with two-layer all *y+* wall treatment. Five base sizes are used in trimmer mesh constructions where the absolute thickness of prism layer is fixed at 0.4 mm. For 2.7-mm bypass gap width, only base size of 1.0, 0.8 and 0.6 mm can be used because the narrowest region (bypass gap) cannot be captured properly when using base size of 2.0 and 1.5 mm. Implicit unsteady scheme with timestep of 1.0 second is employed for all simulations and they are stopped at 100 seconds. Bypass flow fractions and pressure drops from simulations corresponding to each experiment are summarized in Table 15 to Table 17 and are plotted in Figure 27 to Figure 29. Because the height of models for all bypass flow simulations are 25 inches, pressure drops in Table 17 and Figure 29 are added by hydrostatic pressure of water to remove its effects.

Table 15 Bypass flow fraction and pressure drop from bypass flow simulation using k-epsilon model corresponding to air flow experiments with flow meters

Base Size	Bypass Gap 6.1 mm		Bypass Gap 4.4 mm		Bypass Gap 2.7 mm	
(mm)	Bypass (%)	Δp (Pa)	Bypass (%)	Δp (Pa)	Bypass (%)	Δp (Pa)
2.0	76.67	1868.99	69.41	3222.38	-	-
1.5	76.70	1837.13	69.53	3165.12	-	-
1.0	77.40	1750.89	70.38	3021.26	57.34	6204.10
0.8	77.43	1735.67	70.35	2963.07	57.50	6146.38
0.6	77.09	1714.02	69.98	2916.77	57.05	6051.41

Table 16 Bypass flow fraction and pressure drop from bypass flow simulation using k-epsilon model corresponding to air flow experiments without flow meter

Base Size	Bypass Gap 6.1 mm		Bypass Gap 4.4 mm		Bypass Gap 2.7 mm	
	Bypass	Δp	Bypass	Δp	Bypass	Δp
(mm)	(%)	(Pa)	(%)	(Pa)	(%)	(Pa)
2.0	36.85	437.85	28.36	562.51	-	-
1.5	36.98	433.99	28.42	557.77	-	-
1.0	37.07	408.81	28.60	526.00	17.77	695.02
0.8	37.05	406.61	28.69	520.58	17.85	690.82
0.6	36.89	401.37	28.54	514.02	17.73	679.44

Table 17 Bypass flow fraction and pressure drop from bypass flow simulation using k-epsilon model corresponding to water flow experiments

Base Size	Bypass Gap 6.1 mm		Bypass Gap 4.4 mm		Bypass Gap 2.7 mm	
	Bypass	Δp	Bypass	Δp	Bypass	Δp
(mm)	(%)	(Pa)	(%)	(Pa)	(%)	(Pa)
2.0	57.68	15994.04	48.72	23700.60	-	-
1.5	58.29	15733.86	48.84	22992.94	-	-
1.0	58.29	14618.58	49.23	21730.69	35.58	29922.73
0.8	58.25	14471.06	49.24	21339.55	35.75	29861.00
0.6	58.07	14315.08	49.10	21110.58	35.40	29144.20

From above tables, all base sizes yield almost the same bypass flow fraction. This is not true for pressure drop because its values obtained from the finest and coarsest cell can be 10% different for 6.1- and 4.4-mm bypass gap width. Therefore, pressure drop should be used in specifying base size that grid independence starts.

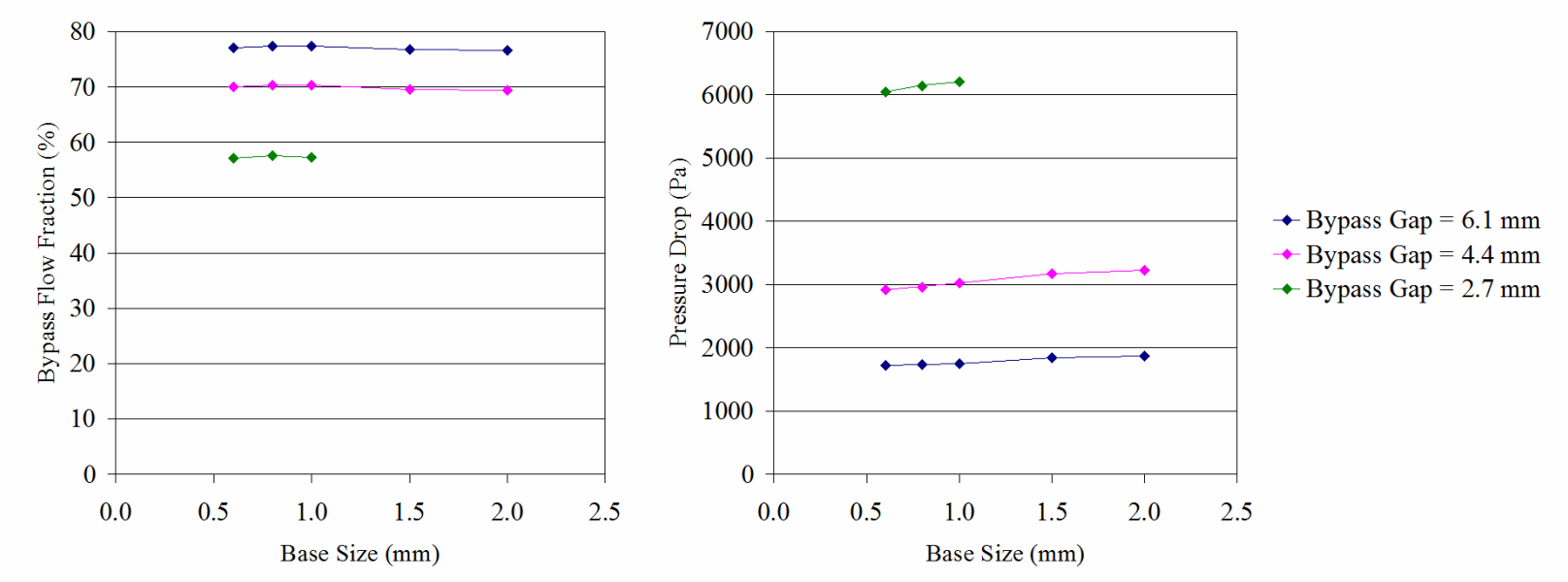

Figure 27. Bypass flow fraction and pressure drop from bypass flow simulation using k-epsilon model corresponding to air flow experiments with flow meters

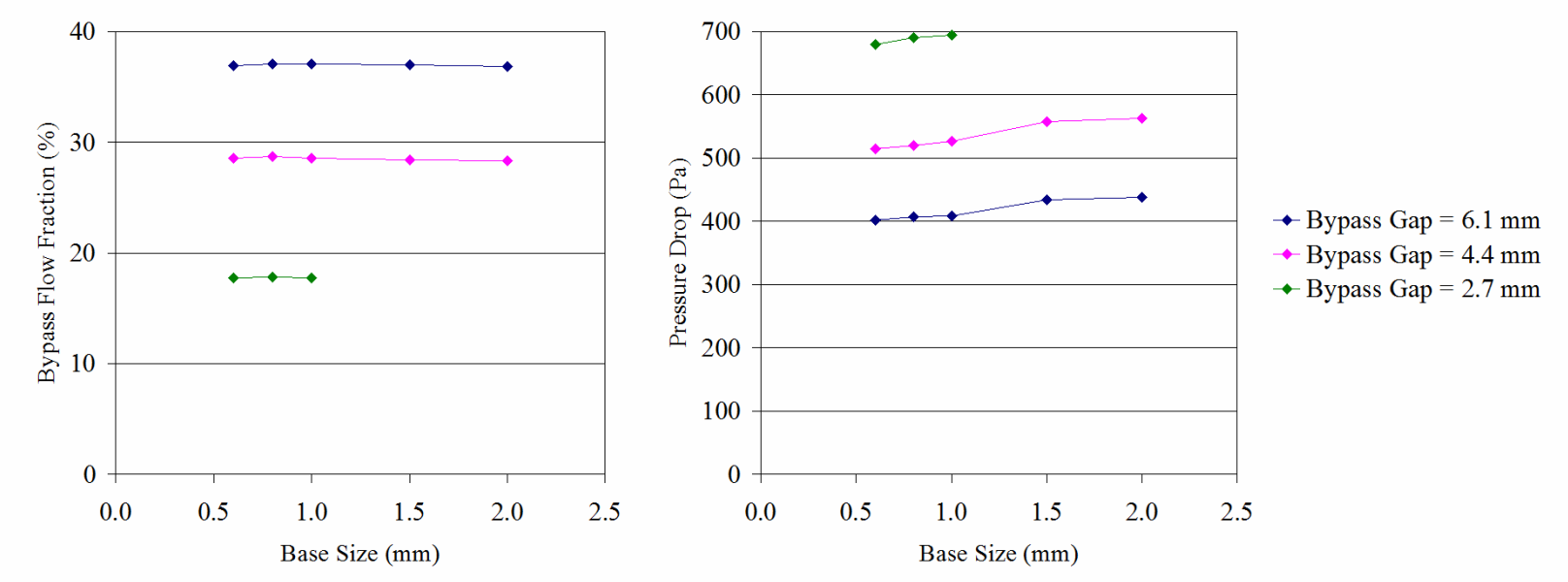

Figure 28. Bypass flow fraction and pressure drop from bypass flow simulation using k-epsilon model corresponding to air flow experiments without flow meter

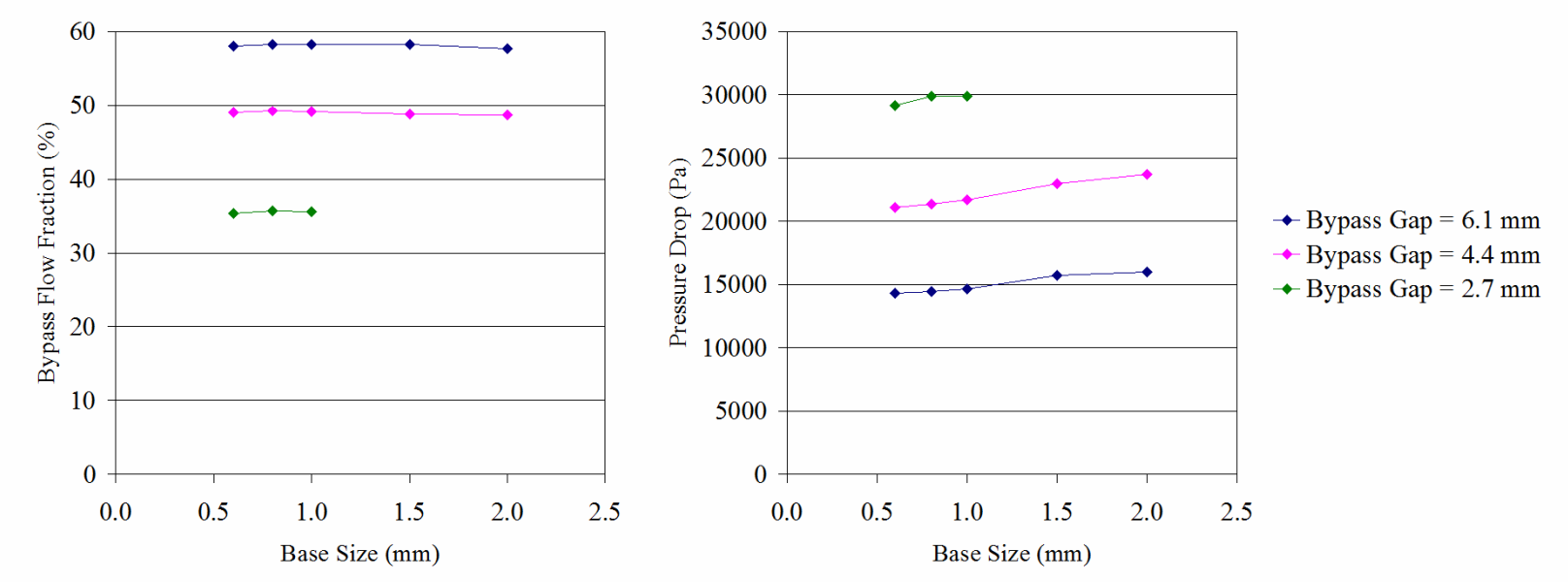

Figure 29. Bypass flow fraction and pressure drop from bypass flow simulation using k-epsilon model corresponding to water flow experiments

From pressure drops shown in Figure 27 to Figure 29, it can be said that grid independence can be observed when base size is 1.0 mm for 6.1- and 4.4-mm bypass gap width because pressure drop remarkably reduces from next larger base size and it is at most 3% smaller when base size is decreased to 0.6 mm. Based on the data from 4.4-mm bypass gap width case, the narrowest length between two walls after subtracted by absolute prism layer thickness is 3.6 mm. It may be suggested that the ratio of this length and base size should be greater than 3.5 to obtain grid independence solutions.

For 2.7-mm bypass gap width, the same observation in pressure drop as in other two bypass gap widths can be detected when base size reduces from 0.8 to 0.6 mm. The narrowest length between two walls subtracted by absolute prism layer thickness is 1.9 mm. The ratio between this length and base size about 3.17 is acceptable for obtaining grid independence solution. However, all numerical results reported in present study are from the simulations using trimmer meshed models with *base size of 1.0 mm* to keep consistency in base size for all simulations and save computational resources.

3.3 Air Flow Simulations

In air flow experiments, there are some downstream components from prismatic blocks (besides flow meters) that cannot be modeled in air flow simulations. All of them cause considerable discrepancies between the results (bypass flow fraction and pressure drop) from experiments and simulations. Although they can be indirectly compared, the procedures are cumbersome and two features are added to the computational models to remove these difficulties. The sudden contraction at the exit of flow passage connected from the block (Figure 24) is the most important one because it can contribute more

affects on bypass flow fraction and pressure drop than the existence of three obstructions which is another feature added to the models. The inner diameter of sudden contraction is adjusted until the simulation (turbulence model is realizable k-epsilon model with two-layer all *y*+ wall treatment, implicit unsteady scheme is employed with timestep of 1.0 second and stopped at 100 seconds) yields the same bypass flow fraction as obtained from the experiment with 6.1-mm bypass gap. The widest bypass gap is selected for this purpose because the effects from tilting of the blocks on experimental data are smallest compared with two remaining bypass gap widths. It can be said that this data set is used for geometry calibration and two remaining data sets are used for software validation.

In air flow experiments with flow meters, bypass flow fraction of 6.1-mm bypass gap width is about 77% at flow rate of 100 cfm as shown in Table 2. The inner diameter of sudden contraction that yields the same bypass flow fraction from air flow simulation is 0.416 inch. Sudden contraction with inner diameter of 0.994 inch yields bypass flow fraction about 37% at flow rate of 100 cfm as from air flow experiments without flow meter shown in Table 5. For convenience in referring of bypass flow simulations, all tables and plots presented after this point will be referred to the conditions in bypass flow experiments in Section 2 instead of referring to the inner diameter of sudden contraction found from geometry calibration.

Bypass flow simulations are performed by using three turbulence models which are realizable k-epsilon model with two-layer all *y*+ wall treatment, SST (Menter) k-omega model with all *y*+ wall treatment and Reynolds stress model with linear pressure strain and high *y*+ wall treatment. Bypass flow fraction, coolant channel Reynolds

number (Re_C), bypass gap Reynolds number (Re_B) and pressure drop obtained from air flow simulations using three turbulence models are plotted in Figure 30 to Figure 37 to compare with experimental data. Pressure distributions on plane v-1 (Figure 26) at flow rate of 100 cfm for 6.1-mm bypass gap width are shown in Figure 38 to Figure 40.

It is not surprised that bypass flow fractions, coolant channel Reynolds numbers (Re_C) and bypass gap Reynolds numbers (Re_B) for 6.1-mm bypass gap width in Figure 30 to Figure 35 match very well with experimental data because the data from this gap width was used in model constructions. For 4.4-mm bypass gap width, bypass flow fractions from air flow simulations in Figure 30 and Figure 31 are slightly higher than those from air flow experiments. This results in slightly lower Re_C and higher Re_B than experimental data in Figure 32 to Figure 35.

For 2.7-mm bypass gap, bypass flow fractions from air flow simulations in Figure 30 and Figure 31 are higher than those from air flow experiments. The most important source of error is that flow rate calculation through bypass gap for this case yields smaller flow rates than their actual values as mentioned in Section 2.

Another source of error is from the simulations employ selected turbulence model throughout computational domain which results in slightly *lower* flow rate through bypass gap if Re_B is in laminar or transition regime. If this source of error is removed, bypass flow fraction will be slightly larger than the values in Figure 30 and Figure 31. This can increase small discrepancy in bypass flow fractions but it may be neglected because it is very small compare with error caused by flow rate estimation in circular pipe when Reynolds number is between 3000 and 10000.

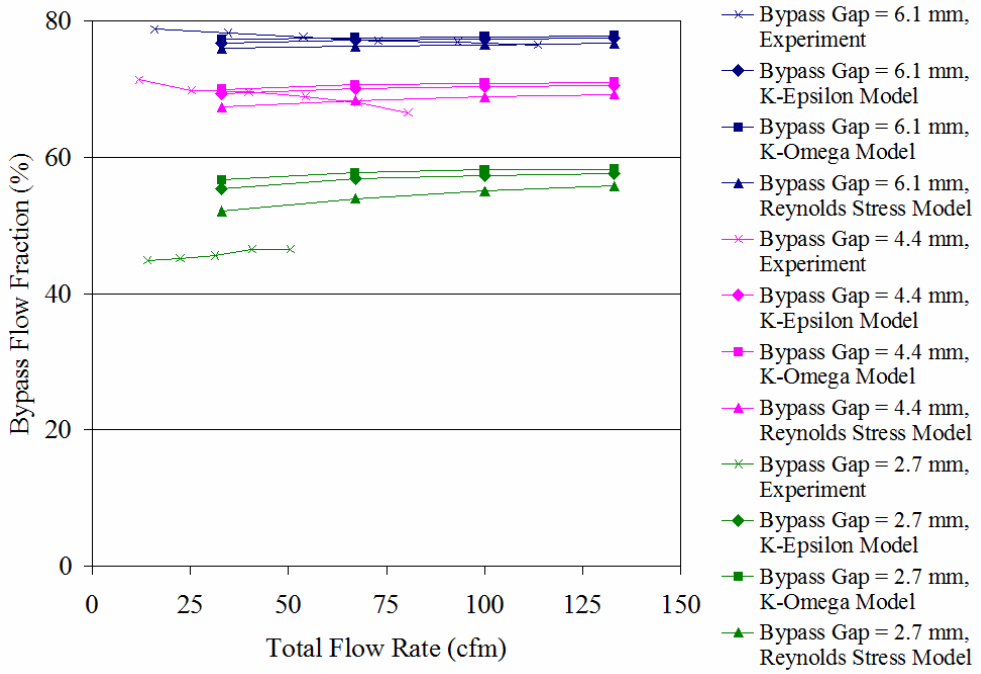

Figure 30. Bypass flow fraction comparison for air flow experiments with flow meters

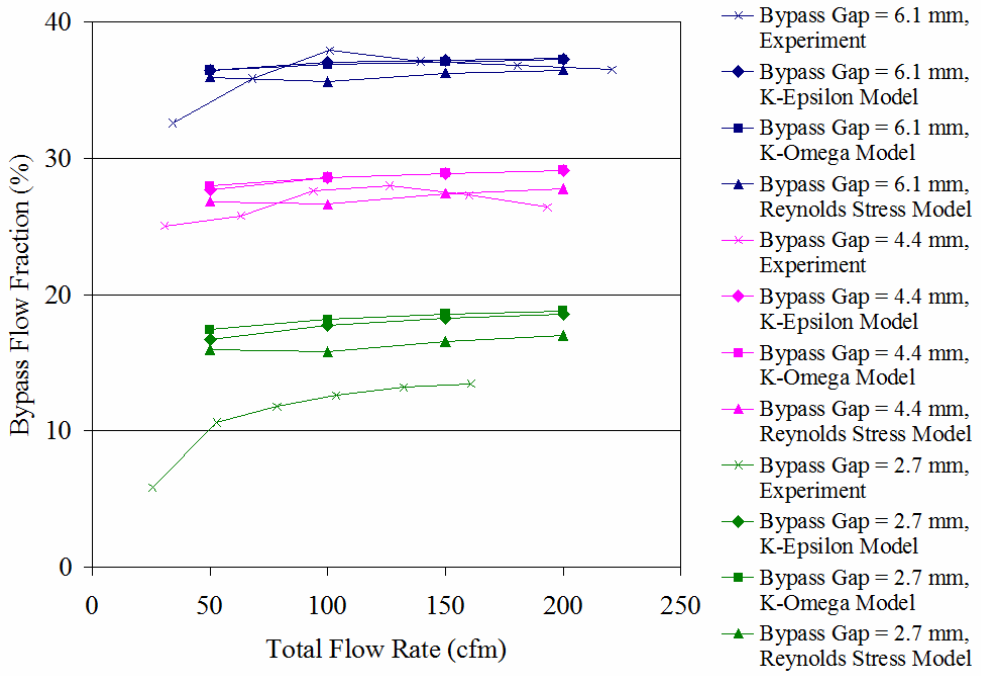

Figure 31. Bypass flow fraction comparison for air flow experiments without flow meter

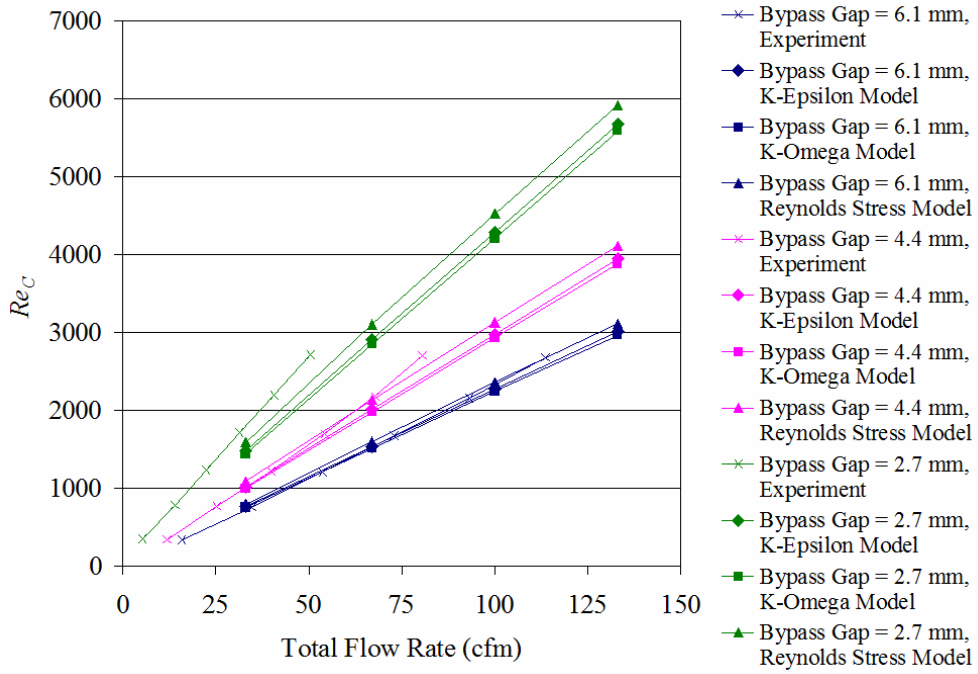

Figure 32. Re_C comparison for air flow experiments with flow meters

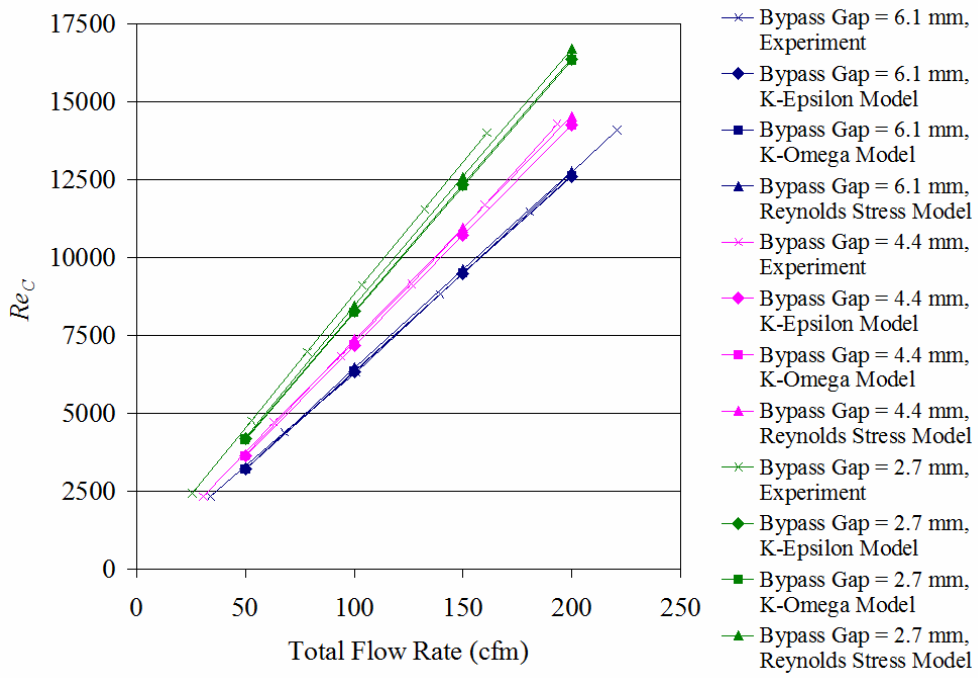

Figure 33. Re_C comparison for air flow experiments without flow meter

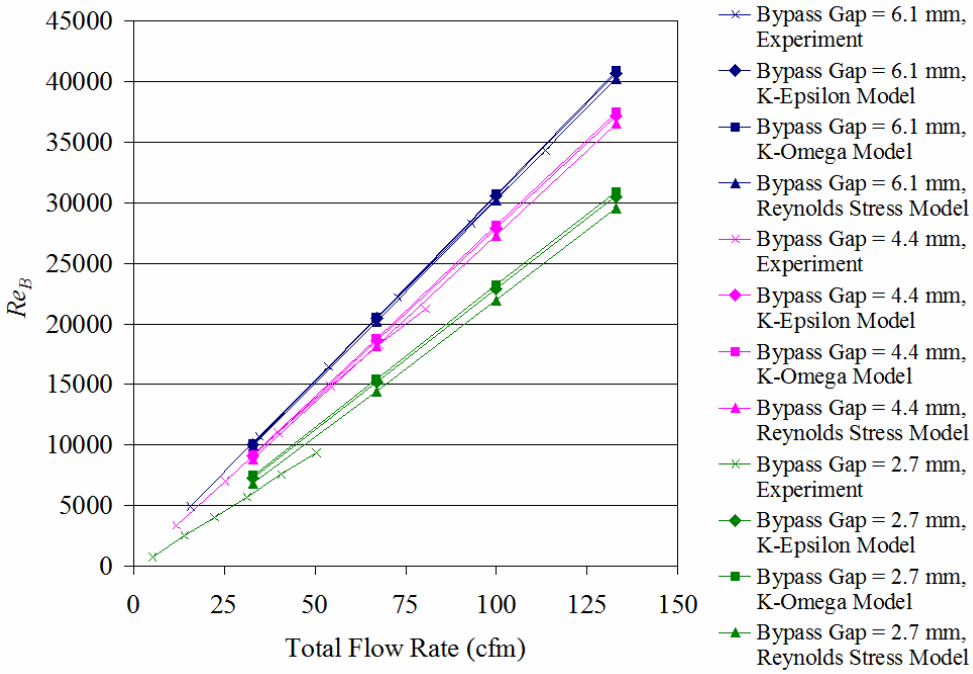

Figure 34. Re_B comparison for air flow experiments with flow meters

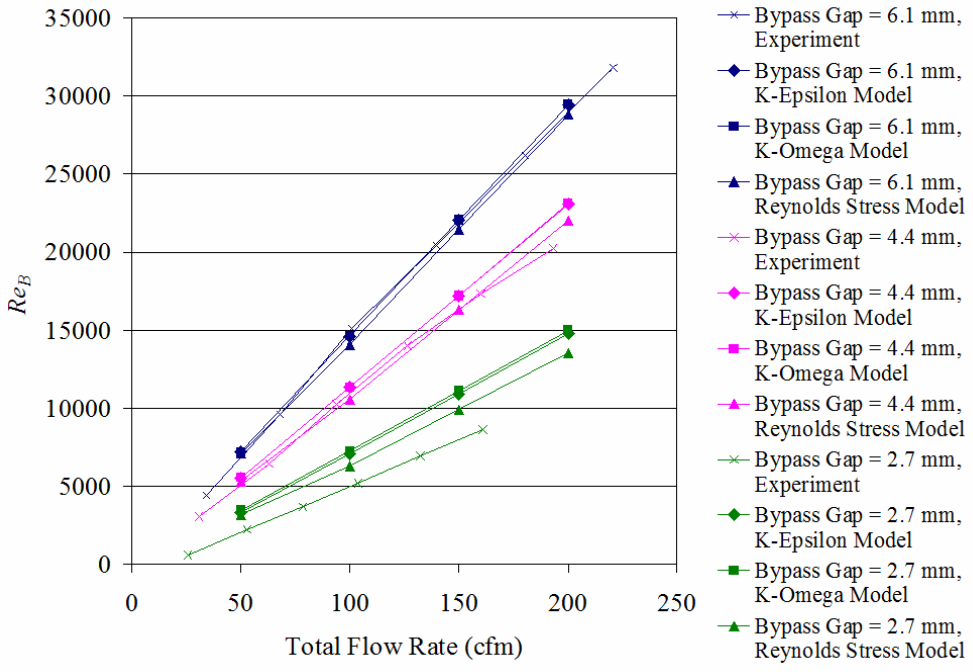

Figure 35. Re_B comparison for air flow experiments without flow meter

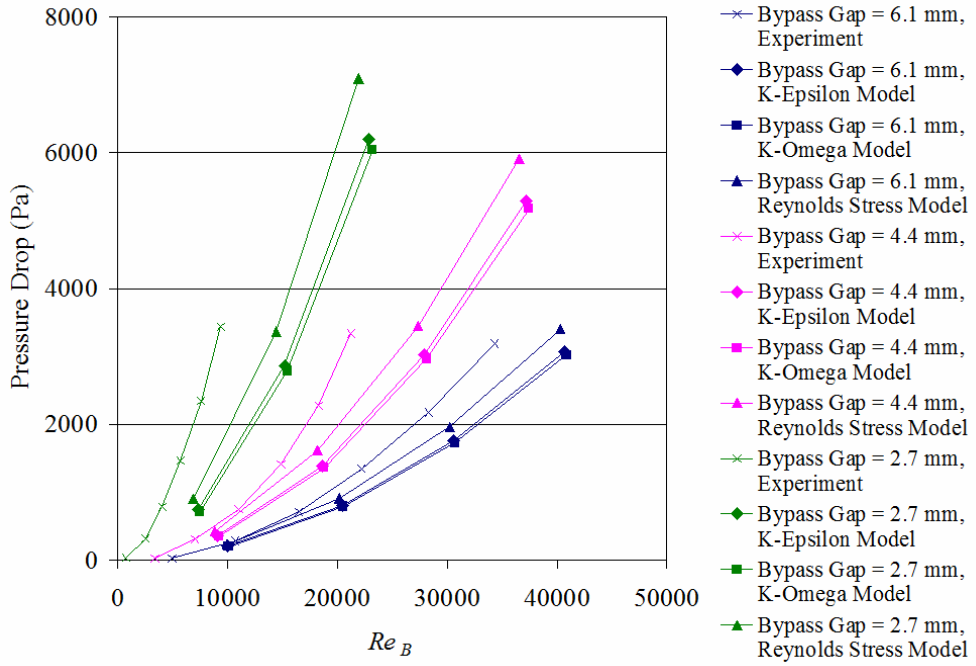

Figure 36. Pressure drop comparison for air flow experiments with flow meters

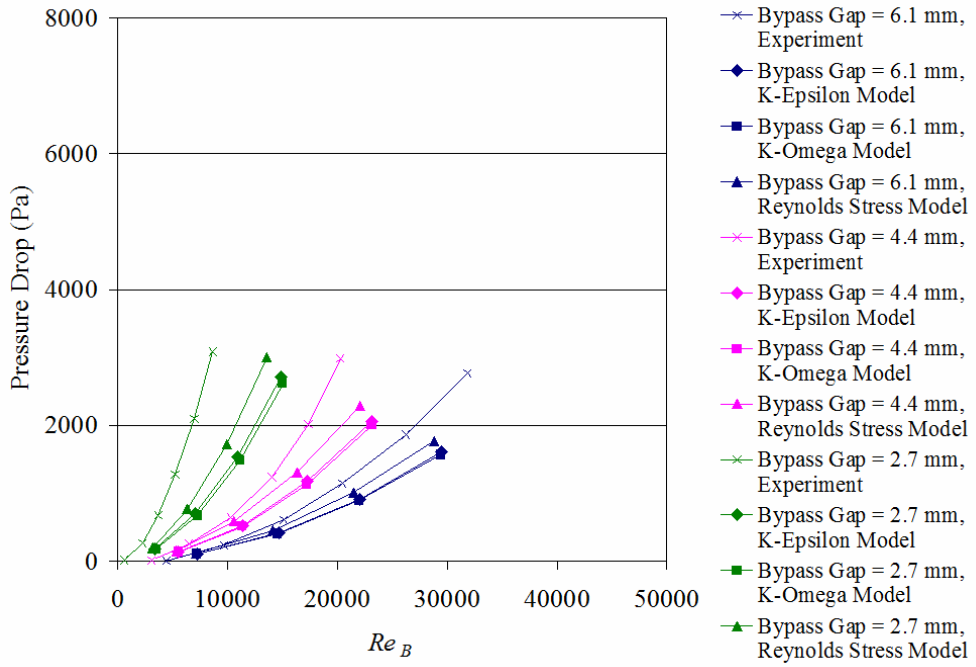

Figure 37. Pressure drop comparison for air flow experiments without flow meter

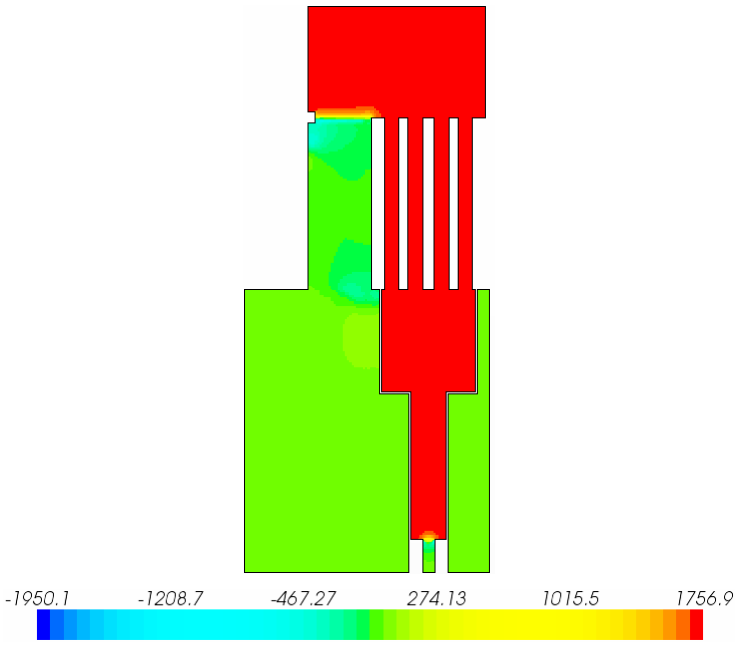

(a) the case corresponding to air flow experiments with flow meters

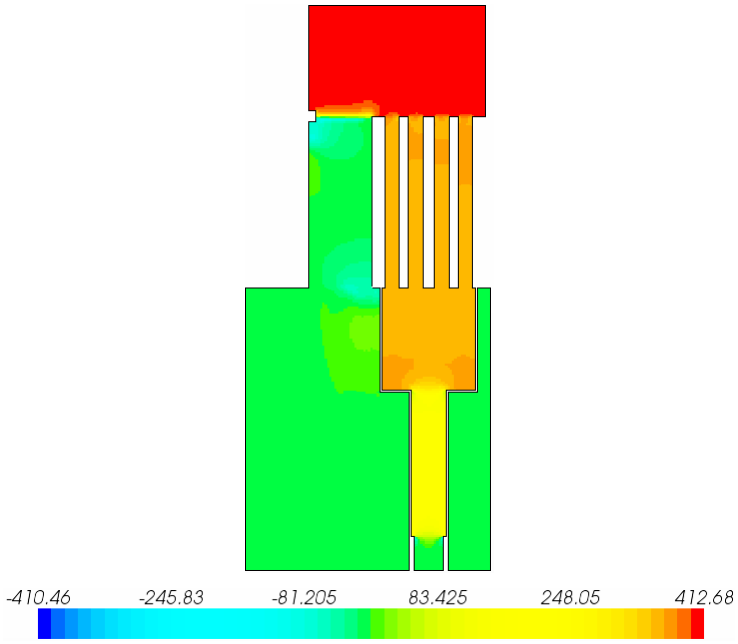

(b) the case corresponding to air flow experiments without flow meter

Figure 38. Pressure distribution on plane v-1 at flow rate of 100 cfm and 6.1-mm bypass gap from air flow simulation using k-epsilon model

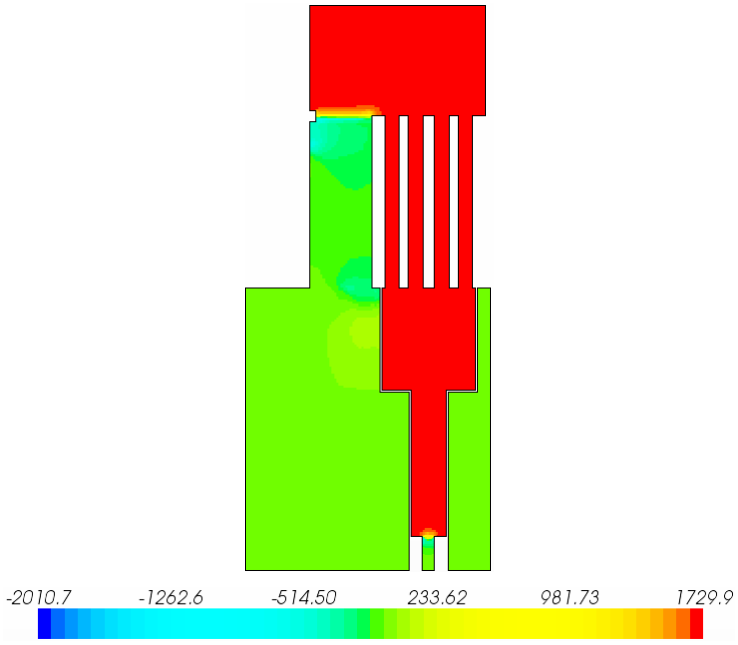

(a) the case corresponding to air flow experiments with flow meters

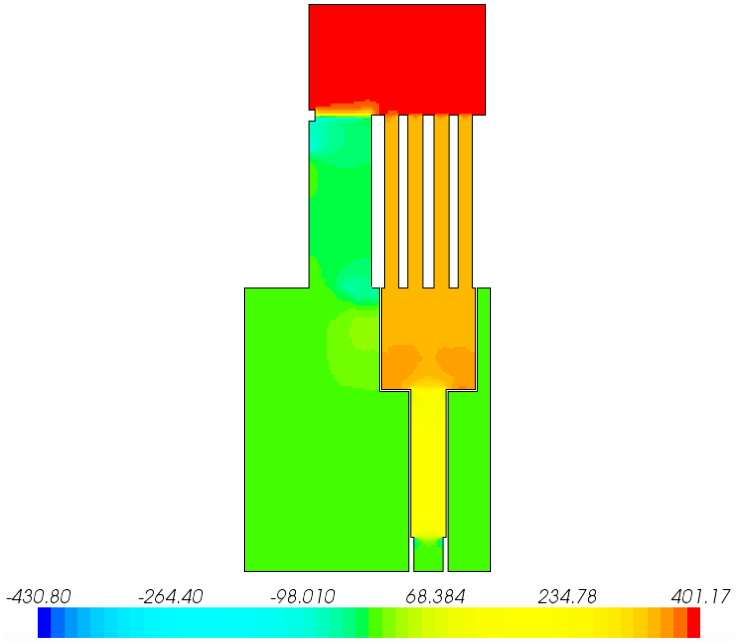

(b) the case corresponding to air flow experiments without flow meter

Figure 39. Pressure distribution on plane v-1 at flow rate of 100 cfm and 6.1-mm bypass gap from air flow simulation using k-omega model

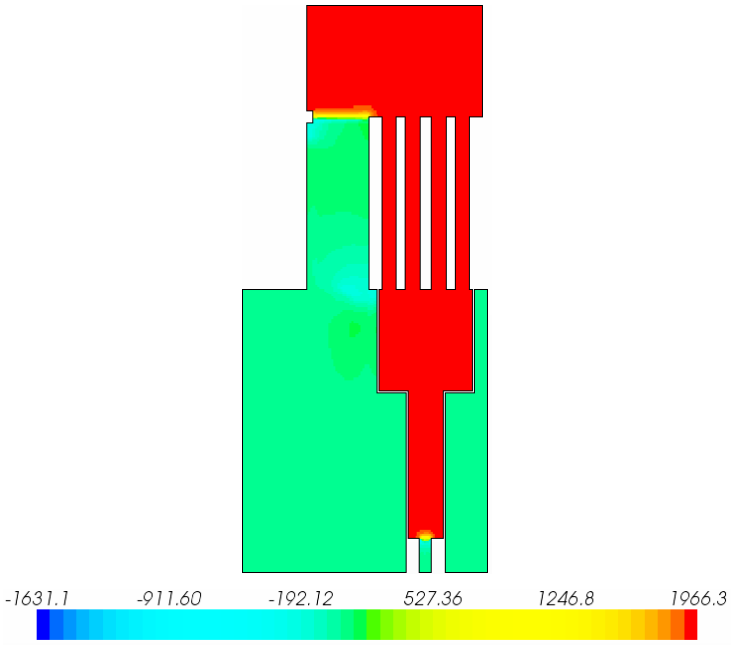

(a) the case corresponding to air flow experiments with flow meters

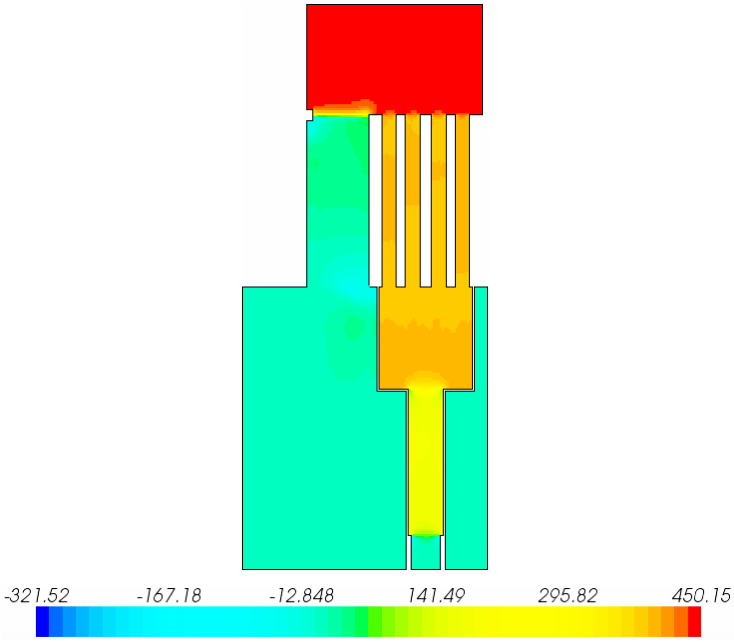

(b) the case corresponding to air flow experiments without flow meter

Figure 40. Pressure distribution on plane v-1 at flow rate of 100 cfm and 6.1-mm bypass gap from air flow simulation using Reynolds stress model

Pressure drops obtained from air flow simulations are remarkably lower than those obtained from air flow experiments for 6.1-mm bypass gap width. Same situation occurs for data obtained from air flow experiments with two remaining gap widths. This is resulted from block tilting due to block arrangement method and flow rate estimation in Section 2 that yields bypass flow rates smaller than their actual values. Also, small error in calibrating of sudden contraction inner diameter at the exit of flow passage connected from the blocks to match bypass flow fraction can cause considerably error in pressure drops obtained from simulations.

In bypass flow experiments, pressure drop is the difference of pressures taken from two locations where pressure taps or pressure transducers are placed. In bypass flow simulations, pressure drop is the difference of averaged pressure at inflow boundary and pressure specified at outflow boundary from bypass gap shown in Figure 25. From an example of pressure distribution along a line passes through bypass gap from air flow simulation in Figure 41, pressure drops reported in present study is sum of pressure losses due to:

(1) flow through bypass gaps which is flow through sudden contraction,

(2) flow between two parallel plates formed by two walls of bypass gaps, and

(3) flow through sudden expansion after the flow exits bypass gaps.

It is obvious that the first component of pressure drop is the most important one. Another issue that can be observed is that flow through bypass gaps is fully-developed at almost the bottom of the blocks. In real reactors which there are up to 10 blocks in one column, pressure drop from (2) may be comparable with pressure drop from (1).

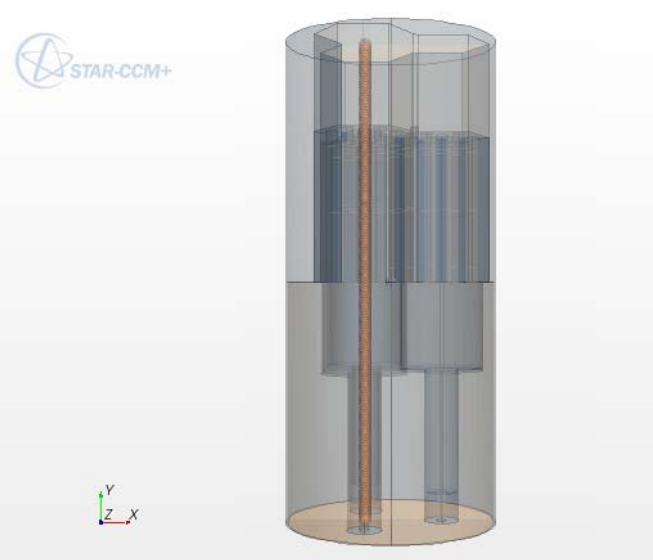

(a) line probe for plotting pressure distribution along bypass gap

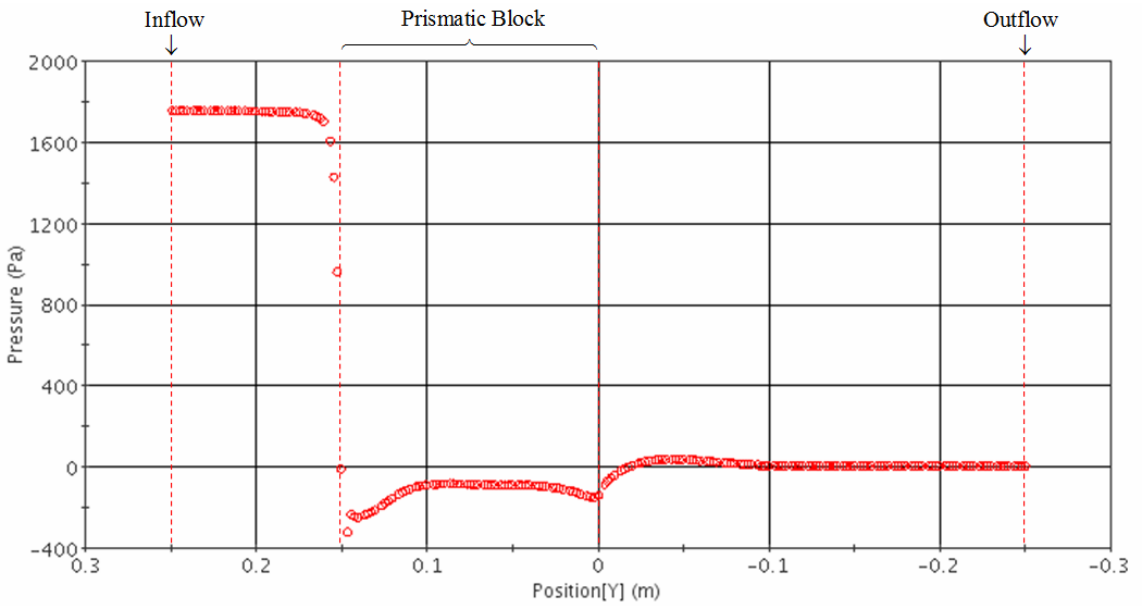

(b) pressure distribution from air flow simulation corresponding to air flow experiments with flow meters at flow rate of 100 cfm using k-epsilon model

Figure 41. Pressure distribution along a line passes through bypass gap

It should be emphasized that hydrostatic pressure of liquid equal to the height between two locations used in obtaining pressure drop in each case (experiment and simulation) must be added to recorded values of pressure drop to remove hydrostatic effects. All pressure drops presented before and after this paragraph when working fluid is liquid are treated as explained already.

Although *bypass flow rate* that is *lower* than usual when flow through bypass gap is in laminar or transition regime (for 2.7-mm bypass gap) can result in *lower pressure drop* of flow between two walls of bypass gaps, pressure drop contributed from this cause is very small portion of pressure drop reported in every case. The larger portion of pressure drop is resulted from area reduction when the flow goes into bypass gap as seen from change of several colors of pressure distributions in Figure 38 to Figure 40. Also, pressure distribution along a line passes through bypass gap in Figure 41. This means that pressure drops obtained from simulations are few Pascals smaller than usual due to this source of error and can contribute very small discrepancy in pressure drops.

Before leaving this section, the reason for getting lower flow rate through bypass gap and lower pressure drop when employing turbulence model throughout the domain, while flow between the walls of bypass gaps is laminar in the preceding paragraph (for 2.7-mm bypass gap width) is explained as closure because it seems to be a contradiction.

Firstly, two simulations of flow between two parallel plates (working fluid is air for this verification) employing turbulence model (realizable k-epsilon model with two-layer all $y+$ wall treatment) and laminar flow option are performed at same flow rate. The results show that pressure drop from laminar flow simulation is lower than that from

turbulent flow simulation. If this is the case in bypass flow simulation, more flow from coolant channels will go into bypass gap and bypass flow fraction will increase. This confirms getting of lower bypass flow fraction when employing a turbulence model throughout the domain while flow between the walls of bypass gap is laminar.

The reason for getting lower pressure drop under the condition mentioned above is that the increasing of pressure drop due to additional flow from coolant channels if the flow between the walls of bypass gaps is treated as laminar is smaller than the amount of pressure drop decreased due to the change of flow regime from turbulent to laminar through this flow passage. In fact, it can be expected that higher pressure drop through bypass gaps will result in lower bypass flow rate for *multiple-path flow* but this cannot be applied here because there is a change in flow regime in bypass gaps.

3.4 Water Flow Simulations

By employing the same concept as in air flow simulations, data taken from water flow experiments with bypass gap width of 6.1 mm is spent for calibrating geometry of the model analyzed by simulations using the same turbulence model, computational scheme, timestep, and stopping time as in the cases of air. The geometry calibration results in sudden contraction with inner diameter of 0.646 inch which yields bypass flow fraction about 58% at total flow rate of 100 gpm as in water flow experiments.

Bypass flow fraction, coolant channel Reynolds number (Re_C), bypass gap Reynolds number (Re_B) and pressure drop obtained from water flow simulations using three different turbulence models are plotted in Figure 42 to Figure 45 to compare with experimental data. Pressure distributions on the plane v-1 (Figure 26) with hydrostatic

effects obtained from simulations using k-epsilon model at flow rate of 50 and 150 cfm for bypass gap width of 6.1 mm are shown in Figure 46 and Figure 47. The purpose of showing these two figures is to reveal the hydrostatic effects on pressure distributions which can produce *negative* pressure drop in water flow experiments at low flow rates.

For 6.1-mm bypass gap width, all quantities plotted in Figure 42 to Figure 45 match very well with experimental data. It should be mentioned that *pressure drop* from simulations for this bypass gap width shows good agreement with pressure drop from experiments because total flow rate and flow rate through each block are taken from flow meters. Therefore, there is no flow rate estimation which is the major source of error in the cases of air. Also, pressure forces in water flow experiments can push the blocks to more favorable positions, while this is not the case for air.

For 4.4-mm and 2.7-mm bypass gap width, bypass flow fractions obtained from water flow simulations are almost constant and higher than those obtained from water flow experiments. Differences in bypass flow fractions at higher flow rate is smaller than those at lower flow rate because larger pressure forces of flow between the walls of bypass gaps pushes tilted blocks caused by the method of gap width varying to more favorable positions which can reduce pressure drop of flow through bypass gaps.

However, bypass flow fractions at the highest flow rate that can be attained in water flow experiments still be lower than those from water flow simulations because any imperfection in experiments can reduce flow area in bypass gap or produce more pressure drop. Therefore, difference in bypass flow fraction still exists but its magnitude is depended on how good is the experimental setup.

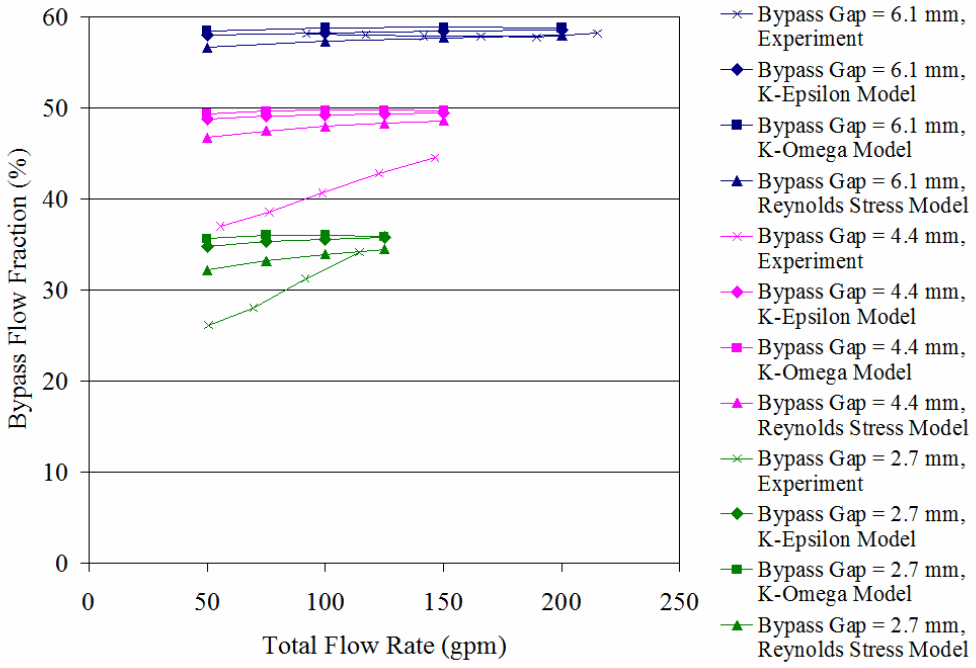

Figure 42. Bypass flow fraction comparison for water flow experiments

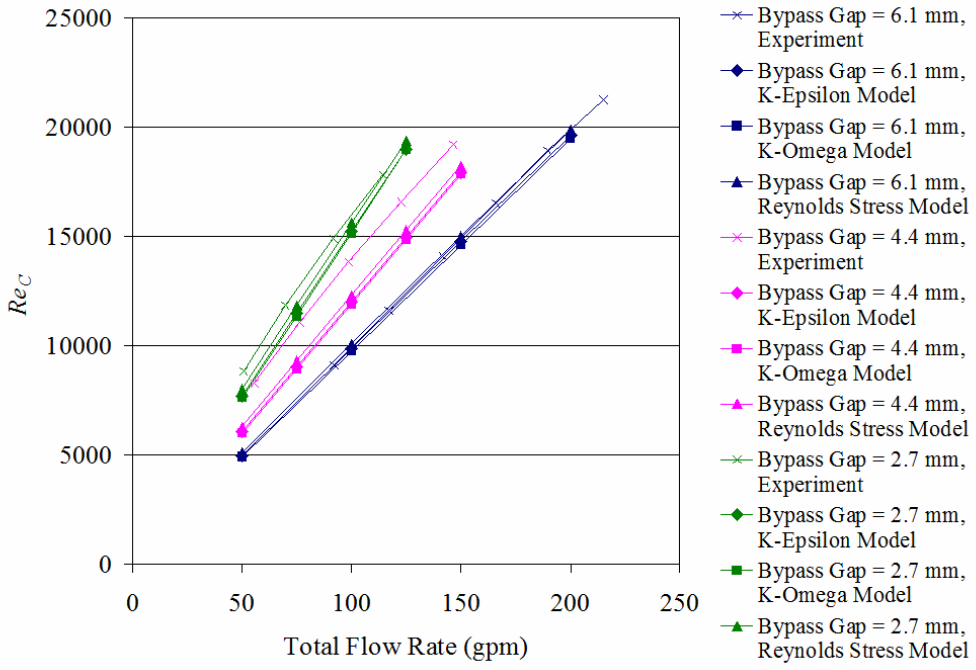

Figure 43. Re_C comparison for water flow experiments

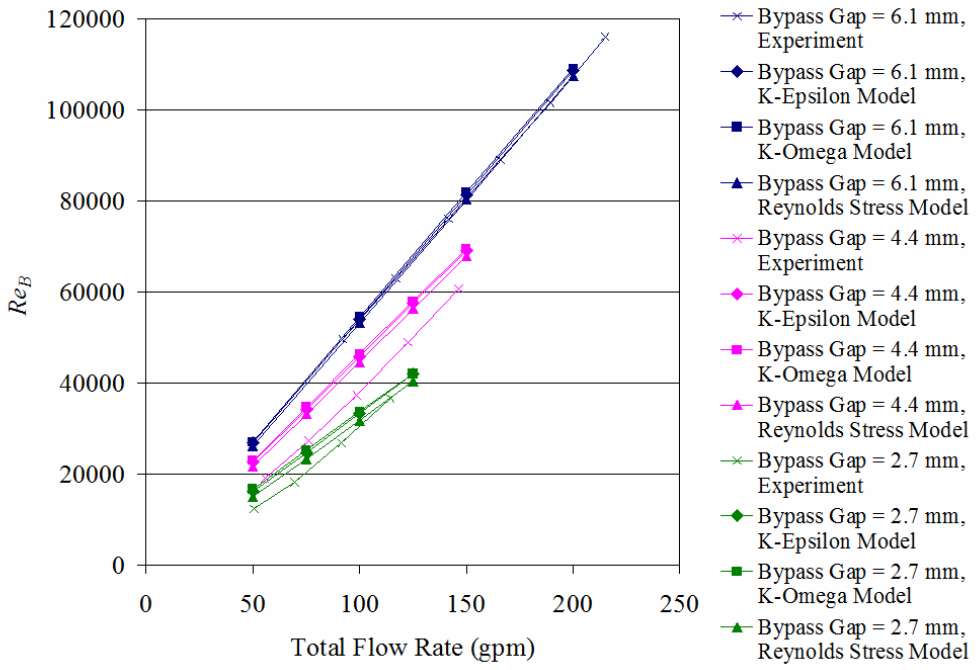

Figure 44. Re_B comparison for water flow experiments

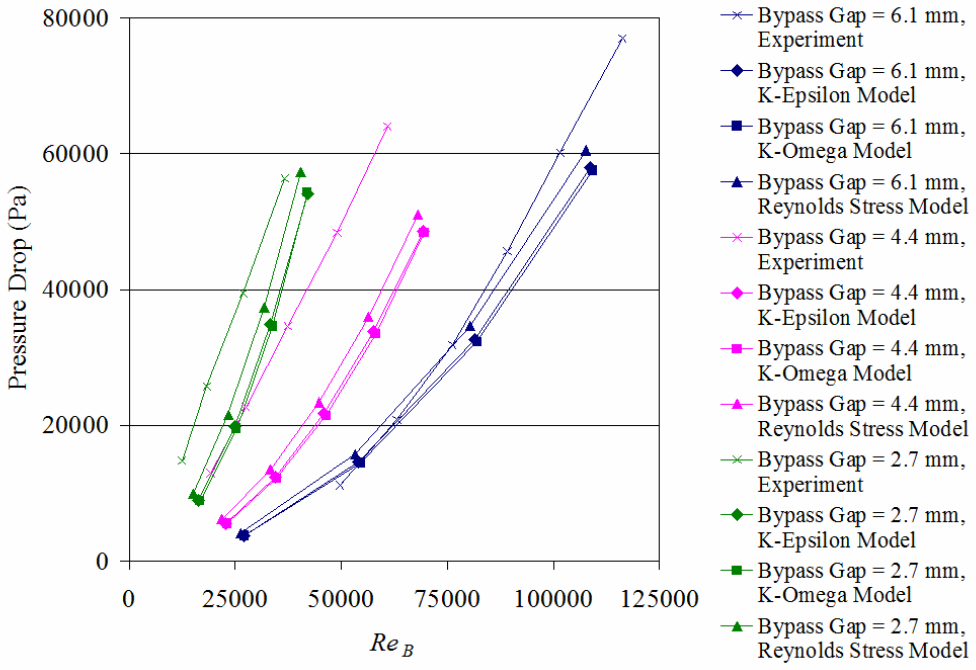

Figure 45. Pressure drop comparison for water flow experiments

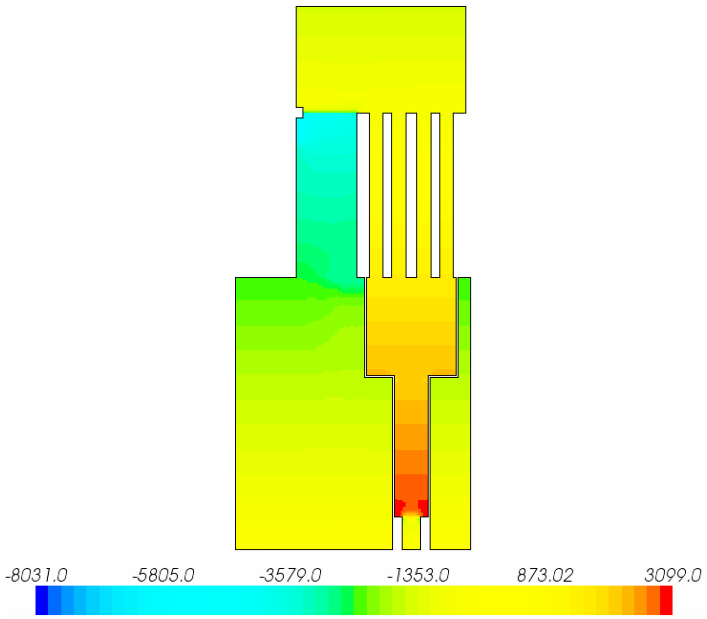

Figure 46. Pressure distribution on plane v-1 at flow rate of 50 cfm and 6.1-mm bypass gap from water flow simulation using k-epsilon model

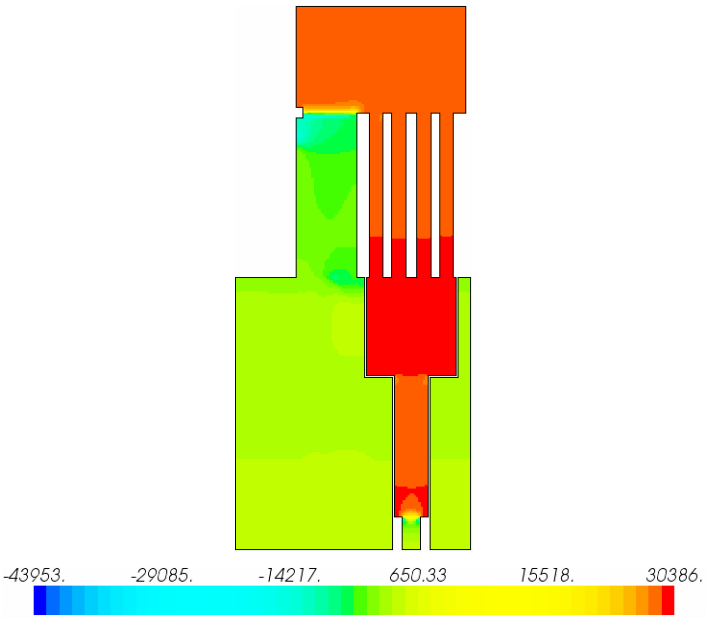

Figure 47. Pressure distribution on plane v-1 at flow rate of 150 cfm and 6.1-mm bypass gap from water flow simulation using k-epsilon model

Due to the higher bypass flow fractions from water flow simulations than those from water flow experiments for these two gap widths, bypass gap Reynolds numbers (Re_B) and coolant channel Reynolds numbers (Re_C) from water flow simulations are higher and lower than those from water flow experiments, respectively. The minimum value of Re_B indicates that there is no change in flow regime for water flow through bypass gap in present study. Finally, lower pressure drops from water flow simulations are obtained as obtained in the cases of air.

3.5 P-Cymene Flow Simulations

The model used in water flow simulations (inner diameter of sudden contraction of flow passage connected from the block is equal to 0.646 inch.) is employed in p-cymene flow simulations again but only 4.0-mm bypass gap is analyzed because only this gap width can be prepared in p-cymene flow experiments.

Bypass flow fraction, Re_C, Re_B and pressure drop obtained from p-cymene flow simulations using three different turbulence models are plotted in Figure 48 to Figure 51. They are prepared for comparison with experimental data. Velocity distributions on plane v-1 and v-2 (in Figure 26) are shown in Figure 52 and Figure 54. Two scenes in Figure 53 and Figure 55 are zoomed from bottom region along the height of the blocks to reveal details of velocity distributions in coolant channel and bypass gap that are closest to fully-developed flow and to show capability of the software for flow visualization. Color and length of velocity vectors in the plots are varied with their magnitudes. Number of color levels is changed from default at 32 to 50 and vector length is adjusted to represent velocity distribution properly in each plot.

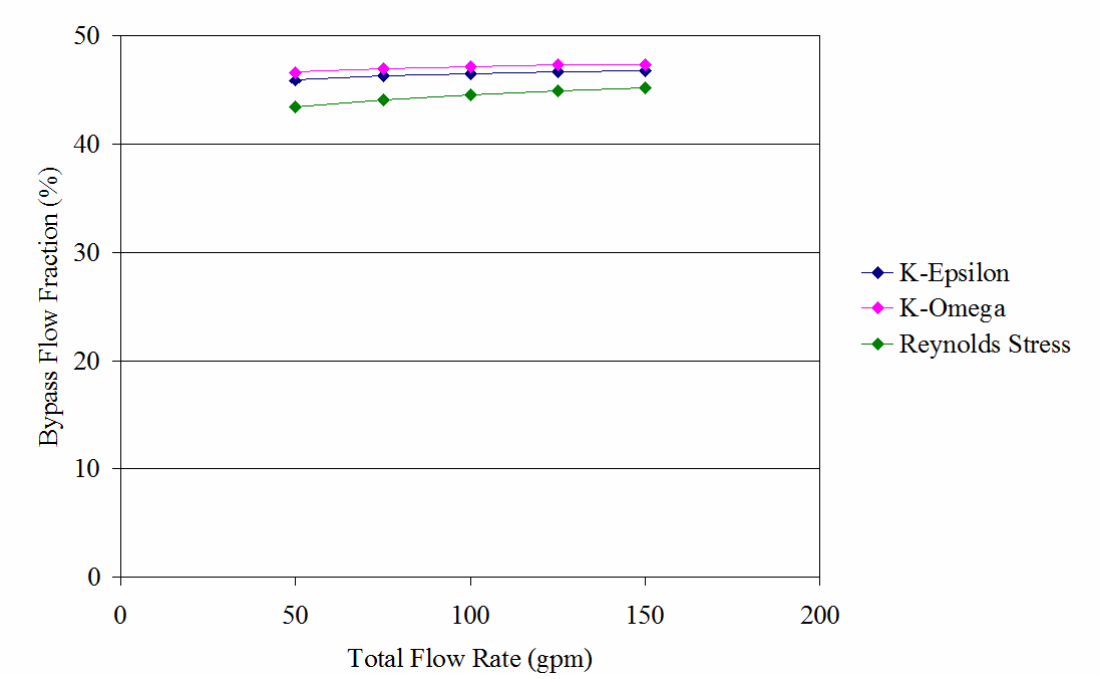

Figure 48. Bypass flow fraction from p-cymene flow simulations

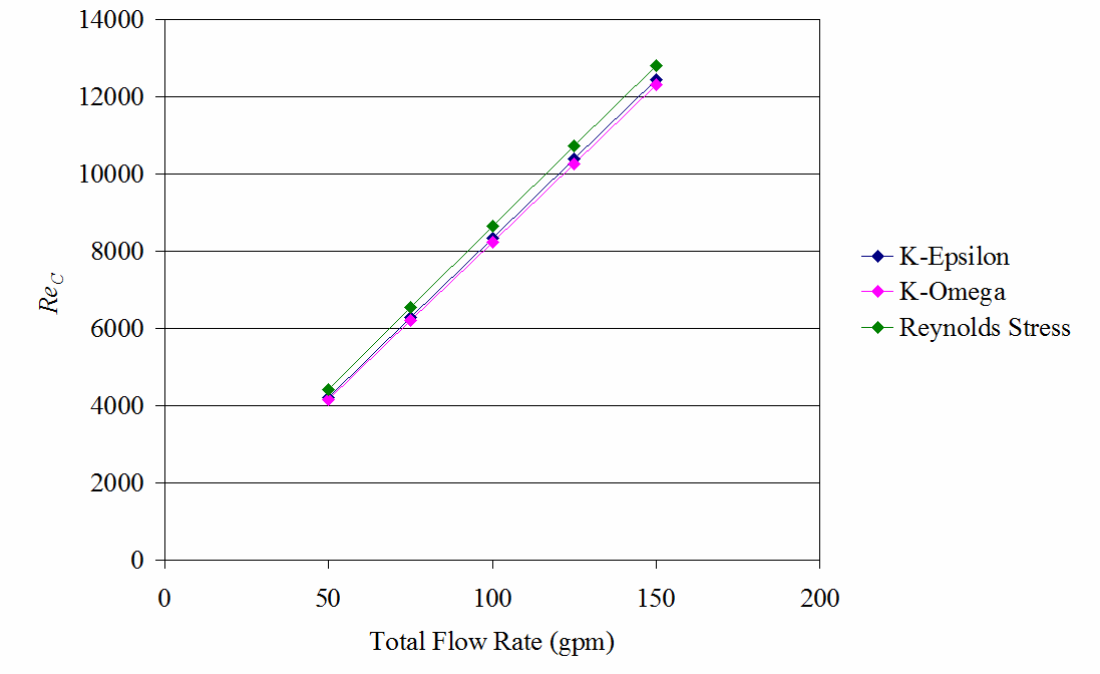

Figure 49. Re_C from p-cymene flow simulations

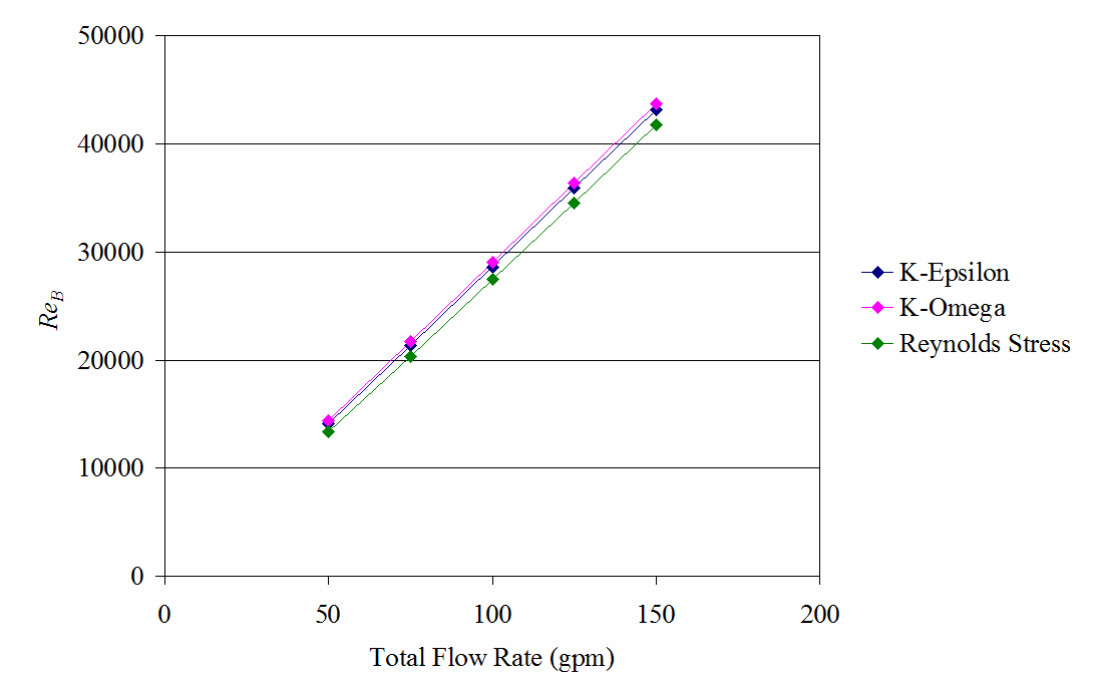

Figure 50. Re_B from p-cymene flow simulations

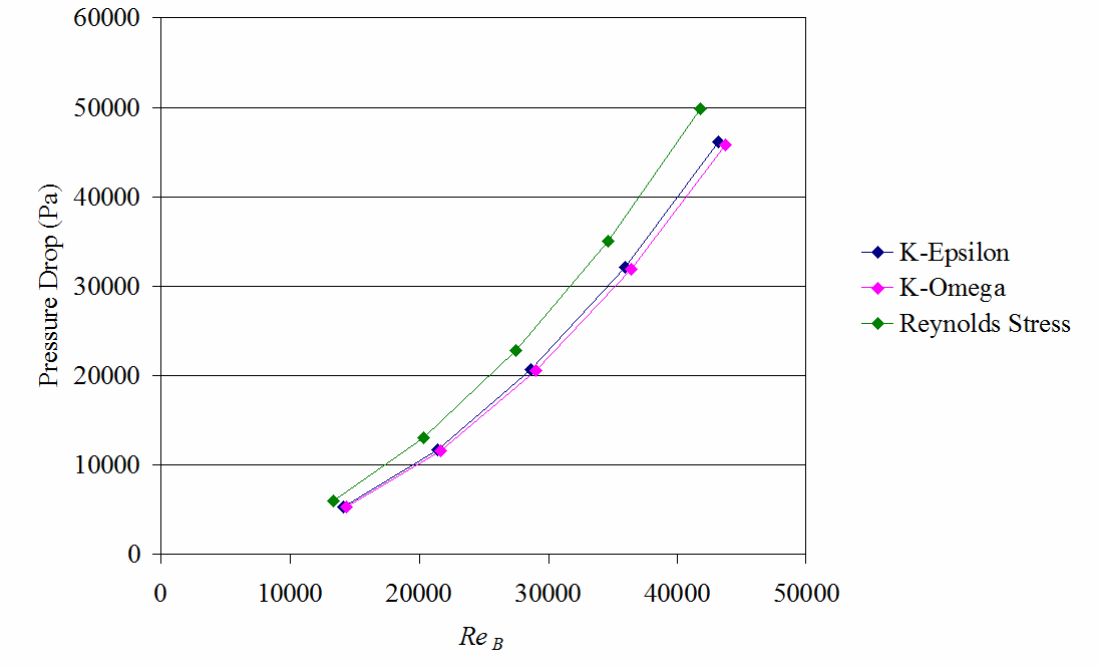

Figure 51. Pressure drop from p-cymene flow simulations

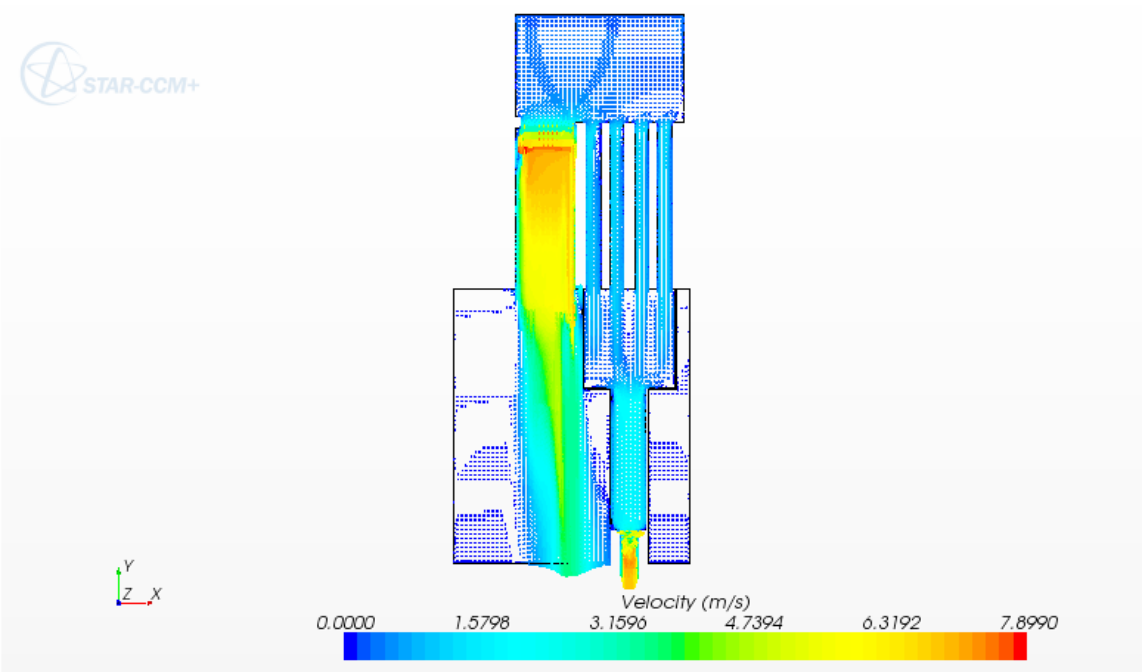

Figure 52. Velocity distribution on plane v-1 from p-cymene flow simulation

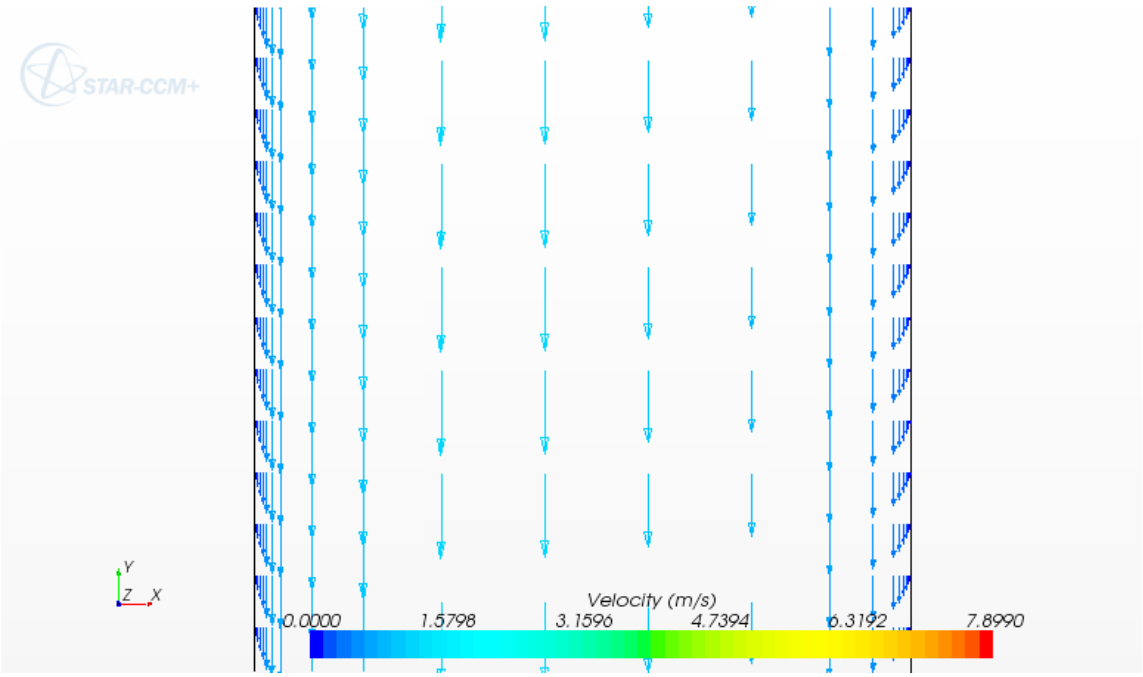

Figure 53. Velocity distribution in a coolant channel from p-cymene flow simulation

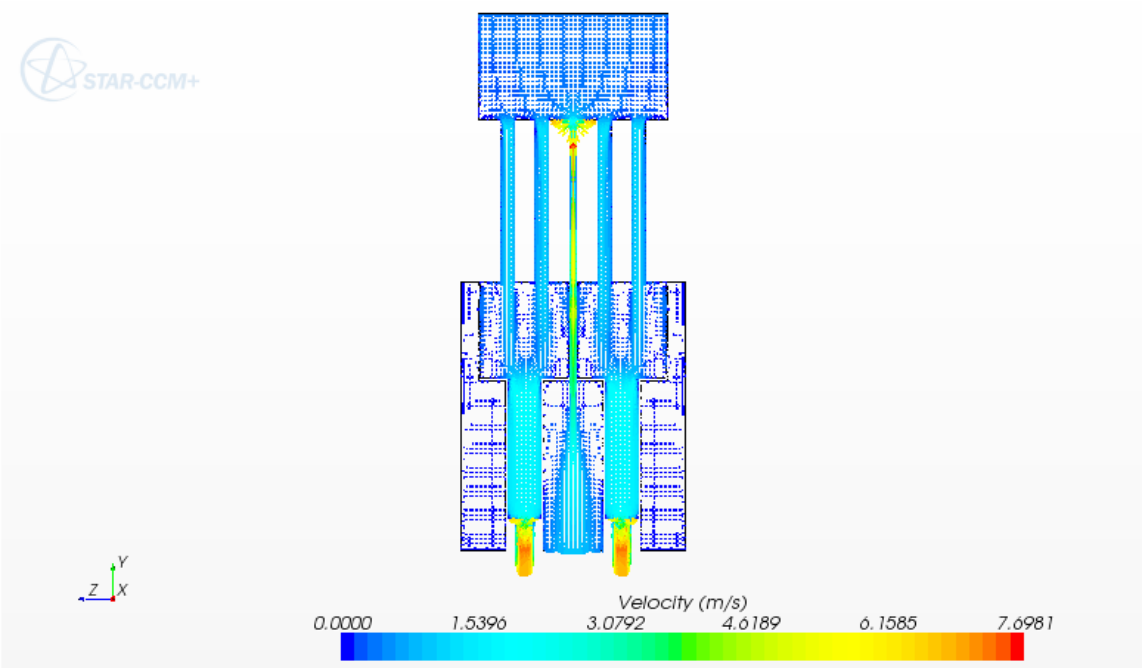

Figure 54. Velocity distribution on plane v-2 from p-cymene flow simulation

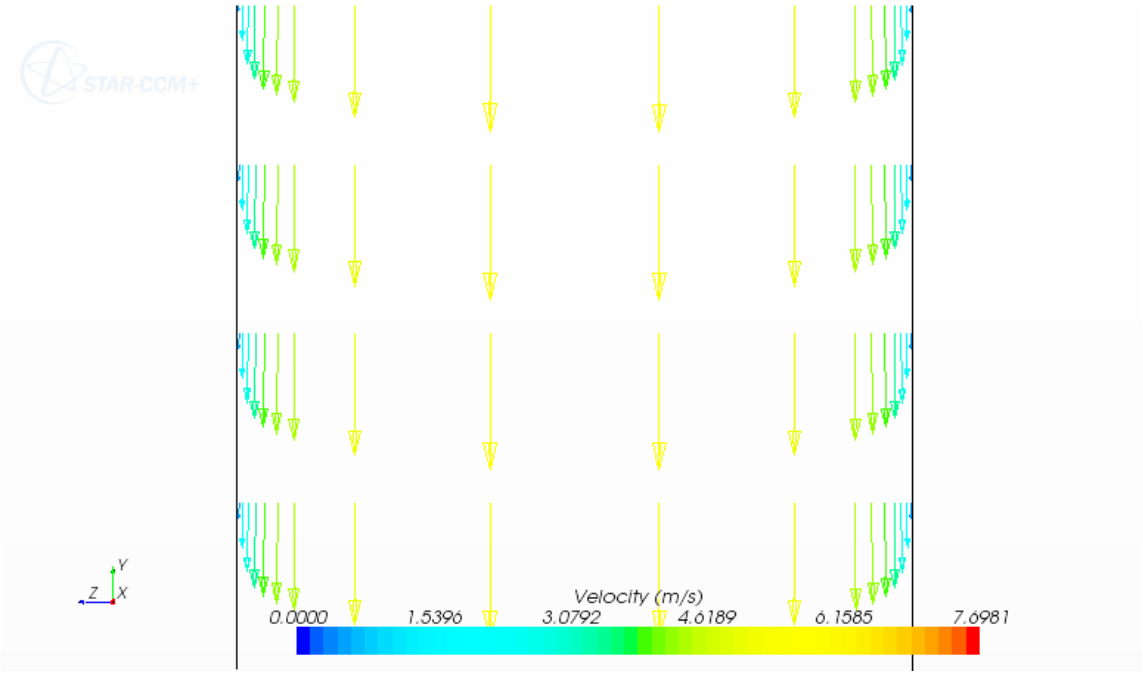

Figure 55. Velocity distribution in a bypass gap from p-cymene flow simulation

Velocity distribution in a coolant channel in Figure 53 shows that it is not a symmetric velocity profile. Same situation occurs in other coolant channels with slight difference in shape of velocity profile from Figure 53, so they are not shown for brevity. Although different velocity profiles yield different coolant channel Reynolds numbers (Re_C), their differences are very small and they are approximated by dividing volume flow rate of flow through the block with the sum of flow area of all coolant channels on that block.

Velocity distribution in a bypass gap in Figure 55 shows that it is a symmetric velocity profile. Therefore, a suggestion for PIV technique is that flow visualization should be taken on a plane lies at the middle of block side length to minimize any disturbance that may occur in flow through bypass gaps.

3.6 Conclusion

Flow in circular pipe and flow between two parallel plates are flow problems used for simulation exercises with trimmer meshes. Among three turbulence models, realizable k-epsilon model with two-layer all $y+$ wall treatment yields the best matching of friction factor in the range of Reynolds number attained in bypass flow experiments. Meshing parameters determined from these exercises are absolute prism layer thickness of 0.4 mm which employs seven prism layers with stretching ratio of 1.35.

Grid independence study is performed by using the models that will be used in bypass flow simulations. They are constructed by adjusting downstream flow passage from the blocks to yield the same bypass flow fraction in each bypass flow experiment for 6.1-mm bypass gap. Therefore, only experimental data from other two bypass gaps

can be compared with results from simulations to examine reliability of the software. Pressure drop of flow through bypass gap is the physical quantities used for indicating grid independent solution because it is much more sensitive than bypass flow fraction. It is suggested that the ratio between the narrowest distance between two walls (bypass gap in present study) substracted by absolute prism layer thickness and cell base size should be 3.5 or greater to obtain grid independent solution.

From air flow simulations, the discrepancies in bypass flow fraction and pressure drop of flow through bypass gaps increases with decreasing bypass gap width. The imperfection in air flow experiments is not only one cause of these discrepancies, but also the method of flow rate estimation. Therefore, air flow experiments set up should be improved and flow rate should be directly measured in bypass flow experiments in the future. The sensitivity of pressure drop of flow through bypass gaps can be observed from air flow experiments with 6.1-mm bypass gap because bypass flow fractions can be matched very well with air flow simulations but pressure drops of flow through bypass gaps cannot. However, pressure drops of flow through bypass gaps predicted from simulations does not depend on downstream condition as in air flow experiments.

It should be noted that pressure drops of flow through bypass gaps predicted from water flow simulations with 6.1-mm bypass gap show good agreement with those obtained from water flow experiments. The trends of discrepancies in bypass flow fraction and pressure drop of flow through bypass gaps are different from air flow simulations due to the method of bypass gap varying that differs from the case of air which should be improved in the future.

In comparing the results with different turbulence models, bypass flow fraction predicted by SST (Menter) k-omega model is slightly higher than that predicted by realizable k-epsilon model which results in lower pressure drop of flow through bypass gaps. For Reynolds stress model, bypass flow fraction is lower than that predicted by realizable k-epsilon model which results in higher pressure drop of flow through bypass gaps.

Because hydraulic diameter of flow through bypass gaps is smaller than that of flow through coolant channels, flow through bypass gaps should be referred when mention about pressure drop. From conclusion in the preceding paragraph, it can be said that SST (Menter) k-omega model under-predicts, while Reynolds stress model over-predicts pressure drop of flow through bypass gaps.

Bypass flow fractions from bypass flow simulations using realizable k-epsilon model with two-layer all y+ treatment corresponding to each bypass flow experiment are plotted together in Figure 56. All curves from simulations show the trend of bypass flow fraction as bypass gap width decreases that are expected in bypass flow experiments. It should nonlinearly decrease with decreasing of bypass gap width when flow through bypass gaps is turbulent and linearly decrease to zero with decreasing of bypass gap width when laminar flow exists in bypass gaps. The plots for other two turbulent models are skipped because they are slightly different from the plot in Figure 56.

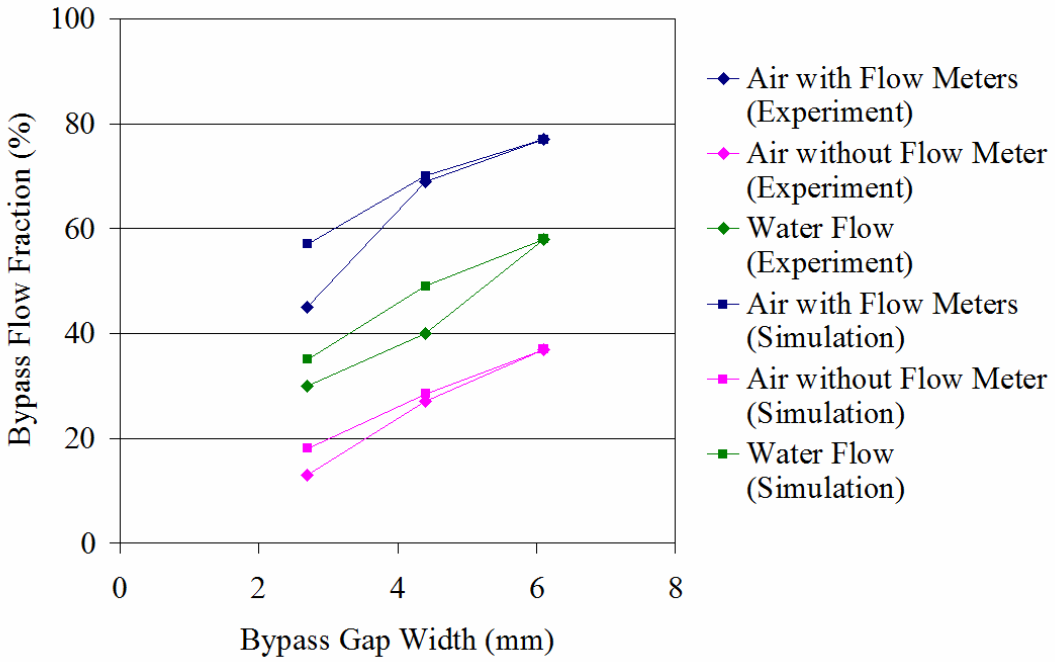

Figure 56. Bypass flow fraction as function of bypass gap width from experiments and simulations using k-epsilon model

4. DATA REDUCTION

In this section, all parameters related to bypass flow in HTR core appeared in literature review are summarized and are grouped to yield dimensionless parameters. Pressure loss coefficients obtained from all bypass flow experiments and simulations are reduced into a diagram as a function of bypass gap Reynolds number (Re_B) and block side length to bypass gap width ratio (b/l). Generic pressure loss coefficient diagram for bypass flow phenomenon under ideal condition is imagined as closure of this section.

4.1 Parameters Related to Bypass Flow in HTR Core

Geometry of prismatic block in Figure 10 is shown again in this section. Its parameters are block height (h), block side length (l), coolant channel diameter (d), number of coolant channels (n) and their locations. Block porosity (ε) which is the ratio of flow area (cross-sectional area of all coolant channels) and cross-sectional area of the block is a *dependent parameter* because it can be computed after specifying of d and n.

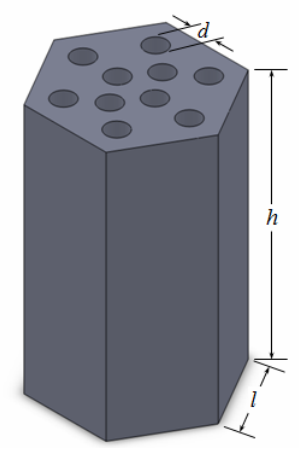

Figure 10. Geometry of prismatic block

When a number of prismatic blocks are arranged to form a part of a block layer in reactor core as in Figure 11 which is shown again below, the additional parameters related to bypass flow are number of block columns stacked in test section (N_C), bypass gap width (b), side gap width (s), and seal mechanism. Actually, bypass gaps and side gaps are not designed features of nuclear reactor but they are inevitably arisen from combination of several causes and are treated as independent parameters in present study. If there are more than one block layer in test section, another two additional parameters are number of block layers (N) and crossflow gap width (c).

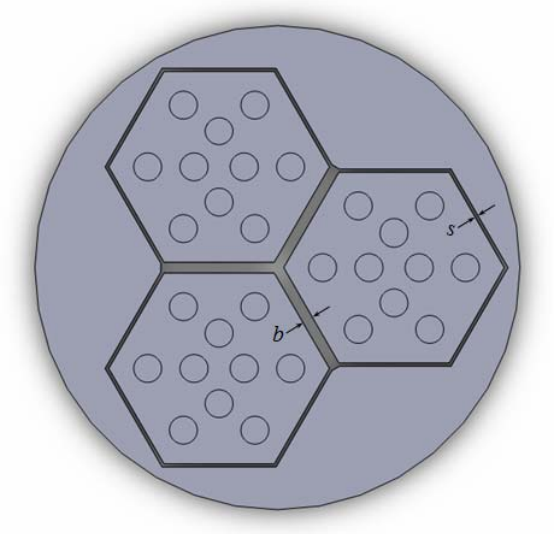

Figure 11. Top view of block combination

Many physical phenomena such as flow-induced vibration and thermal expansion of several elements can occur during the operations of nuclear reactor. They can change some structural configurations and initiate more parameters related to bypass flow, for example, seal mechanism configurations under motions of prismatic blocks and bending of fuel elements contained in same column which can cause some changes in bypass gap

and crossflow gap configurations. The most important change of parameter that may occur in nuclear reactor operations and is focused in present study is the variation of bypass gap width. All parameters mentioned in this section, relevant dimensionless parameters, their values and comments are summarized in Table 18.

4.2 Pressure Loss Coefficient Diagram

The concept in getting pressure loss coefficient diagram is modified from the same concept used in simple pipe flow. For fully-developed flow in constant-area pipe in horizontal plane with no minor loss as shown in Figure 57, pressure drop between section 1 and 2 (Δp or $p_1 - p_2$) is a function of pipe diameter (D), pipe length (L), pipe roughness (e), average flow speed (V), fluid density (ρ), and fluid viscosity (μ).

$$\Delta p = \mathcal{F}_1(d, l, e, V, \rho, \mu) \tag{4.1}$$

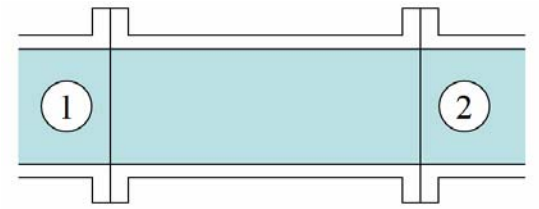

Figure 57. Flow in constant-area pipe

By applying dimensional analysis, equation (4.1) can be written as

$$\frac{\Delta p}{\frac{1}{2}\rho V^2} = \mathcal{F}_2\left(\frac{\rho V d}{\mu}, \frac{l}{d}, \frac{e}{d}\right), \tag{4.2}$$

where $\frac{\Delta p}{\frac{1}{2}\rho V^2}$ is pressure loss coefficient, $\frac{\rho V d}{\mu}$ is Reynolds number (Re), $\frac{l}{d}$ is dimensionless pipe length and $\frac{e}{d}$ is relative roughness of pipe.

Table 18 Parameters related to bypass flow in HTR core

Parameter Related to Bypass Flow		Dimensionless Parameter		Comments
Physical Quantity	Value	Definition	Value	
Block Side Length (l)	50 mm	-	-	- l is used as repeating parameter in normalizing almost all lengths.
Block Height (h)	152 mm	h/l	~3	- h/l is about 4 for standard fuel element and will be increased with h/d in new bypass flow facility.
Coolant Channel Diameter (d)	12.7 mm	h/d	~12	- h/d is about 50 for standard fuel element. - Attaining geometric similarity is very hard due to difficulties arisen in block model fabrication.
Number of Coolant Channels (n)	10	ε	0.1950	- ε is known after specifying d and n and it is close to 0.1867 for standard fuel element.
Locations of Coolant Channels	-	-	-	- They should be symmetric, not be difficult to fabricated, and do not reduce block strength. - They will not affect bypass flow fraction if n is high enough.
Number of Block Columns (N_C)	3	-	-	- Next N_C for larger portion of the core is 7.
Bypass Gap Width (b)	varied	b/l	varied	- Effects of b/l on bypass flow are studied because b/l varies in nuclear reactor operations. - The minimum value of b/l is limited by laser sheet thickness used in PIV technique.
Bypass Gap Configuration	rectan-gular	-	-	- Only rectangular gap will be studied, wedge-shaped gap is omitted as future works.
Side Gap Width (s)	0 mm	s/l	0	- No side gap benefits in reducing a large number of cells in simulations. - If the effects of side gap flow are focuses, s/l should be varied with more number of block columns.
Number of Block Layers (N)	1	-	-	- N is up to 10 in existing nuclear reactor cores.

Table 18 continued

Parameter Related to Bypass Flow		Dimensionless Parameter		Comments
Physical Quantity	Value	Definition	Value	
Crossflow Gap Width (c)	N/A	c/l	-	- There is no crossflow gap because N is equal to 1.
Crossflow Gap Configuration	N/A	-	-	
Seal Mechanisms	N/A	-	-	- There is no seal mechanism.
Seal Mechanism Configuration	N/A	-	-	

For flow in vertical pipeline, equation (4.2) can be applied if hydrostatic pressure is removed from pressure difference of two sections. If there are minor losses due to area reduction in flow passage, additional dimensionless parameters related to configurations listed in Table 18 should be included as independent parameters. These conditions are mentioned because they are situations occur in bypass flow experiments and simulations in present study.

$$\frac{\Delta p}{\frac{1}{2}\rho V^2} = \mathcal{F}_3\left(\frac{\rho V d}{\mu}, \frac{l}{d}, \frac{e}{d}, \text{system configurations}\right) \tag{4.3}$$

If all surfaces are assumed to be smooth, relative roughness can be dropped from equation (4.3). Furthermore, if there is no sufficient length (l) of straight flow path that can contribute significant pressure drop compared to pressure drop caused by other components, l/d can be dropped from equation (4.3). Finally, flow passage diameter (d) used in Reynolds number calculation must be changed to another characteristic length (ℓ) because diameter, d, is not the most important dimension that characterizes the flow.

$$\frac{\Delta p}{\frac{1}{2}\rho V^2} = \mathcal{F}_4\left(\frac{\rho V \ell}{\mu}, \text{system configuration}\right) \tag{4.4}$$

Based on the fact in continuity equation, sum of flow through bypass gaps and all blocks is total flow. This means that bypass flow fraction or percentage of flow through each block can characterize bypass flow. Therefore, only one of characteristic lengths of the block or bypass gap width can be used as characteristic length. Because flow fields within bypass gaps are focused, bypass gap width (*b*) should be selected as characteristic length appears in equation (4.4).

As seen in Table 18, bypass gap width to block side length ratio (*b*/*l*) is the most important dimensionless parameter in present study because bypass gap width can be varied in actual operations while other parameters may be fixed. Although crossflow gap width to block side length ratio (*c*/*l*) can be varied in actual operations, it does not exist in present study. Therefore, the relation for pressure loss coefficient should be in the form as shown in equation (4.5) and it should be noted that average velocity (*V*) should be average velocity of flow through bypass gaps.

$$\frac{\Delta p}{\frac{1}{2}\rho V^2} = \mathcal{F}\left(\frac{\rho V b}{\mu}, \frac{b}{l}\right) = \mathcal{F}\left(Re_B, \frac{b}{l}\right) \tag{4.5}$$

Pressure loss coefficients from experiments are plotted in Figure 58, while those from simulations are plotted in Figure 59. Because pressure drops obtained from bypass flow experiments and simulations are quite different for bypass gap width of 4.4 and 2.7 mm, pressure loss coefficients correspond to these data are far apart in the diagrams. However, the ideal diagram for pressure loss coefficient can be imagined based on all existing data (from experiments and simulations) as shown in Figure 60.

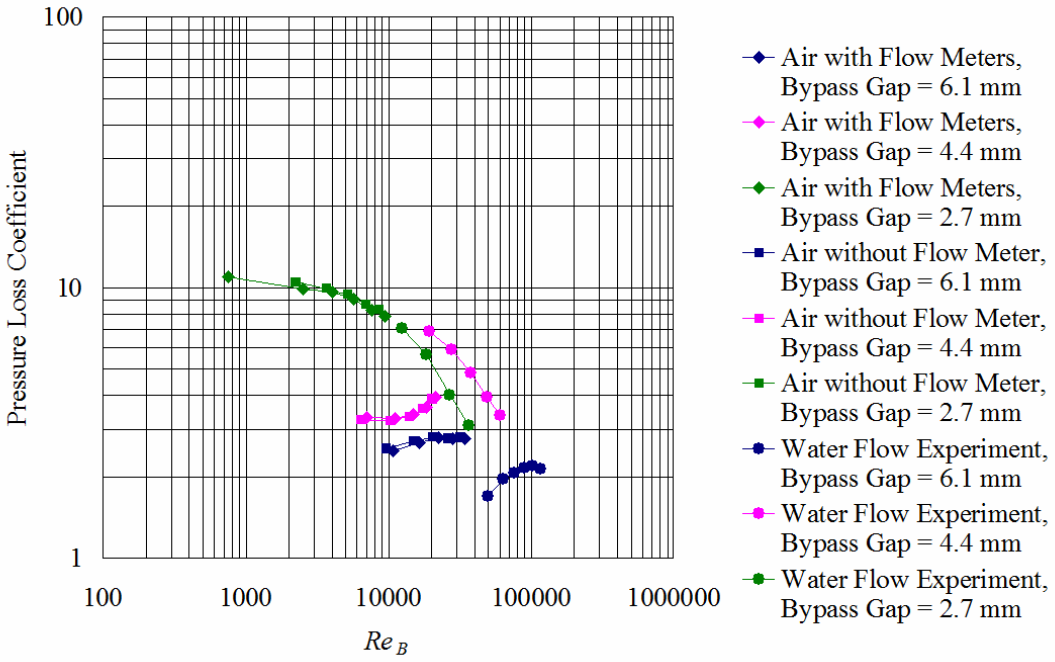

Figure 58. Pressure loss coefficients from bypass flow experiments

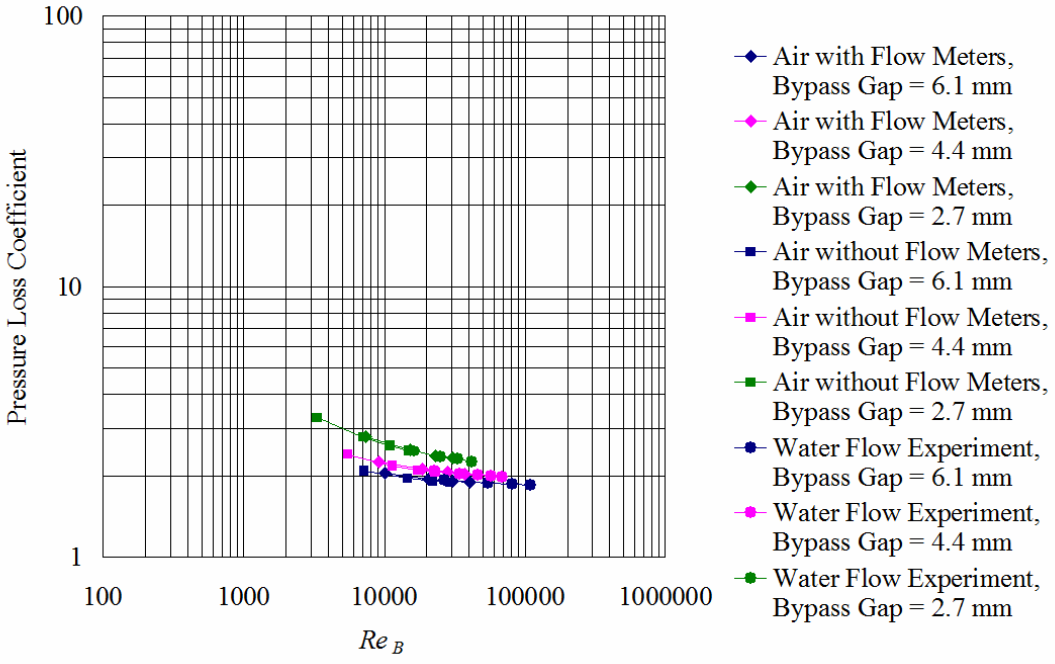

Figure 59. Pressure loss coefficients from bypass flow simulations

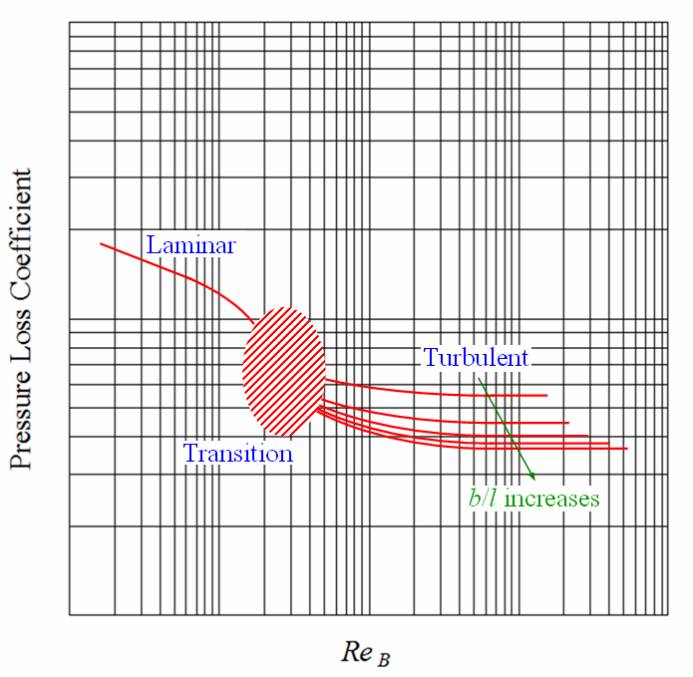

Figure 60. Imagination of ideal pressure loss coefficient diagram

The first issue that should be mentioned is pressure drop of flow through bypass gaps taken from bypass flow experiments and simulation is the combination of pressure losses resulted from (1) sudden contraction from flow passage before upstream of the blocks to bypass gaps, (2) flow between two walls of bypass gaps which can be treated as flow between two parallel plates, and (3) sudden expansion from bypass gaps to flow passage downstream of the blocks.

Results from bypass flow simulations show that pressure loss coefficient depends on *b*/*l* only, does not depend on both downstream condition and working fluid. Although experimental data from air and water flow experiments does not confirm this issue, better results can be expected in new bypass flow experiments after some improvements has been included in new design for bypass flow facility.

The curve of pressure loss coefficient when Re_B is very low in laminar flow regime is almost a straight line. When Re_B in laminar flow regime increases to reach transition flow regime, the curve of pressure loss coefficient becomes a concave function of Re_B which can be observed from experimental data. In turbulent flow regime, pressure loss coefficient should be constant when Re_B is very high. For Re_B that is not far from transition flow regime, the curve of pressure loss coefficient becomes a convex function of Re_B. This is the same situation as friction factor of flow in circular pipe (Moody diagram) [41] and friction factor of flow along flat plate [43]. The larger b/l (or larger area ratio between smaller and larger flow passage) should result in lower pressure loss coefficient as indicated in Figure 60. Range of Re_B for transition flow regime is not specified because pressure loss coefficients from experiments are scattered, while pressure loss coefficients from simulations do not give any information about it because of employing of a turbulence model throughout the domain.

5. CONCLUSION AND FUTURE WORKS

As closure of the study, experiences grasped from bypass flow experiments and bypass flow simulations are drawn as conclusion, and their possible extensions and improvements are suggested as future works.

5.1 Conclusion

The capabilities of present bypass flow facility are approximately summarized in Table 19 followed by conclusions drawn from experimental data and simulation results.

Table 19 Capability of bypass flow facility

	Air Flow Experiments with Flow Meters			Air Flow Experiments without Flow Meter			Water Flow Experiments		
	Bypass Gap (mm)			Bypass Gap (mm)			Bypass Gap (mm)		
	6.1	4.4	2.7	6.1	4.4	2.7	6.1	4.4	2.7
Maximum Flow Rate (cfm or gpm)	115	80	50	220	200	160	215	150	115
Bypass Flow Fraction (%)	77	69	45	37	27	13	58	40	30
Maximum Re_C	2680	2710	2720	14100	14300	14000	21300	19200	17800
Maximum Re_B	34300	21200	9360	31800	20200	8630	116000	60800	36600
Pressure Drop of Flow through Bypass Gaps (kPa)	3.27	3.39	3.45	2.94	3.13	3.20	68.3	54.4	46.4

From Table 19, there are few issues about *air flow experiments* that should be mentioned again. Maximum coolant channel Reynolds number (Re_C) does not depend on bypass gap width but depends on downstream condition of the blocks, while maximum bypass gap Reynolds number (Re_B) strongly depends on bypass gap width and slightly depends on downstream condition of the blocks. For *water flow experiments*, maximum

Re_C changes with bypass gap width due to method of bypass gap varying. No conclusion about Re_B can be drawn because there is only one set of water flow experiments.

5.1.1 Bypass Flow Experiments

Firstly, air flow experiments with flow meters are conducted to test the facility and to examine flow measurement method and flow rate estimation. This set of air flow experiments results in high bypass flow fractions which are much higher than bypass flow fraction in nuclear reactor operation. So air flow experiments are modified by removing all flow meters connected from the blocks. As expected, bypass flow fraction is decreased.

Because flow meters cannot be attached to all flow passages, VelociCalc air velocity meter is used in measuring maximum speed of air at center line of the pipe. These two sets of air flow experiments reveal that flow rate estimation yield accurate values when Reynolds number of flow in pipe is greater than 10000.

The experimental data shows that bypass flow fraction should be constant if flow regime in bypass gaps is turbulent and it will decrease considerably when flow regime in bypass gaps is laminar. The plot of pressure drop versus Re_B shows that pressure drop of flow through bypass gaps is not affected by downstream condition of the blocks. Therefore, changing downstream condition of the blocks is an approach to vary bypass flow fraction in bypass flow experiment to attain actual condition of nuclear reactor operation.

After obtaining ranges of Re_C and Re_B from air flow experiments, water flow experiments are conducted to get higher ranges of those Reynolds numbers. It is found

that bypass flow fraction increases with increasing of total flow rate. This is because larger pressure force at higher flow rate pushes slightly tilted blocks to their favorable positions in vertical planes which is not the case in air flow experiments.

To clarify conclusion from bypass flow experiments, all features mentioned in the preceding paragraphs are restated as follows.

Effects of Bypass Gap Width

It is obvious from all bypass flow experiments and simulations that bypass flow fraction, Re_B and pressure drop are strongly depended on bypass gap width while Re_C is not. Decrease in bypass gap width results in higher pressure drop of flow through bypass gaps and lower bypass flow fraction as a consequence.

Effects of Downstream Condition of the Blocks

Downstream condition of the blocks can alter bypass flow fraction considerably but does not effect pressure drop of flow through bypass gaps (also, pressure loss coefficient) as a function of Re_B. These issues can be observed from data of two sets of air flow experiments (air flow with flow meters and without flow meter) plotted in Figure 15 and Figure 18, respectively. Because there is no change in upstream condition of the blocks and in bypass flow passage, the conclusion on pressure drop of flow through bypass gaps is limited to downstream condition of the blocks only.

Varying of Bypass Flow Fraction

From two air flow experiments, bypass flow fraction can be varied by changing pressure loss of flow through the blocks. In present study, this can be accomplished by removing all flow meters connected from the blocks to reduce bypass flow fraction.

Another example in the work of Kaburaki and Takizuka [22] is that an orifice plate was placed on the top of each coolant channel to simulate the coolant flow in the blocks at the periphery of reactor core. Because bypass flow fractions from almost all bypass flow experiments are higher than the range between 10% and 25% [42], any modification in experiments that results in reduction of bypass flow fraction is preferred.

Inclination of the Blocks

The arrangement method of the blocks in present study cannot exactly place them in vertical planes and results in slight inclination of them as shown in Figure 61. Their inclinations cause larger pressure drop of flow through bypass gaps, at the same time, smaller bypass flow fraction than the values as it should be when all blocks are in vertical planes. Consequently, this can increase discrepancies in pressure drop and bypass flow fraction from experiments and simulations. Furthermore, block arrangement method should be improved in new bypass flow facility design.

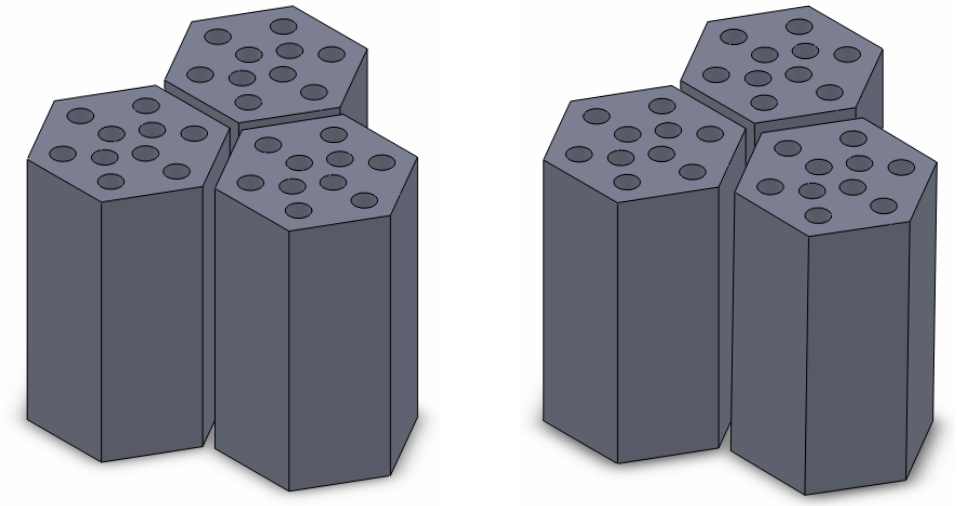

(a) vertical blocks (b) inclined blocks

Figure 61. Inclination of the blocks in bypass flow experiments

Attaining of Higher Reynolds Number in Experiments

Higher Reynolds numbers of flow through coolant channels (Re_C) and bypass gaps (Re_B) can be attained when working fluid is liquid. This will benefit in extending the range of Reynolds number in bypass flow experiments.

Avoiding of Flow Rate Estimation

Based on the data obtained from bypass flow experiments and simulations for 6.1-mm bypass gap width (used in calibrating geometry of the models), pressure drops from water flow simulations and pressure drops from water flow experiments are closer to each other than the cases when working fluid is air. The most plausible cause for this situation is that bypass flow fraction in the case of water is more accurate than that in the case of air. Only one different process in bypass flow fraction calculations is that all flow rates in water flow experiments are measured directly, while there is at least one flow rate in air flow experiments estimated by using the power law for velocity profile. Therefore, the first approach should be employed if possible.

5.1.2 Bypass Flow Simulations

Pipe flow and channel flow are two problems selected for validation exercises of STAR-CCM+ software to find meshing parameters which consist of absolute prism layer thickness, number of prism layers and stretching ratio. Among three turbulence models, realizable k-epsilon model with two-layer all y+ wall treatment yields closest values of friction factor for both pipe flow and channel flow.

Models for bypass flow simulations are constructed using meshing parameters obtained from validation exercises by matching bypass flow fraction from bypass flow

experiments with 6.1-mm bypass gap. These models are used in grid independent study to specify appropriate base size for bypass flow simulations. It is suggested that the narrowest gap between two walls substracted by (absolute) prism layer thickness should be at least 3.5 times of base size used in bypass flow simulations.

Results from air and water flow simulations for 4.4- and 2.7-mm bypass gap are compared with those from experiments. Results from the case of 4.4-mm bypass gap show better agreements with experiments than the case of 2.7-mm bypass gap because there are many sources of error when bypass gap is varied. In bypass flow experiments, the blocks may be tilted because of the method of block arrangement. When bypass gap becomes narrower, flow regime in bypass gaps will change to be laminar which cannot be handled in bypass flow simulations because selected turbulence model is employed throughout the computational domain.

However, bypass flow simulations predict that pressure loss coefficient should depend on Re_B and bypass gap width, although the experimental data cannot confirm it. Additionally, p-cymene flow simulations are performed to provide velocity profiles of flow in coolant channels and bypass gaps. Also, suggestion for flow visualization can be made.

Because the guidelines for bypass flow simulations are very important, they are restated as follows.

Guideline for Base Size in Bypass Flow Simulations

From the section of grid independent study, a guideline for base size of cells used in simulations can be drawn. The narrowest gap in computational domain (bypass gap in

present study) excludes prism layer thickness should be *at least 3.5 times* of base size. For example, if bypass gap width is 4.0 mm and prism layer thickness is 0.4 mm, the distance used in estimating base size will be 3.2 mm and the appropriate base size that should be set in meshing process to get grid independent solution should be less than 0.9 mm. The idea of this guideline is clarified in Figure 62.

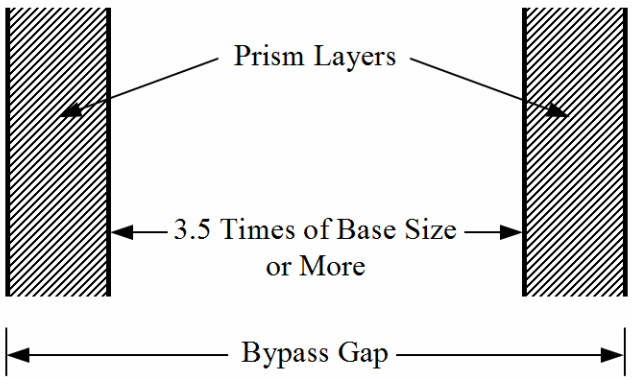

Figure 62. Guideline about base size for bypass flow simulations

Guideline for Prism Layers in Bypass Flow Simulations

From the validation exercises in Appendix C, two guidelines about prism layers used in simulations can be suggested. The first one is that *absolute thickness* should be set in meshing process instead of relative thickness. The reason behind this guideline is that using relative thickness will lead to too thin prism layer thickness when base size is too small. This can cause very large normalized residual of turbulent energy dissipation rate in older version of STAR-CCM+ which affects other variables in the simulations. It is suggested in the validation exercises that absolute thickness should be *0.4 mm* for the range of Reynolds number of flow in circular pipe and flow between two parallel plates that can be attained in experiments of present study.

Another guideline about prism layers is number of prism layers set in meshing process. The minimum number of prism layer that yields the first layer adjacent to the wall lies within viscous sublayer depends on prism layer thickness and stretching ratio. Based on absolute thickness of 0.4 mm given in the preceding paragraph, the minimum number of prism layer is varied with stretching ratio. For default value of stretching ratio at 1.5, number of prism layers should be 12 or more. For stretching ratio of 1.35 used in all bypass flow simulations, number of prism layers should be 15 or more. In present study, only seven prism layers are sufficient because near wall phenomena such as wall shear stress and wall heat flux are not focused and default damping functions can model turbulent kinetic energy and turbulent dissipation rate in the region very close to solid walls efficiently. It can prevent stopping of simulation due to overflow problem caused by very large normalized residual of turbulent dissipation rate, especially in the older version of STAR-CCM+, while the values taken from surface integral and surface average still be accurate as seen from very good agreements of bypass flow fractions in bypass flow simulation using several base sizes in the section of grid independent study.

5.2 Future Works

Because there are many features in present study that can be improved, future works related to bypass flow experiments and simulations may be suggested as follows.

5.2.1 Bypass Flow Experiments

As seen from Table 18, block height to block side length ratio (h/l) and block height to coolant channel diameter ratio (h/d) are less than their values for standard fuel

element using in real reactors. New bypass flow facility should be larger than this bypass flow facility to reduce the difference in these geometric parameters between experiments and real reactors and to attain the desired values of Re_C and Re_B. Additionally, more pressure taps may be located in coolant channels and bypass gaps to investigate more details of pressure drops of flow through coolant channels and bypass gaps. The example of pressure distribution along a line passes through bypass gap that will be compared with experiments in the future is shown in Figure 41.

Two features that can be included to new bypass flow facility are new block arrangement method and changing the shape of flow passage connected from the blocks. Bypass gap width must be varied precisely and inclination of the blocks must be minimized by new block arrangement method, while sudden contraction of flow passage connected from the blocks must be change to gradual contraction in new bypass flow facility to reduce pressure drop of flow through the blocks.

Another layer of prismatic block may be added to the new bypass flow facility to study effects of uniform crossflow gap on bypass flow fraction and pressure drop of flow through each flow passage. Moreover, wedge-shaped crossflow gap may be arranged by installing a special flange between two layers prismatic block.

After new bypass flow experiments are conducted successfully, thermal issues should be considered for more realistic study of bypass flow because there are so many topics related to bypass flow study when thermal issue arisen such as effects of temperature-dependent properties of working fluid on flow pattern and heat transfer characteristics of bypass flow.

5.2.2 Bypass Flow Simulations

Because pressure drop of flow through bypass gaps is mainly contributed by flow through sudden contraction, it should be added to validation exercises in parallel with pipe flow and channel flow. Also, all constants specified in each turbulence model should be adjusted until they yield satisfactory results. Besides three turbulence models based on Reynolds-averaged equations employed in bypass flow simulations of present study, Large-Eddy Simulation (LES) can be included for comparison and started in validation exercises as done in present study.

Models for new bypass flow simulations can be constructed based on meshing parameters found from new validation exercises by matching bypass flow fraction from bypass flow experiments with the widest bypass gap. These models are used in grid independent study to specify appropriate base size for bypass flow simulations by starting from base size suggested in present study. Furthermore, tetrahedral mesh should be employed to compare with trimmer mesh.

To handle different flow regimes exist simultaneously in computational domain, multi-region domain must be constructed for bypass flow simulations and assigned to each region with appropriate flow regime known as *a priori* from present study.

Air and water flow simulations can be performed and their results can be compared with experimental data for remaining gaps. Also, p-cymene flow simulations should be performed to compare velocity profiles in coolant channels and bypass gaps with those obtained from PIV technique. Furthermore, design of bypass flow facility for thermal/hydraulic experiments may be started with simulation experiences at this state.

REFERENCES

[1] http://www.world-nuclear.org/info/inf77.html

[2] http://www.gen-4.org

[3] http://www.usnuclearenergy.org/GEN%20IV%20Reactors.htm

[4] http://www.inl.gov/technicalpublications/Documents/2559926.pdf

[5] https://inlportal.inl.gov/portal/server.pt?open=514&objID=2251&parentname=CommunityPage&parentid=13&mode=2

[6] http://www.iaea.org/inisnkm/nkm/aws/htgr/fulltext/gcr_review_01.pdf

[7] http://www.inl.gov/research/very-high-temperature-reactor

[8] http://www.iaea.org/inisnkm/nkm/aws/htgr/fulltext/gcr_review_02.pdf

[9] C. R. McCullough, "Summary Report on Design and Development of High Temperature Gas-Cooled Power Pile," Oak Ridge, TN, September 15, 1947.

[10] F. Carre, P. Yvon, W. J. Lee, Y. Dong, Y. Tachibana, and D. Petti, "VHTR – Ongoing International Projects," *GIF Symposium*, Paris, France, September 9-10, 2009.

[11] Z. Zhang, Z. Wu, D. Wang, Y. Xu, Y. Sun, F. Li, and Y. Dong, "Current Status and Technical Description of Chinese 2×250 MW_{th} HTR-PM Demonstration Plant," *Nuclear Engineering and Design*, vol.239, pp.1212-1219, 2009.

[12] http://www.iaea.org/inisnkm/nkm/aws/htgr/fulltext/gcr_review_04.pdf

[13] http://gt-mhr.ga.com

[14] P. E. MacDonald, "NGNP Preliminary Point Design – Results of the Initial Neutronics and Thermal-Hydraulic Assessments," *INEEL/EXT-03-00870 Rev.1*, Idaho National Engineering and Environmental Laboratory, September 2003.

[15] G. Melese and R. Katz, *Thermal and Flow Design of Helium-Cooled Reactors*, American Nuclear Society, La Grange Park, Illinois, USA, 1984.

[16] S. Maruyama, K. Yamashita, N. Fujimoto, I. Murata, and Y. Sudo, "Evaluation of Hot Spot Factors for Thermal and Hydraulic Design of HTTR," *Journal of Nuclear Science and Technology*, vol.30, pp.1186-1194, 1993.

[17] H. G. Olson, H. L. Brey, and D. W. Warembough, "The Fort St. Vrain High Temperature Gas-Cooled Reactor: X. Core Temperature Fluctuations," *Nuclear Engineering and Design*, vol.72, pp.125-137, 1982.

[18] H. G. Groehn, "Disturbance of the Cooling Gas Distribution in HTGR Fuel Blocks due to Bypass Flow," *Proceedings of ANS/ASME/NRC International Topical Meeting on Nuclear Reactor Thermal-Hydraulics*, NY, USA, October 5-8, 1980.

[19] H. G. Groehn, "Estimate of Cross Flow in High Temperature Gas-Cooled Reactor Fuel Block," *Nuclear Technology*, vol.56, pp.392-400, 1982.

[20] S. Shiozawa, S. Fujikawa, T. Iyoku, K. Kunitomi, and Y. Tachibana, "Overview of HTTR Design Features," *Nuclear Engineering and Design*, vol.233, pp.11-21, 2004.

[21] H. Kaburaki and T. Takizuka, "Leakage Flows in High-Temperature Gas-Cooled Reactor Graphite Fuel Element," *Journal of Nuclear Science and Technology*, vol.22, pp.387-397, 1985.

[22] H. Kaburaki and T. Takizuka, “Effect of Crossflow on Flow Distribution in HTGR Core Column,” *Journal of Nuclear Science and Technology*, vol.24, pp.516-525, 1987.

[23] H. Kaburaki and T. Takizuka, “Crossflow Characteristics of HTGR Fuel Blocks,” *Nuclear Engineering and Design*, vol.120, pp.425-434, 1990.

[24] H. Kaburaki and T. Takizuka, “Leakage Flow Characteristics of Seal Mechanism for HTGR Core Support Blocks,” *Journal of Nuclear Science and Technology*, vol.24, pp.742-747, 1987.

[25] H. Kaburaki and T. Takizuka, “Leakage Flow Characteristics of Highly Effective Graphite Seal Mechanism for HTGR Core Support Blocks,” *Journal of Nuclear Science and Technology*, vol.25, pp.92-99, 1988.

[26] S. Maruyama, K. Takase, R. Hino, N. Izawa, M. Hishida, and H. Shimomura, “Experimental Studies on the Thermal and Hydraulic Performance of the Fuel Stack of the VHTR Part I: HENDEL Multi-Channel Test Rig with Twelve Fuel Rods,” *Nuclear Engineering and Design*, vol.102, pp.1-9, 1987.

[27] S. Maruyama, K. Takase, R. Hino, N. Izawa, M. Hishida, and H. Shimomura, “Experimental Studies on the Thermal and Hydraulic Performance of the Fuel Stack of the VHTR Part II: HENDEL Single-Channel Tests with Uniform Heat Flux,” *Nuclear Engineering and Design*, vol.102, pp.11-20, 1987.

[28] S. Maruyama, N. Fujimoto, Y. Sudo, T. Murakami, and S. Fujii, “Evaluation of Core Thermal and Hydraulic Characteristics of HTTR,” *Nuclear Engineering and Design*, vol.152, pp.183-196, 1994.

[29] E. Takada, S. Nakagawa, N. Fujimoto, and D. Tochio, "Core Thermal-Hydraulic Design," *Nuclear Engineering and Design*, vol.233, pp.37-43, 2004.

[30] M. Nakano, N. Tsuji, and Y. Tazawa, "Conceptual Reactor Design Study of Very High Temperature Reactor (VHTR) with Prismatic-Core Type," *Journal of Power and Energy Systems*, vol.2, pp.768-774, 2008.

[31] N.-I. Tak, M.-H. Kim, and W. J. Lee, "Numerical Investigation of a Heat Transfer within the Prismatic Fuel Assembly of a Very High Temperature Reactor," *Annals of Nuclear Energy*, vol.35, pp.1892-1899, 2008.

[32] H. Sato, R. Johnson, and R. Schultz, "Computational Fluid Dynamic Analysis of Core Bypass Flow Phenomena in a Prismatic VHTR," *Annals of Nuclear Energy*, vol.37, pp.1172-1185, 2010.

[33] R. W. Johson and H. Sato, "Bypass Flow Computations Using A One-Twelfth Symmetric Sector for Normal Operation in A 350 MWth Prismatic VHTR," *Nuclear Engineering and Design*, vol.251, pp.84-91, 2012.

[34] Y. H. Tung, R. W. Johnson, and H. Sato, "Effects of Graphite Surface Roughness on Bypass Flow Computations for An HTGR," *Proceedings of the ASME 2011 Pressure Vessels and Piping Division Conference*, Baltimore, Maryland, USA, July 17-21, 2011.

[35] S.-J. Yoon, Y.-J. Cho, K.-Y. Kim, M.-H. Kim, W.-J. Lee, and G.-C. Park, "Experimental Evaluation of the Bypass Flow in the VHTR Core," *Transactions*, SMiRT19, Toronto, August 2007.

[36] S.-J. Yoon, C.-Y. Jin, J.-H. Lee, M.-H. Kim, and G.-C. Park, "Study on the Flow Distribution in Prismatic VHTR Core with A Multiple-Block Experiment and CFD Analysis," *Nuclear Engineering and Design*, vol.241, pp.5174-5182, 2011.

[37] S.-J. Yoon, J.-H. Lee, M.-H. Kim, and G.-C. Park, "The Effects of Crossflow Gap and Axial Bypass Gap Distribution on the Flow Characteristics in Prismatic VHTR Core," *Nuclear Engineering and Design*, vol.250, pp.465-479, 2012.

[38] M.-H. Kim and H.-S. Lim, "Evaluation of the Influence of Bypass Flow Gap Distribution on the Core Hot Spot in A Prismatic VHTR Core," *Nuclear Engineering and Design*, vol.241, pp.3076-3085, 2011.

[39] TSI Series 4000/4100 General Purpose Thermal Mass Flowmeters, *Operation and Service Manual*, October 2002.

[40] J. O. Hinze, *Turbulence*, 2nd edition, McGraw-Hill, USA, 1975.

[41] R. W. Fox, A. T. McDonald, and P. J. Pritchard, *Introduction to Fluid Mechanics*, 6th edition, John Wiley & Sons, USA, 2004.

[42] Idaho National Engineering and Environmental Laboratory, "*Next Generation Nuclear Plant Research and Development Program Plan*," INEEL/EXT-05-02581, Idaho, USA, 2005.

[43] H. Schlichting, *Boundary Layer Theory*, 7th edition, McGraw-Hill, USA, 1979.

[44] S. W. Churchill and C. Chan, "Improved Correlating Equations for the Friction Factor for Fully Turbulent Flow in Round Tubes and between Identical Parallel Plates, both Smooth and Naturally Rough," *Industrial & Engineering Chemistry Research*, vol. 33, pp. 2016-2019, 1994.

APPENDIX A

EXPERIMENTAL DATA AND CALCULATION DETAILS

Five sets of data are taken for each bypass flow experiment. Sample mean ($\bar{x}$) and sample standard deviation (s) of physical quantities are calculated and summarized in following tables. All numbers for sample standard deviation are in italic style and, if necessary, calculation details for some physical quantities are provided.

Sample Mean:
$$\bar{x} = \frac{1}{n}\sum_{i=1}^{n} x_i \tag{A.1}$$

Sample Standard Deviation:
$$s = \sqrt{\frac{1}{n-1}\sum_{i=1}^{n}(x_i - \bar{x})^2} \tag{A.2}$$

Table 20 Data from air flow experiments with flow meters with 6.1-mm bypass gap

No.	Volume Flow Rate			Δp	V_{inlet}	V_{bypass}
	Block 1 (cfm)	Block 2 (cfm)	Block 3 (cfm)	(in.-H_2O)	at Centerline (ft/min)	at Centerline (ft/min)
1	1.122	1.147	1.087	0.13	68.2	330.0
	0.003	*0.004*	*0.006*	*0.005*	*1.304*	*4.637*
2	2.528	2.588	2.412	1.22	134.6	700.0
	0.012	*0.006*	*0.002*	*0.045*	*2.302*	*8.660*
3	4.049	4.107	3.809	3.00	201.0	1066.0
	0.006	*0.007*	*0.007*	*0.000*	*1.414*	*8.944*
4	5.707	5.703	5.236	5.60	265.0	1424.0
	0.006	*0.016*	*0.004*	*0.000*	*1.732*	*5.477*
5	7.377	7.390	6.666	9.00	330.6	1806.0
	0.010	*0.026*	*0.006*	*0.000*	*2.074*	*5.477*
6	9.181	9.219	8.237	13.12	402.2	2180.0
	0.011	*0.031*	*0.016*	*0.045*	*3.194*	*10.000*

Table 21 Flow rate calculations in 8-inch diameter inlet pipe of air flow experiments with flow meters with 6.1-mm bypass gap

No.	V_{bypass} at Centerline (m/s)	Index *n* for Power Law (-)	V_{av} (m/s)	*Re* (-)	Flow Regime Re_{cr} = 2300 (-)	Flow Rate (cfm)
1	0.3465	4.8803	0.2608	3383	Turbulent	17.922
2	0.6838	5.4062	0.5282	6851	Turbulent	36.293
3	1.0211	5.7181	0.7992	10366	Turbulent	54.917
4	1.3462	5.9324	1.0625	13781	Turbulent	73.006
5	1.6794	6.1053	1.3338	17301	Turbulent	91.654
6	2.0432	6.2584	1.6313	21160	Turbulent	112.096

Table 22 Flow rate calculations in 3-inch diameter pipe connected from bypass passage of air flow experiments with flow meters with 6.1-mm bypass gap

No.	V_{bypass} at Centerline (m/s)	Index *n* for Power Law (-)	V_{av} (m/s)	*Re* (-)	Flow Regime Re_{cr} = 2300 (-)	Flow Rate (cfm)
1	1.6764	5.3407	1.2911	6280	Turbulent	12.476
2	3.5560	5.9255	2.8058	13647	Turbulent	27.112
3	5.4153	6.2538	4.3231	21028	Turbulent	41.774
4	7.2339	6.4809	5.8181	28300	Turbulent	56.219
5	9.1745	6.6677	7.4215	36098	Turbulent	71.713
6	11.0744	6.8160	8.9957	43764	Turbulent	86.942

Table 23 Data from air flow experiments with flow meters with 4.4-mm bypass gap

No.	Volume Flow Rate			Δp	V_{inlet}	V_{bypass}
	Block 1 (cfm)	Block 2 (cfm)	Block 3 (cfm)	(in.-H_2O)	at Centerline (ft/min)	at Centerline (ft/min)
1	1.137	1.159	1.104	0.13	50.8	227.4
	0.005	*0.006*	*0.005*	*0.008*	*0.837*	*3.286*
2	2.561	2.607	2.455	1.30	101.2	462.0
	0.010	*0.012*	*0.007*	*0.000*	*1.095*	*4.899*
3	4.107	4.132	3.868	3.12	147.6	716.0
	0.016	*0.016*	*0.011*	*0.045*	*2.408*	*6.519*
4	5.784	5.735	5.325	5.80	196.8	959.0
	0.022	*0.033*	*0.011*	*0.000*	*3.347*	*11.937*
5	7.449	7.413	6.788	9.32	246.0	1174.0
	0.026	*0.038*	*0.012*	*0.045*	*5.339*	*5.477*
6	9.263	9.235	8.394	13.62	292.2	1358.0
	0.038	*0.050*	*0.027*	*0.045*	*1.924*	*4.472*

Table 24 Flow rate calculations in 8-inch diameter inlet pipe of air flow experiments with flow meters with 4.4-mm bypass gap

No.	V_{bypass} at Centerline (m/s)	Index n for Power Law (-)	V_{av} (m/s)	Re (-)	Flow Regime Re_{cr} = 2300 (-)	Flow Rate (cfm)
1	0.2581	4.6598	0.1919	2489	Turbulent	13.185
2	0.5141	5.1861	0.3931	5099	Turbulent	27.011
3	0.7498	5.4766	0.5810	7536	Turbulent	39.922
4	0.9997	5.7016	0.7820	10143	Turbulent	53.733
5	1.2497	5.8753	0.9842	12765	Turbulent	67.625
6	1.4844	6.0095	1.1749	15239	Turbulent	80.729

Table 25 Flow rate calculations in 3-inch diameter pipe connected from bypass passage of air flow experiments with flow meters with 4.4-mm bypass gap

No.	V_{bypass} at Centerline (m/s)	Index n for Power Law (-)	V_{av} (m/s)	Re (-)	Flow Regime Re_{cr} = 2300 (-)	Flow Rate (cfm)
1	1.1552	5.0551	0.8776	4269	Turbulent	8.480
2	2.3470	5.6026	1.8283	8893	Turbulent	17.667
3	3.6373	5.9433	2.8718	13969	Turbulent	27.750
4	4.8717	6.1716	3.8782	18864	Turbulent	37.475
5	5.9639	6.3298	4.7732	23217	Turbulent	46.123
6	6.8986	6.4435	5.5418	26956	Turbulent	53.550

Table 26 Data from air flow experiments with flow meters with 2.7-mm bypass gap

No.	Volume Flow Rate			Δp	V_{inlet}	V_{bypass}
	Block 1 (cfm)	Block 2 (cfm)	Block 3 (cfm)	(in.-H_2O)	at Centerline (ft/min)	at Centerline (ft/min)
1	1.162	1.184	1.125	0.14	24.0	76.2
	0.003	*0.003*	*0.004*	*0.009*	*1.000*	*8.955*
2	2.597	2.661	2.498	1.30	54.4	171.4
	0.008	*0.013*	*0.004*	*0.000*	*2.302*	*5.320*
3	4.145	4.195	3.918	3.20	80.8	269.6
	0.015	*0.010*	*0.008*	*0.000*	*1.095*	*4.827*
4	5.824	5.831	5.365	5.96	105.2	375.8
	0.028	*0.011*	*0.013*	*0.055*	*3.347*	*5.404*
5	7.491	7.482	6.821	9.52	133.2	494.6
	0.046	*0.033*	*0.040*	*0.045*	*2.950*	*3.435*
6	9.279	9.279	8.413	13.86	158.0	609.0
	0.074	*0.064*	*0.055*	*0.089*	*4.183*	*8.216*

Table 27 Flow rate calculations in 8-inch diameter inlet pipe of air flow experiments with flow meters with 2.7-mm bypass gap

No.	V_{bypass} at Centerline (m/s)	Index *n* for Power Law (-)	V_{av} (m/s)	*Re* (-)	Flow Regime Re_{cr} = 2300 (-)	Flow Rate (cfm)
1	0.1219	-	0.0610	791	Laminar	4.189
2	0.2764	4.7094	0.2061	2673	Turbulent	14.160
3	0.4105	5.0104	0.3111	4036	Turbulent	21.379
4	0.5344	5.2147	0.4092	5308	Turbulent	28.117
5	0.6767	5.3980	0.5225	6777	Turbulent	35.903
6	0.8026	5.5296	0.6234	8085	Turbulent	42.833

Table 28 Flow rate calculations in 3-inch diameter pipe connected from bypass passage of air flow experiments with flow meters with 2.7-mm bypass gap

No.	V_{bypass} at Centerline (m/s)	Index *n* for Power Law (-)	V_{av} (m/s)	*Re* (-)	Flow Regime Re_{cr} = 2300 (-)	Flow Rate (cfm)
1	0.3871	-	0.1935	941	Laminar	1.870
2	0.8707	4.8353	0.6539	3181	Turbulent	6.318
3	1.3696	5.1861	1.0472	5094	Turbulent	10.119
4	1.9091	5.4409	1.4769	7184	Turbulent	14.272
5	2.5126	5.6557	1.9616	9542	Turbulent	18.955
6	3.0937	5.8169	2.4309	11824	Turbulent	23.490

Table 29 Data from air flow experiments without flow meter with 6.1-mm bypass gap

No.	Volume Flow Rate			Δp	V_{inlet}	V_{bypass}
	Block 1 (cfm)	Block 2 (cfm)	Block 3 (cfm)	(in.-H_2O)	at Centerline (ft/min)	at Centerline (ft/min)
1	-	-	-	0.11	127.0	295.8
				0.004	*2.646*	*5.167*
2	-	-	-	1.12	247.4	632.0
				0.045	*4.669*	*2.739*
3	-	-	-	2.72	363.0	979.0
				0.045	*2.550*	*6.519*
4	-	-	-	5.00	497.4	1314.0
				0.000	*5.727*	*5.477*
5	-	-	-	8.02	640.0	1676.0
				0.045	*5.000*	*5.477*
6	-	-	-	11.80	779.0	2024.0
				0.000	*4.183*	*5.477*

Table 30 Flow rate calculations in 8-inch diameter inlet pipe of air flow experiments without flow meter with 6.1-mm bypass gap

No.	V_{bypass} at Centerline (m/s)	Index *n* for Power Law (-)	V_{av} (m/s)	*Re* (-)	Flow Regime Re_{cr} = 2300 (-)	Flow Rate (cfm)
1	0.6452	5.3612	0.4974	6451	Turbulent	34.175
2	1.2568	5.8797	0.9899	12840	Turbulent	68.022
3	1.8440	6.1787	1.4683	19046	Turbulent	100.895
4	2.5268	6.4256	2.0287	26313	Turbulent	139.396
5	3.2512	6.6234	2.6265	34067	Turbulent	180.473
6	3.9573	6.7777	3.2116	41657	Turbulent	220.681

Table 31 Flow rate calculations in 3-inch diameter pipe connected from bypass passage of air flow experiments without flow meter with 6.1-mm bypass gap

No.	V_{bypass} at Centerline (m/s)	Index n for Power Law (-)	V_{av} (m/s)	Re (-)	Flow Regime Re_{cr} = 2300 (-)	Flow Rate (cfm)
1	1.5027	5.2558	1.1528	5607	Turbulent	11.139
2	3.2106	5.8451	2.5255	12284	Turbulent	24.404
3	4.9733	6.1876	3.9613	19268	Turbulent	38.277
4	6.6751	6.4175	5.3578	26061	Turbulent	51.771
5	8.5141	6.6092	6.8750	33441	Turbulent	66.433
6	10.2819	6.7576	8.3395	40564	Turbulent	80.583

Table 32 Data from air flow experiments without flow meter with 4.4-mm bypass gap

No.	Volume Flow Rate			Δp	V_{inlet}	V_{bypass}
	Block 1 (cfm)	Block 2 (cfm)	Block 3 (cfm)	(in.-H_2O)	at Centerline (ft/min)	at Centerline (ft/min)
1	-	-	-	0.12	114.8	207.4
				0.005	*1.304*	*4.980*
2	-	-	-	1.20	230.0	426.8
				0.000	*2.121*	*5.215*
3	-	-	-	2.84	338.4	670.0
				0.055	*2.510*	*10.000*
4	-	-	-	5.32	451.8	906.0
				0.045	*5.630*	*12.942*
5	-	-	-	8.56	569.0	1114.0
				0.055	*2.236*	*13.416*
6	-	-	-	12.58	684.0	1296.0
				0.084	*4.183*	*5.477*

Table 33 Flow rate calculations in 8-inch diameter inlet pipe of air flow experiments without flow meter with 4.4-mm bypass gap

No.	V_{bypass} at Centerline (m/s)	Index *n* for Power Law (-)	V_{av} (m/s)	*Re* (-)	Flow Regime Re_{cr} = 2300 (-)	Flow Rate (cfm)
1	0.5832	5.2819	0.4479	5810	Turbulent	30.780
2	1.1684	5.8217	0.9183	11911	Turbulent	63.097
3	1.7191	6.1238	1.3662	17721	Turbulent	93.877
4	2.2951	6.3501	1.8381	23842	Turbulent	126.306
5	2.8905	6.5307	2.3284	30202	Turbulent	159.995
6	3.4747	6.6757	2.8115	36467	Turbulent	193.185

Table 34 Flow rate calculations in 3-inch diameter pipe connected from bypass passage of air flow experiments without flow meter with 4.4-mm bypass gap

No.	V_{bypass} at Centerline (m/s)	Index *n* for Power Law (-)	V_{av} (m/s)	*Re* (-)	Flow Regime Re_{cr} = 2300 (-)	Flow Rate (cfm)
1	1.0536	4.9823	0.7974	3879	Turbulent	7.706
2	2.1681	5.5411	1.6847	8194	Turbulent	16.279
3	3.4036	5.8914	2.6821	13046	Turbulent	25.917
4	4.6025	6.1270	3.6582	17794	Turbulent	35.348
5	5.6591	6.2884	4.5230	22000	Turbulent	43.705
6	6.5837	6.4072	5.2826	25695	Turbulent	51.045

Table 35 Data from air flow experiments without flow meter with 2.7-mm bypass gap

No.	Volume Flow Rate			Δp	V_{inlet}	V_{bypass}
	Block 1 (cfm)	Block 2 (cfm)	Block 3 (cfm)	(in.-H_2O)	at Centerline (ft/min)	at Centerline (ft/min)
1	-	-	-	0.12 *0.004*	96.2 *1.304*	61.0 *4.472*
2	-	-	-	1.20 *0.000*	193.8 *1.924*	153.0 *1.871*
3	-	-	-	2.92 *0.045*	284.2 *2.168*	247.0 *1.871*
4	-	-	-	5.42 *0.045*	372.6 *2.074*	345.0 *1.581*
5	-	-	-	8.80 *0.000*	472.6 *5.983*	456.8 *3.271*
6	-	-	-	12.86 *0.055*	572.0 *2.739*	563.0 *2.739*

Table 36 Flow rate calculations in 8-inch diameter inlet pipe of air flow experiments without flow meter with 2.7-mm bypass gap

No.	V_{bypass} at Centerline (m/s)	Index *n* for Power Law (-)	V_{av} (m/s)	*Re* (-)	Flow Regime Re_{cr} = 2300 (-)	Flow Rate (cfm)
1	0.4887	5.1449	0.3729	4837	Turbulent	25.625
2	0.9845	5.6885	0.7697	9983	Turbulent	52.886
3	1.4437	5.9868	1.1417	14809	Turbulent	78.453
4	1.8928	6.1984	1.5082	19563	Turbulent	103.634
5	2.4008	6.3853	1.9250	24969	Turbulent	132.273
6	2.9058	6.5352	2.3410	30365	Turbulent	160.861

Table 37 Flow rate calculations in 3-inch diameter pipe connected from bypass passage of air flow experiments without flow meter with 2.7-mm bypass gap

No.	V_{bypass} at Centerline (m/s)	Index n for Power Law (-)	V_{av} (m/s)	Re (-)	Flow Regime Re_{cr} = 2300 (-)	Flow Rate (cfm)
1	0.3099	-	0.1549	754	Laminar	1.497
2	0.7772	4.7494	0.5809	2826	Turbulent	5.613
3	1.2548	5.1175	0.9562	4651	Turbulent	9.240
4	1.7526	5.3756	1.3520	6576	Turbulent	13.064
5	2.3205	5.5941	1.8071	8790	Turbulent	17.462
6	2.8600	5.7554	2.2419	10905	Turbulent	21.663

Table 38 Data from water flow experiments with 6.1-mm bypass gap

No.	Total Flow (gpm)	Block 1 (gpm)	Block 2 (gpm)	Block 3 (gpm)	Δp (psi)
1	92.0	12.00	13.20	13.30	0.151
	0.000	*0.000*	*0.000*	*0.000*	*0.027*
2	117.0	15.50	16.64	16.94	1.577
	0.000	*0.000*	*0.055*	*0.055*	*0.029*
3	141.6	18.90	20.10	20.60	3.209
	0.548	*0.000*	*0.000*	*0.000*	*0.041*
4	165.8	22.20	23.42	24.20	5.252
	0.837	*0.071*	*0.045*	*0.000*	*0.057*
5	189.4	25.52	26.76	27.70	7.406
	0.548	*0.045*	*0.055*	*0.000*	*0.114*
6	215.0	28.68	30.02	31.14	9.908
	0.000	*0.045*	*0.045*	*0.055*	*0.090*

Table 39 Data from water flow experiments with 4.4-mm bypass gap

No.	Total Flow (gpm)	Block 1 (gpm)	Block 2 (gpm)	Block 3 (gpm)	Δp (psi)
1	55.6	11.48	11.60	11.94	0.384
	0.548	*0.045*	*0.000*	*0.055*	*0.012*
2	76.2	15.40	15.50	15.90	1.809
	0.447	*0.000*	*0.000*	*0.071*	*0.017*
3	98.6	19.20	19.38	19.90	3.559
	0.548	*0.000*	*0.045*	*0.071*	*0.029*
4	122.6	22.98	23.20	23.90	5.581
	0.894	*0.045*	*0.000*	*0.071*	*0.043*
5	146.4	26.58	26.84	27.76	7.887
	1.342	*0.045*	*0.055*	*0.089*	*0.039*

Table 40 Data from water flow experiments with 2.7-mm bypass gap

No.	Total Flow (gpm)	Block 1 (gpm)	Block 2 (gpm)	Block 3 (gpm)	Δp (psi)
1	50.6	12.24	12.36	12.76	0.641
	1.140	*0.055*	*0.055*	*0.055*	*0.024*
2	69.6	16.40	16.58	17.10	2.248
	0.548	*0.000*	*0.045*	*0.000*	*0.074*
3	91.6	20.58	20.78	21.58	4.258
	0.548	*0.084*	*0.045*	*0.045*	*0.030*
4	114.4	24.66	24.80	25.86	6.734
	0.548	*0.055*	*0.000*	*0.055*	*0.061*

APPENDIX B

PRESSURE DROP OF FLOW THROUGH FLOW STRAIGHTENERS

In all experiments, flow straighteners (Figure 63) are placed in the loop before fluid reaches prismatic blocks stacked in test section. Therefore, pressure drops obtained from bypass flow simulations and experiments cannot be compared directly as seen, for example, in the diagram of air flow experiments with flow meters in Figure 64.

Figure 63. Flow straightener

In Figure 64, the *light blue rectangle* that contains three prismatic blocks is the domain modeled in bypass flow simulations. The *light orange rectangle* that contains three flow meters represents the modification at exit of the pipe connected from each prismatic block of model used in bypass flow simulations. Pressure drop obtained from experiments must be subtracted by pressure drop of flow past flow straighteners before comparing with pressure drop obtained from simulations.

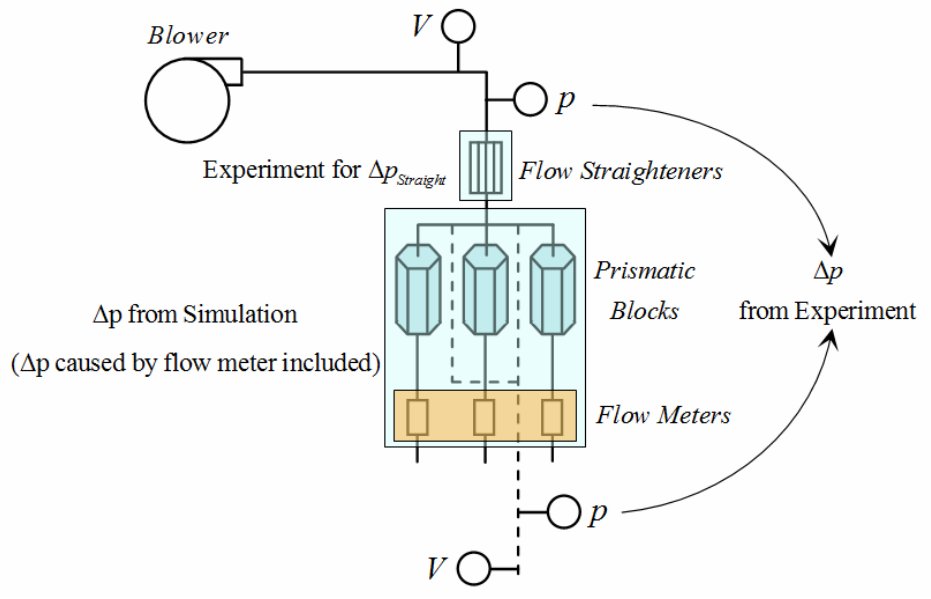

Figure 64. Schematic diagram for pressure drop comparison of air flows

An air flow experiment through flow straighteners was conducted to obtain pressure drop plot in Figure 65. To enable this data for predicting pressure drop of water flow through flow straighteners, all variables are converted to dimensionless form, i.e., volume flow rate and pressure drop are converted to Reynolds number and pressure loss coefficient ($\frac{\Delta p}{\frac{1}{2}\rho V^2}$), respectively. Side length of hexagon that forms flow straightener of 2.0 mm yields hydraulic diameter (d_h) of 3.464 mm was used in Reynolds number calculation. Average velocity is approximately found by dividing flow rate with cross sectional area of three prismatic blocks. Pressure loss coefficients versus Reynolds numbers are plotted in Figure 66 where linear interpolation and extrapolation are employed in predicting of pressure drops at all flow rates in bypass flow experiments.

Reynolds Number: $$Re = \frac{\rho d_h}{\mu}\frac{Q}{A} \qquad \text{(B.1)}$$

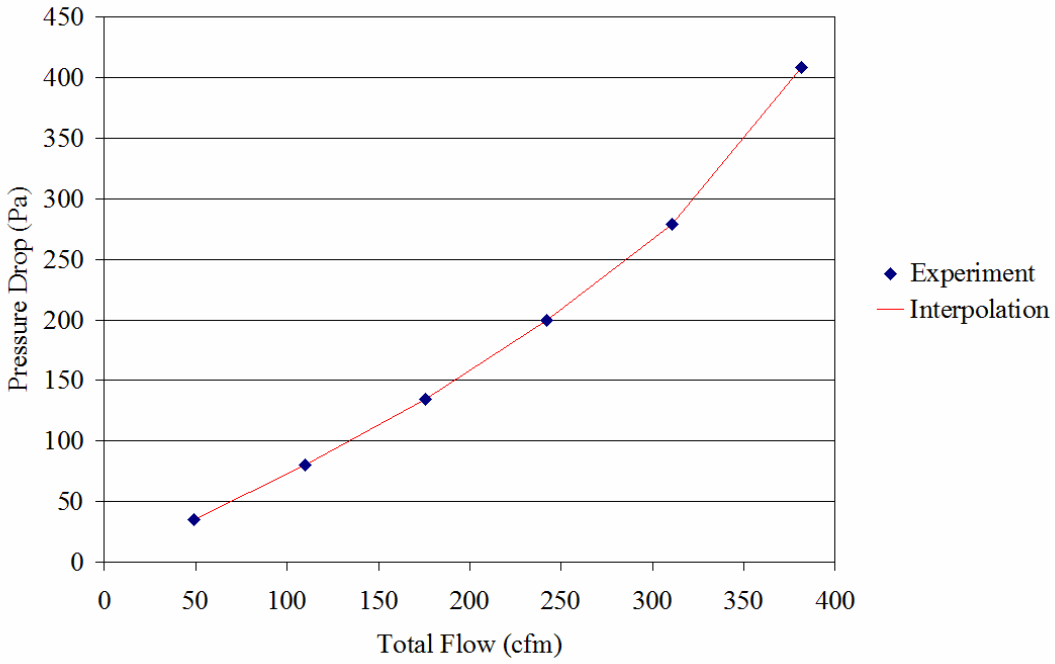

Figure 65. Pressure drop of air flow through flow straighteners

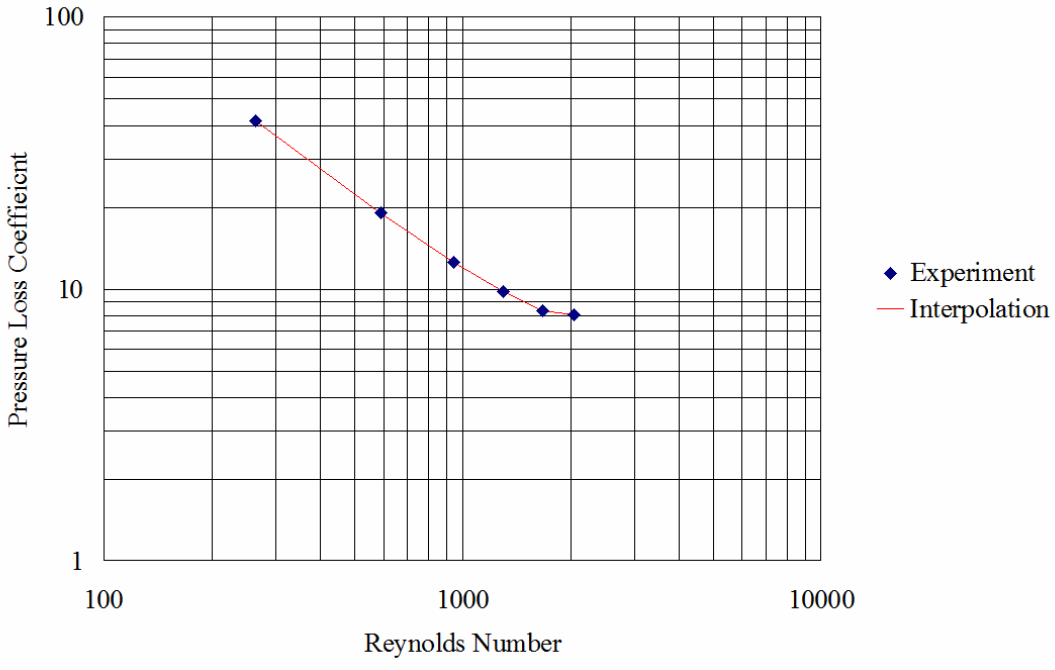

Figure 66. Pressure loss coefficient of flow through flow straighteners

APPENDIX C

VALIDATION EXERCISES OF STAR-CCM+ SOFTWARE

Two simple flow problems used in validating STAR-CCM+ software are flow in circular pipe (pipe flow) and flow between two parallel plates (channel flow) because they can represent physical situations of flow through coolant channels and bypass gaps of the prismatic block models used in present study. Darcy friction factor (*f*) from air and water flow simulations computed from equation (C.1) are compared with ***four times*** of Fanning friction factor (*f*) provided by Churchill & Chan [44] in equation (C.2) for turbulent flow in circular pipe and equation (C.3) for turbulent flow between two parallel plates where *e* contained in them is surface roughness.

Energy equation:
$$\frac{\Delta p}{\rho} = f\,\frac{l}{d_h}\,\frac{V^2}{2} \tag{C.1}$$

Fanning friction factor of fully-developed turbulent flow in circular pipe:

$$\left(\frac{2}{f}\right)^{1/2} = 1.989 - \frac{161.2}{Re(f/8)^{1/2}} + \left[\frac{47.6}{Re(f/8)^{1/2}}\right]^2 + 2.5\ln\left[\frac{Re(f/8)^{1/2}}{1+0.301(2e/d)Re(f/8)^{1/2}}\right] \tag{C.2}$$

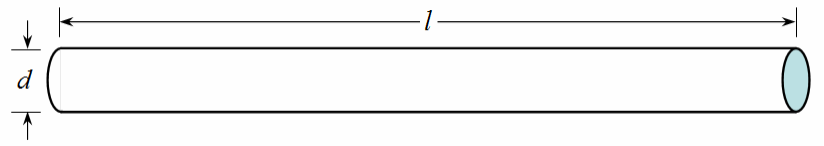

Figure 67. Parameters related to flow in circular pipe

Fanning friction factor of fully-developed turbulent flow between two parallel plates:

$$\left(\frac{2}{f}\right)^{1/2} = 3.3618 - \frac{190.83}{Re(f/32)^{1/2}} + 2.5\ln\left[\frac{Re(f/32)^{1/2}}{1+0.301(2e/b)Re(f/32)^{1/2}}\right] \qquad \text{(C.3)}$$

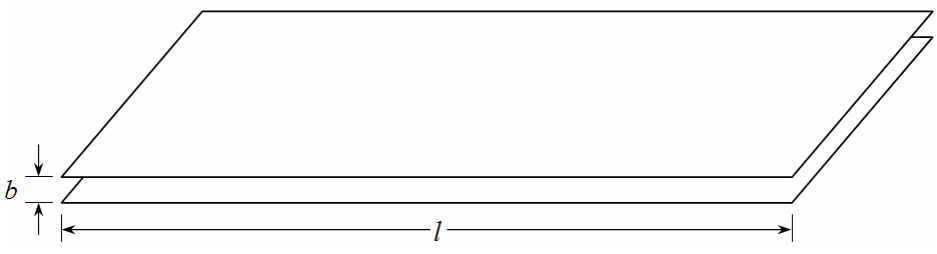

Figure 68. Parameters related to flow between two parallel plates

In Figure 67, diameter (d) of 25 mm and pipe length (l) of 3000 mm are specified in simulations to obtain l/d of 120. Pressure drops (Δp) are computed from difference between *surface-averaged* pressures taken from two cross sections located at l/d equal to 20 and 120 to avoid computational error at location where l/d is very small. In Figure 68, gap width between two parallel plates (b) of 10 mm and plate length (l) of 2000 mm are specified in simulations to obtain l/d_h of 100. Surface-averaged pressures taken from locations where l/d_h equal to 20 and 100 are used in calculating pressure drops with the same reason as for flow in circular pipe.

Mass flow rates and zero gauge pressure are specified on left plane (inlet) and right plane (exit) in both figures, respectively. In Figure 68, front plane and back plane, 100-mm apart, are set as symmetric planes. Air and water properties used in these exercises are same as the values used in bypass flow simulations. Reynolds number based on hydraulic diameter (d_h) in both flow problems is ranged from 10000 to 100000

because it can cover almost all of the range of Reynolds numbers of flow through coolant channels and bypass gap that can be attained in all experiments.

Trimmer mesh with base size of 1.0 mm is selected for mesh constructions. Number of prism layer equal to *seven* with stretching ratio of 1.35 (default value is 1.5) was found to be enough to prevent very large residual of turbulent dissipation rate at the beginning of simulations which caused solutions to be diverged (especially when using older version of STAR-CCM+ such as 3.06.006). Therefore, only *absolute* thickness of prism layer is varied to be 0.250, 0.333 and 0.400 mm to investigate appropriate prism layer thickness for bypass flow simulations.

Turbulence model used in all simulations for validation exercises is realizable k-ε model with two-layer all y^+ wall treatment because it yields the closest values of friction factor to those obtained from Churchill & Chan's correlations compared with k-ω and Reynolds stress model. The *implicit unsteady* scheme is employed for all simulations which are stopped at physical time of 100 seconds. As seen from Figure 69 to Figure 72, Darcy friction factors computed from air and water flow simulations are almost identical for both flow problems. After considering all cases, it can be concluded that absolute prism layer thickness of *0.400 mm* contains seven prism layers with stretching ratio of 1.35 is appropriate for bypass flow simulations in present study. If near-wall phenomena are focused, number of prism layer should be 15 for stretching ratio of 1.35 (or 12 for stretching ratio of 1.5) to make the first layer lies within viscous sublayer at short distance (less than 2 cm) from leading edge.

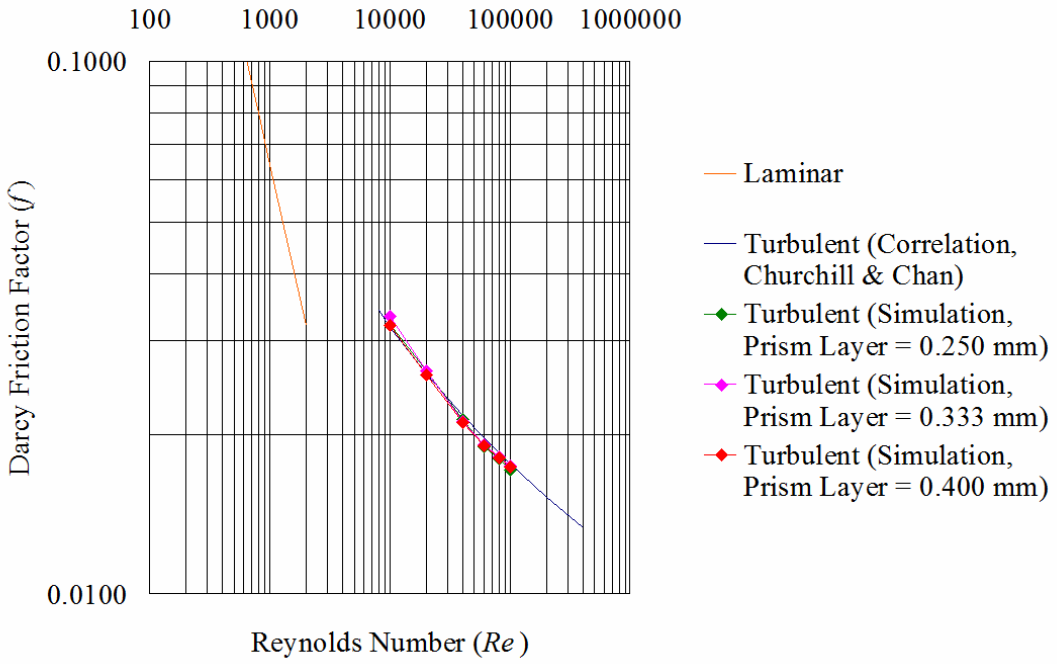

Figure 69. Darcy friction factor of air flow in circular pipe

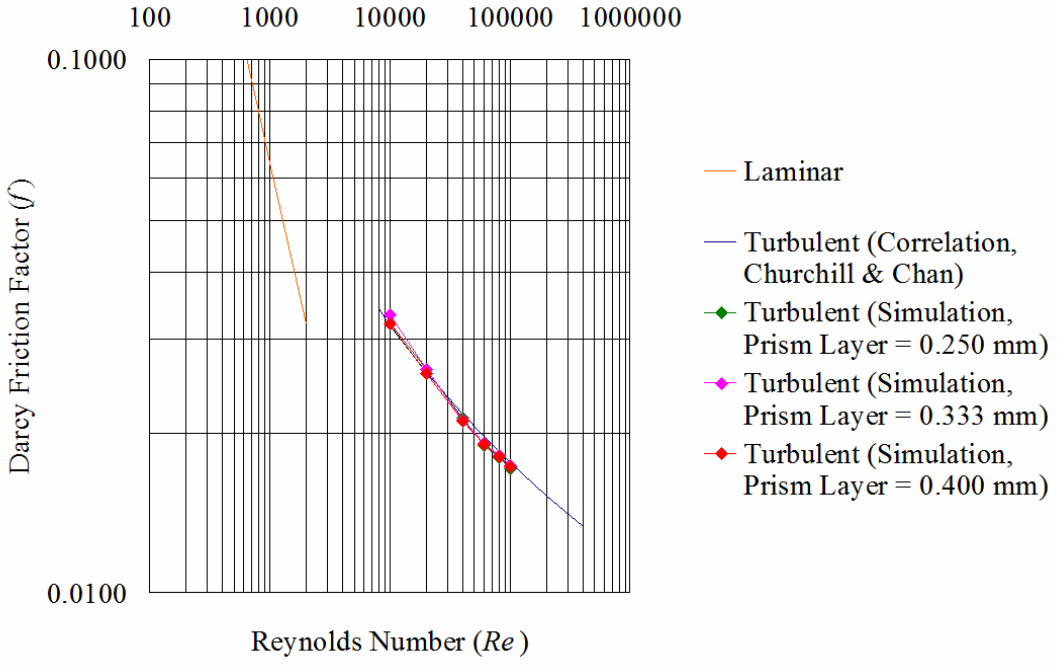

Figure 70. Darcy friction factor of water flow in circular pipe

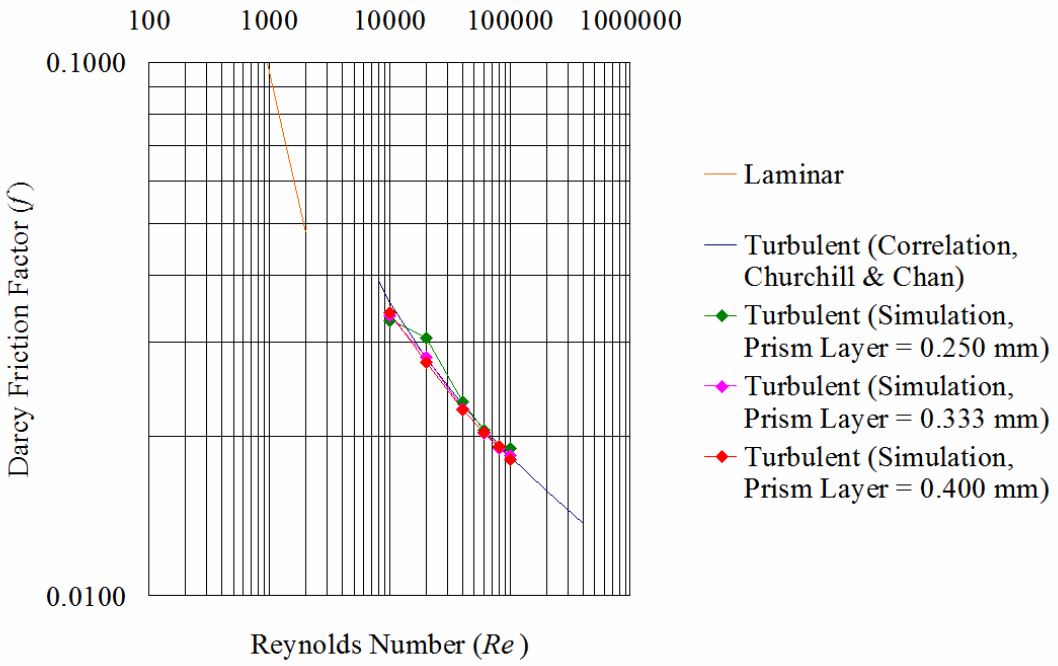

Figure 71. Darcy friction factor of air flow between two parallel plates

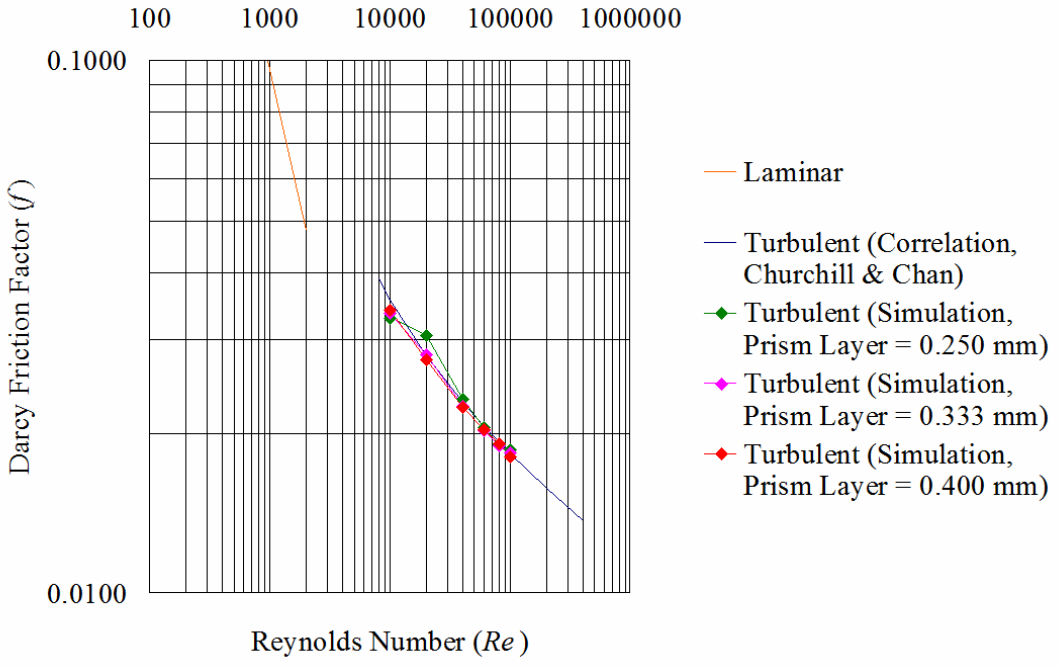

Figure 72. Darcy friction factor of water flow between two parallel plates